ROME AIR DEVELOPMENT CENTER GRIFFISS AFB NY NULL FILTER MOBILE RADAR (NEMRAD): CONCEPT VERIFICATION, (U) OCT 80 W BUCHANAN, H GODLEWSKI, F S HOLT RADC-TR-80-306 AD-A099 079 F/6 17/9 UNCLASSIFIED NL 1 oF 2 An A 099079

IFVELT **RADC-TR-80-30** in-House Reperi NULL FILTER MOBILE RADAR (NFMRAD): CONCEPT VERIFICATION, W./Buchanan/Capt, USAF H. Godlewski 1/Lt, USAF F. Sheppard/Holt P 16) 460P APPROVED FOR PUBLIC RELEASE; DISTRIBUTION UNLIMITED

ROME AIR DEVELOPMENT CENTER
Air Force Systems Command
Griffiss Air Force Base, New York 13441

OTE FILE COPY

309050

This report has been reviewed by the RADC Public Affairs Office (PA) and is releasable to the National Technical Information Service (NTIS). At NTIS it will be releasable to the general public, including foreign nations.

RADC-TR-80-306 has been reviewed and is approved for publication.

APPROVED:

JOHN K. SCHINDLER, Assistant Chief

EM Techniques Branch

Electromagnetic Sciences Division

APPROVED: Weland Scheel

ALLAN C. SCHELL, Chief

Electromagnetic Sciences Division

FOR THE COMMANDER:

JOHN P. HUSS

Acting Chief, Plans Office

kn P. Kluss

SUBJECT TO EXPORT CONTROL LAWS

This document contains information for manufacturing or using munitions of war. Export of the information contained herein, or release to foreign nationals within the United States, without first obtaining an export license, is a violation of the International Traffic in Arms Regulations. Such violation is subject to a penalty of up to 2 years imprisonment and a fine of \$100,000 under 22 U.S.C 2778.

Include this notice with any reproduced portion of this document.

If your address has changed or if you wish to be removed from the RADC mailing list, or if the addressee is no longer employed by your organization, please notify RADC (EEC) Hanscom AFB MA 01731. This will assist us in maintaining a current mailing list.

Do not return this copy. Retain or destroy.

Unclassified SECURITY CLASSIFICATION OF THIS PAGE (When Date Entered)

REPORT DOCUMENTATION PAGE	READ INSTRUCTIONS BEFORE COMPLETING FORM		
RADC-TR-80-306 ALAO 99079	3 RECIPIENT'S CATALOG NUMBER		
4 TITLE (and Submite)	5 TYPE OF REPORT & PERIOD TOVERED		
NULL FILTER MOBILE RADAR (NFMRAD): CONCEPT VERIFICATION	In-House		
CONCEPT VENIFICATION	6 PERFORMING ORG REPORT NUMBER		
7 AUTHOR'S)	B CONTRACT OR GRANT NUMBER: 5.		
W. Buchanan, Capt, USAF H. Godlewski, 1/Lt, USAF F. Sheppard Holt			
9 PERFORMING ORGANIZATION NAME AND ADDRESS Deputy for Electronic Technology (RADC/EEC)	10 PROSPAM ELEMENT PROJECT TASK AREA & WORK UNIT NUMBERS		
Hanscom AFB Massachusetts 01731	62702F 46001502		
Deputy for Electronic Technology (RADC/EEC)	12 REPORT DATE Cottober 1980		
Hanscom AFB Massachusetts 01731	13 NUMBER OF PAGES		
14 MON-TORING AGEN'Y NAME & ADDRESS it different from Controlling Office	15 SECURITY CLASS of this report:		
	Unclassified		
	15# DECLASSIFICATION DOWNGRADING		
16 DISTRIBUTION STATEMENT Of this Reports			
Approved for public release; distribution unlimited.			
17 DISTRIBUTION STATEMENT of the abstract entered in Block 20, if different from Report			
18 SUPPLEMENTARY NOTES			
19 KEY WORDS (Continue on reverse side if necessars and identify by block number)			
Foliage Penetration			
Mobile			
Radar			
The Null Filter Mobile Radar (NFMRAD) concept is described, and the need for narrow-band digital filters that can distinguish between positive and negative frequencies is explained. Two different procedures for realizing complex bandpass and bandstop filters of the infinite impulse response type are described, and their properties evaluated. A procedure for generating complex bandpass and bandstop filters of the finite impulse response type is also described, and the particular applicability of these filters to NFMRAD			
is discussed. The experimental NFMRAD system			

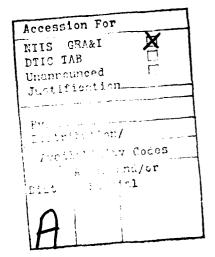
Unclassified
SECURITY CLASSIFICATION OF THIS PAGE(When Data Entered)

20. Abstract (Continued)

installation and test program is explained. A ground based experiment using a truck traveling at about 30 mph (13.4 m/s) as the radar platform is described. Under these experimental conditions, the performance of NFMRAD is computed theoretically and compared to expected performance of systems using Chebyshev and uniform-fed antenna arrays with and without filters. Real-time processing tasks such as antenna pattern synthesis, Doppler filtering, and detection processing are described. Hardware performance and a functional description of the radar hardware is presented. NFMRAD transmitter, receiver, and digital processing specification are reviewed, and experimental system restrictions are made clear. The NFMRAD system is found to have its greatest superiority over other systems for cases in which the differences between the radial velocities of the target and the local clutter is not large.

Unclassifed

SECURITY CLASSIFICATION OF THE PAGE When Date Enter



Preface

The authors are indebted to the following individuals for their contributions during the course of this work:

Dr. William B. Goggins for original system concept and system design work. $^{\mbox{\scriptsize 1}}$

Dr. August Golden for system design, software development, consultation, and continued project guidance.

Mr. Radames Gonzalez, Jr. for system fabrication and support during field testing.

Mr. L. McWilliams for artwork and drafting done in support of this report, and for his perserverance throughout field testing.

Dr. J. K. Schindler and Dr. J. Leon Poirier for providing guidance, suggestions, and relevant questions throughout this effort.

TSgt Dion Shannon for system fabrication, field testing support, and the ADC alignment procedure.

Mr. Richard Taylor for development of efficient real-time radar data processing software which made system realization possible, and for his continued support and interest.

Goggins, W.B., Jr., Sletten, C.J., and Holt, F.S. (1974) New concepts in AMTI radar: Nulling effect of Doppler filter/multielement horn array, Microwave J. 17(No.1):29-33.

		Contents
1.	INTRODUCTION	11
2.	THE NFMRAD CONCEPT AND EXPERIMENTAL SYSTEM	15
-•	2.1 The Null Filter Mobile Radar (NFMRAD) 2.1.1 Concept Description and Filter Requirements 2.1.2 Optimum Receive Antenna Pattern 2.2 Experimental Radar System 2.3 Theoretical Investigations Relative to the NFMRAD Experiment 2.3.1 The NFMRAD Experiment 2.3.2 Optimization of FIR Filters 2.3.3 Comparison With Other Systems	15 16 22 29 29 30 31
3.	NFMRAD RF HARDWARE	33
	3.1 Transmitter 3.1.1 RF Sources 3.1.2 Generation of Carrier 3.1.3 Transmit Pulse Formation 3.1.4 Traveling Wave Tube Amplification 3.1.5 Transmit Antenna 3.1.6 Diagnostic Facilities 3.1.7 Summary of Transmitter Specifications 3.2 Receiver 3.2.1 Receive Antenna 3.2.2 Receiver Front End 3.2.3 Receiver Gain Control 3.2.4 IF Eandpass Characteristics and Detection	35 35 36 38 43 43 46 47 50 50
	of Moving Targets 3.2.5 Summary of Receiver Specifications	56 6 0

Contents

4.	REC	EIVER DIGITAL HARDWARE	61
	4.1	NFMRAD (AMTI) System Timing	64
	4.2	Ultra-High-Speed Sample and Hold	67
	4.3	Ultra-High-Speed Analog-to-Digital Converter	67
	4.4	Radar Data Buffer	68
		4.4.1 Mantissa Buffer	71
		4.4.2 Base 2 Exponent Buffer	72
	4.5	Data Format Conversion Logic	72
		4.5.1 Analog-to-Digital Converter (Input and Output	
		Specifications)	73
		4.5.2 8-Bit Inverted ()ffset Binary Format Conversion	
		to 8-Bit Sign/Magnitude Format	73
		4.5.3 8-Bit Sign/Magnitude Mantissa with Positive 3-Bit	
		Base 2 Exponent Conversion to 16-Bit Floating	
		Point Format with Base 16 Exponent	74
		4.5.4 Normalization of 16-Bit Floating Point Word	77
	4.6	Input/Output Scroll (IOS) Interface	77
		4.6.1 16-Bit Normalized Floating Point Word Transfer	7.5
		from Radar to IOS Interface	77
		4.6.2 Radar/MAP-300 IOS Interface Control and	70
		Timing Signals	78 79
	4.7	4.6.3 Data Status Indicator Receiver Simulator Hardware	80
	4.1	Receiver Summator nardware	00
5.	SYS	TEM SOFTWARE	83
	5.1	CSP-30/MAP-300 System Initialization Software	83
		CSP-30/MAP-300 Real-Time Operation	84
	5.3	Maintenance Software	85
	5 .4	MAP Software	86
		5.4.1 MAP Initialization	86
		5.4.2 MAP Real-Time Processing	87
		5.4.3 MAP Software Test Mode	90
	5, 5	MAP-300 Double Buffered Input	90
6.	FIE	LD INSTALLATION AND TESTS	93
	6.1	Experimental Set-Up	94
		6.1.1 Van Installation	94
		6.1.2 Remote Test Facility	94
		6.1.3 Enhanced Radar Target	97
		6.1.3.1 Pickup/Corner Reflector Combination	
		Target	97
		6.1.3.2 Flat Plate Reflector	97
	6.2	Field Tests	100
		6.2.1 Measurement of Two-Way Antenna Patterns	102
		6.2.2 Measurement of Doppler Filter Characteristic	105
		6.2.3 Target Detection Threshold Voltage Determination	107
		6.2.4 NFMRAD (AMTI) P _d Determination	110
7.	EXP	ERIMENTAL RESULTS AND CONCLUSIONS	116
	7.1	Two-Way Antenna Patterns	116
		7.1.1 Uniformly Weighted Antenna Pattern	116
		7.1.2 NFMRAD Antenna Pattern	117
	7.2	Doppler Filter Characteristic	118

		Contents
	 7.3 Threshold Voltage Determination 7.4 Receiver I/O Characteristic 7.4 Receiver Noise Histogram 7.6 Preference Conclusions and Future Direction 	118 118 120 121
RE	FERENCES	123
ΑP	PENDIX A: Complex Recursive Infinite Impulse Response (IIR) Digital Filters	125
ΑP	PENDIX B: Complex Nonrecursive Finite Impulse Response (FIR) Digital Filters	137
ΑP	PENDIX C: Control Panel Operational Range Equations	141
ΑP	PENDIX D: ADC Alignment Procedures	145
ΑP	PENDIX E: System Component Identification	159
		Illustrations
1.	Example of Doppler Clutter Interference	14
2.	NFMRAD Antenna Patterns, Filter Power Transfer Functions, and Clutter Distributions (a) Transmit Antenna Pattern (b) Doppler Filter Power Transfer Function (c) Bandstop Filter Power Transfer Function (d) Optimum Receive Array Pattern (e) Composite Doppler Filter Characteristic (f) Clutter Power vs Azimuth After Filtering but Before NFMRAD Processing (g) Clutter Power vs Azimuth After Filtering and NFMRAD Processing (h) Two-Way NFMRAD Antenna Pattern	17
3.	Simplified NFMRAD System	23
4.	NFMRAD/AMTI Experimental Radar System	23
5.	NFMRAD/AMTI Transmit and Receive Antennas (a) Transmit and Receive Array (Front View) (b) Transmit Antenna (Three Views) (c) Eight-Element Receive Array (Side View) (d) Eight-Element Receive Array (Top View)	24
6.	Radar Van and Target Tracks for NFMRAD Experiment (Diverging Case)	30
7.	Improvement of NFMRAD System Over a System Using Uniform Patterns on Both Transmit and Receive	39

Illustrations

8.	Improvement of NFMRAD System ()ver a System Using Chebyshev Array Patterns on Both Transmit and Receive (a) Without Filters, (b) With Filters	32
9.	NFMRAD System Functional Breakdown	34
10.	Simplified Diagram of NFMRAD Receiver and Transmitter	3.5
11.	Typical Microwave PIN Diode Switch	39
12.	Timing Diagram: Transmit Pulse Formation	4 1
13.	Diode Switch Firing Circuitry	42
14.	TWTA Gain Characteristic	43
15.	Transmitter Horn	44
16.	Theoretical and Experimental Transmit Horn Azimuth Power Patterns	4.5
17.	Experimental Transmit Horn Elevation Power Pattern	45
18.	Doppler Target Simulator	47
19.	NFMRAD Transmitter Subsystem	49
20.	Theoretical and Experimental Receive Horn Single Element Directivity Pattern	50
21.	Illustration of Relationship for Derivation of Single Receive Element Pattern	51
22.	Theoretical and Experimental Azimuth Power Pattern for Receiver Eight-Element Array	53
23.	Receiver Front End	54
24.	Diagram of I and Q Outputs with Respect to Reference Signal Vector	59
25.	NFMRAD Receiver Subsystem	62
26.	Receiver Realization	63
27.	Timing Signal Binary Counter Outputs	65
28.	ADC Board Timing Signals	68
29.	Mantissa and Exponent Shift Register Buffer with 8-Bit Wide Data Multiplexer	70
30.	Radar Receiver Mantissa Buffer (256 8-Bit Words)	71
31.	Radar/IOS Interface Control and Timing Signals	78
3 2.	Receiver Digital Hardware	81
33.	Receiver Simulator Hardware	81
34.	Double Buffered Input Timing	91
35.	Radar Van Installation with Generator	95
36.	Radar Equipment Layout (Top View of Van)	95
37.	Radar Equipment Layout (End View of Van)	96
38.	Floating Radar Platform with Shocks and Sway Braces	96
39.	Base Plate Shocks	97

Illustrations

40.	Sway Braces	98
41.	Remote Test Facility	90
42.	Enhanced Radar Target	90
43.	Corner Reflector	100
44.	Flat Plate Reflector	101
45.	Field Site Used for Antenna Pattern Measurements (Top View)	101
46.	Field Site Used for Antenna Pattern Measurements (Side View)	102
47.	Field Site Used for Measurement of Deppler Filter Characteristic (Top View)	10%
48.	Field Site Used to Determine NUMRAD {AMTI} Threshold Voltages and NEMRAD {AMTI} P _d Curves (Top View)	108
49.	Taxiway Whiskey Divided into Tape Records	113
50.	AMTI Two-Way Azimuth Pattern (Theoretical and Experimental)	117
51.	NEMRAD Two-Way Azimuth Pattern (Theoretical and Experimental)	118
52.	Doppler Filter Characteristic (Theoretical and Experimental)	119
53.	Receiver 1 O Characacteristic	119
54.	Receiver Noise Histogram	120
55.	Effect of Uniformly Distributed Error in the Scattering Matrix on the Null Region of Receive Pattern	122
A1.	Power Transfer Loss Function of a Caver CO4a Type Filter	127
A2.	Power Transfer Functions of Filters Used to Realize an Asymmetrical Single-Band Lowpass Filter	129
A3.	Power Transfer Functions of Filters Used to Realize an Asymmetrical Single-Band Lowstop Filter	131
A4.	HR Digital Filter Response Times	135
B1.	Specification of Filter Response Values for BP 33-3-2 F.1.R. Filter	139
(1.	Radar Control Panel	141
D1.	8-Bit ADC Alignment Configuration	146
D2.	Receiver Digital Hardware (Backplane Connector Panel)	147
D3.	8-Bit ADC Assembly (a) Pin Locations (Top View) (b) Calibration Adjustments (Side View)	148
)4.	8-Bit ADC Calibration	150
D5.	LED Display	150
) 6,	4-Bit ADC Assembly	152
07.	4-Bit ADC Bias Adjustment	154
08.	ADC Dynamic Test Configuration	156

Illustrations

EI.	Receiver Transmitter Equipment Racks	162
	(a) Receiver	
	(b) Transmitter	
E2.	CSP-30 (MAP-300 Equipment Racks	162
	(a) CSP-30	
	(b) MAP-300	

Tables 1. NFMRAD AMTI System Characteristics Summary 26 2. IF Attenuation as a Function of Base 2 Exponent 56 3. Timing Command Sequence 66 4. System Timing Signals 67 5. Mantissa Buffer Data Multiplexer Pecking Order 69 6. Datel ADC Output Format 73 7. Sign Magnitude Format 74 8. Radar Base 2 Floating Point Format 75 9. MAP Base 16 Floating Point Half-Word Format 76 10. Radar/IOS Interface Control and Timing Signals 79 11. Receiver Digital Circuit Card Functions 82 12. Tape Record 105 B1. FIR Filters Used in NFMRAD Investigation 139 C1. Radar Operating Range Mode 142 C2. DCBA₁₀ Equivalent for Range Calculations 143 D1. 4-Bit ADC Output 153 D2. ADC to Digital Hardware Backplane Cable List 155

Null Filter Mobile Radar (NFMRAD): Concept Verification

1. INTRODUCTION

Pulse-Doppler radars may be used in a side-looking airborne configuration for the detection of slow-moving stand-off targets embedded in clutter (that is, foliage). Such a radar experiences interference from this background clutter. Clutter signals received through the mainbeam may be distinguished from a target of interest by appropriate Doppler filtering. This is possible, since the mainbeam clutter returns possess near-zero Doppler and can be effectively separated from a moving target signal possessing a Doppler frequency shift. However, clutter received through receive antenna sidelobes possesses motion relative to the moving radar platform. This sidelobe clutter can easily possess a Doppler equal to that of a moving target in the receive antenna mainbeam. Doppler filtering of this sidelobe clutter signal will not separate it from the target Doppler signal received through the mainbeam. Hence, with sufficient power, the sidelobe clutter signal can obscure the mainbeam target; thus, moving target detection is rendered difficult or impossible. The detection of a moving target will be made where no such target exists in the mainbeam.

This phenomenon results from the mechanism which generates a Doppler frequency and may be referenced to the forward motion of the radar platform by the following relation:

(Received for publication 3 October 1980)

$$f_{\rm d} = \frac{2V_{\rm o}}{\lambda} \cos \theta$$

where λ is the wavelength of the radar frequency; $V_{_{O}}$ is the forward velocity of the airborne radar platform; θ is measured from the line of forward motion of the radar platform, and $f_{_{\rm d}}$ is the resultant Doppler frequency. Targets with motion parallel to the radar platform and with position in the receiver mainbeam would be at a θ angle of $90^{\rm O}$ and produce a zero Doppler frequency in their radar returns.

Targets illuminated by the mainbeam and producing nonzero Doppler frequencies are following courses nonparallel to that of the radar platform; hence they possess radial velocities with respect to the radar platform. A problem arises when ground clutter possesses a radial velocity with respect to the moving radar platform. This is true of ground clutter received through the receive antenna sidelobes.

To illustrate this matter, assume that the radar platform possesses a forward velocity of 180 miles per hour (mph) (80 meters per second (m s)). A signal is being received in an antenna sidelobe from a large patch of ground clutter at a bearing of roughly 95° from the radar platform course heading. The return signal power would be large and detectable above the radar systems minimum discernible signal level. In addition, the sidelobe signal Doppler would be 14 m s λ . For a radar wavelength of 1.8 ft (0.6 m or 500 MHz), the Doppler frequency of the return would be 23.3 Hz, indicating a target moving away from the radar platform with a radial speed of 31.3 mph (14 m/s).

The returned signal Doppler frequency may also be referenced to radial velocity from the moving radar platform with the following relation:

$$I_d = \frac{2V_r}{\lambda}$$

where \mathbf{V}_{v} is the apparent target radial velocity from the moving radar platform. A moving target in the mainbeam may possess the same radial velocity as sidelobe clutter:

$$V_r = V_o \cos 80^\circ$$
 .

Such a target, embedded in foliage, could be traveling away from the radar platform at 31.3 mph (14 m/s). The course of the mainbeam target would be 80° from that of the radar platform, with a velocity of approximately 32 mph (14.2 m/s) on its own course.

Examining the two cases illustrated above highlights the problem from the radar reception standpoint. With reception of clutter alone, an erroneous detection of a target may be made. With the reception of the discrete clutter at a bearing from the radar line of travel of 95°, and the simultaneous presence of the moving target in the receive antenna mainbeam, detection of the mainbeam target is rendered a difficult if not impossible task. Figure 1 illustrates the situation of clutter at 95° and the above target on a course 80° from that of the radar platform.

One possible answer to this sidelobe clutter problem is the use of a narrow-beam, low-sidelobe high-gain antenna. Unfortunately, this approach suffers from physical unmanagability. The radar operating frequencies that afford good foliage penetration performance lie well below 900 MHz. The antenna apertures required to realize a narrow mainbeam become prohibitively large at these optimum foliage penetration frequencies, and would result in an antenna size physically unmanageable in a side-looking airborne configuration.

One approach to the solution of the Doppler clutter problem is the use of antenna receive-pattern nulls placed or stirred such that the interfering clutter is attenuated. This technique could be used in conjunction with mainbeam target Doppler filtering to reveal the presence or absence of a tactical target in the mainbeam. It is for the investigation of this antenna null filtering technique that the Null Filter Mobile Radar (NFMRAD) project has been conducted.

NFMRAD is a proof-of-concept investigation. In any proof-of-concept program, economy of performance in the attainment of new information is important. To this end NFMRAD has been designed. Hardware design in both the areas of radio frequency and digital signal processing technology has been directed toward implementation of one antenna null and one Doppler filter with a similar design of processing software.

Rather than implementing NFMRAD in a costly airframe design, a truck-based moving platform has been used. This NFMRAD configuration is similar to that of a side-looking Airborne Moving Target Indicator (AMTI) on a moving platform. The moving system may be field tested against another moving target (truck), greatly simplifying field testing while addressing the objective of the most economic experimental investigation possible. Additionally, facility exists in the design for comparison of NFMRAD performance to that of conventional standoff, side-looking AMTI without the null filtering capability.

NFMRAD, as an experimental system, has been implemented in X-band. In keeping with constraints of simplicity and economy, the X-band implementation

Brown, Dr. Gary S., and Curry, William J. (1979) An Analytical Study of Wave Propagation Through Foliage, RADC-TR-79-359.

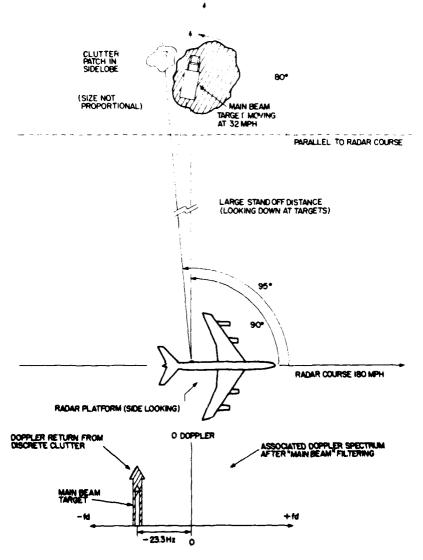


Figure 1. Example of Doppler Clutter Interference

affords the use of readily available components within a compact experimental configuration. This again not only simplifies the design of the experimental richar platform but also eases field testing requirements.

Section 2 of this report covers in detail the theoretical aspects of the NFMRAD concept. Sections 3 and 4 describe the hardware design, both radio frequency and digital circuitry. Section 5 covers the design of supporting system software, while Section 6 deals with the experimental system field installation and testing. Results and conclusions are presented in Section 7 of the report.

2. THE NEMBAD CONCEPT AND EXPERIMENTAL SYSTEM

2.1 The Null Filter Mobile Radar (NFMRAD)

2.1.1 CONCEPT DESCRIPTION AND FILTER REQUIREMENTS

The NFMRAD system operates from a moving platform and uses Doppler bandpass and bandstop filters together with null control in the receive internal array pattern to reduce clutter return when detecting a target that is in notion relative to the ground. For a radar moving with velocity is relative to the ground, there is a simple relationship between the clutter Doppler frequency shift Δf_d and the azimuth angle θ given by the formula

$$\Delta f_{d} = \frac{2\nu \cos \theta}{\lambda}$$

where λ is the wavelength of the transmitted frequency and θ is measured clockwise relative to the direction of motion of the NFMRAD platform. By means of this relationship, all Doppler filter plots between the maximum and minimum clutter Doppler frequency shifts $(2\sqrt{\lambda} \text{ and } -2\sqrt{\lambda})$ can be exhibited as functions of azimuth angle θ , rather than clutter Doppler frequency shift. Throughout this report, we will assume that the clutter distribution is uniform in θ . The Doppler filter patterns in θ thus represent the clutter distribution as modified by the filters.

The NFMRAD system converts to baseband, using inphase and quadrature mixing. The received signal thus processed will contain only the Doppler frequency shifts; these will be positive or negative according to whether the objects producing the reflected signals are approaching or receding relative to the radar. Discrimination between these two cases is possible because both inphase and quadrature information is present. To quantitatively measure the frequency shifts and hence the relative velocities, bandpass filters must be designed that can measure both positive and negative frequencies and distinguish between them. At the same time, to discriminate against signals due to ground clutter, it is

steed that play be centered in the order to a Winess all big as state there. The our steed that play be centered in the order negative or a positive trequer will there in as a read voltage transfer and that is, read on the read exist, the place transfer turn from as a function of the access with last be synchotten with respect there of remiency, and the filter countries are note between positive and togrative frequencies. What is needed his confine that will produce a single possibility of stappand) that is not synchetic with respect to zero frequency. The will are transfer function for such a filter will necessarily be complex that will be read axis).

In the operation of NFMRAD, many infferent filters and many different actions, array patterns need to be implemented, and the only, practical way this can be accomplished as by digital processing. Two general types of complex is, stal offers have been considered. One type has an infinite impulse response (HRO act is recorded by means of a recursive algorithm. The second type has a canto in online response (HRO) and is realized by means of a nonrecoursive algorithm.

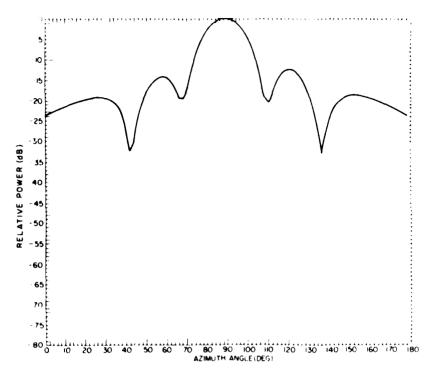
2. 1. 2 CPTIMUM RECEIVE ANTENNA PATTERN

In the XEMRAD system concept, the spatial azimuth sector is a very the aset of fixed transmitting bear positions, and the Doppler frequency shall be tage is covered by a set of bandrass filters. Figure 2(a) shows a typical transmit afterm pattern and Figure 2(b) shows a typical Doppler bandrass filter power transfer function both plotted with "as abscissa. For each transmitting bear position the its also an associated bandstor Doppler tilter than blanks the clutter of the first main labe of the transmitted pattern. Figure 2(c) shows the bandstor tilter power transfer function corresponding to the transmitt antenna pattern. Figure 2(d).

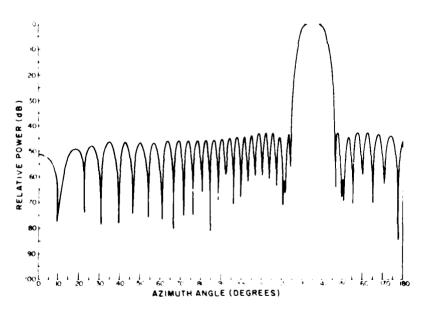
Assume there is a target located at the reak of the main is best the mass of antenna pattern of Figure 2(a) with maked velocity trelative to the NEMEND plate such that its return signal has a Doupler frequency shift that lies in the grassband the Doupler filter of Figure 2(b). Then for the transmit antenna pattern of Figure 2(a) and the alter power transfer runs trons of Figures 2(b) and 2(c), there exists a unique receive antenna array pattern that is optimum in the sense that it maximizes the ratio of the power of the received target signal to the total clutter boxes, ², ⁴. All optimum received patterns that appear in this report were computed in a

Cherry, D.K. and Tseng, F.L. (1965) Gain optimization for arbitrary antenna arrays, IEEE Tr. APAP-13(No. 6):973.

Drane, C.J., Jr. and McIlvenna, J.F. (1969) Gain Maximization and Controlled Null Placement Simultaneously Achieved in Aerial Array Patterns, AFCRL-69-0257.

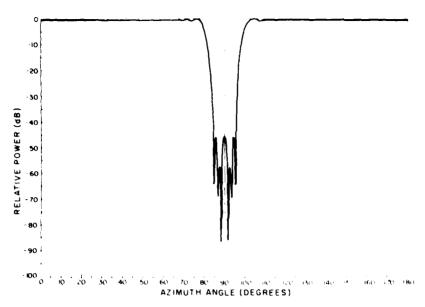


(a) Transmit Antenna Pattern

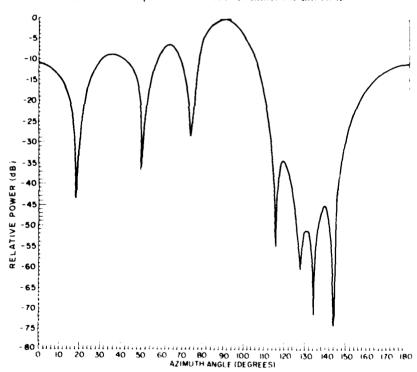


(b) Doppler Filter Power Transfer Function

Figure 2. NFMRAD Antenna Patterns, Filter Power Transfer Functions, and Clutter Distributions

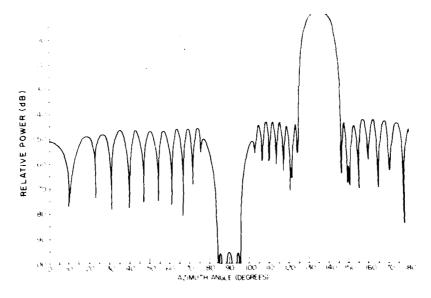


(c) Bandstop Filter Power Transfer Function



(d) Optimum Receive Array Pattern

Figure 2. NEMRAD Antenna Patterns, Filter Power Transfer Functions, and Clutter Distributions (Cont.)



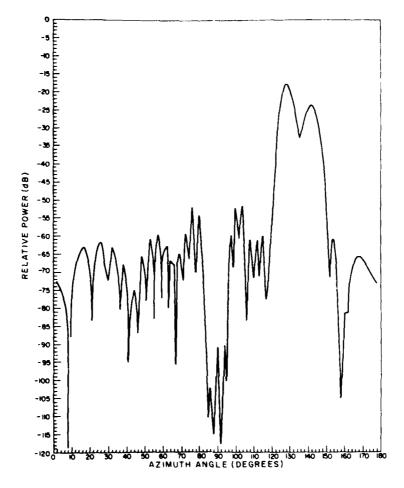
(e) Composite Doppler Filter Characteristic

Figure 2. NFMRAD Antenna Patterns, Filter Power Transfer Functions, and Clutter Distributions (Cont.)

CDC-6600, using modifications of a FORTRAN program devised by Goggins and Schindler. 5 Figure 2(d) shows a typical optimum receive antenna array pattern for the present case. It is characteristic of this optimum pattern that it has a null region in the angular sector whose clutter Doppler return lies in the passband of the Doppler bandpass filter.

The power filter transfer function for the composite filter obtained by caseading the bandpass filter (Figure 2(b)) with the bandstop filter (Figure 2(c)), is shown in Figure 2(e). A plot of clutter power vs angle, as observed after illumination of the assumed uniformly distributed clutter by the transmit antenna pattern followed by filtering but before receive antenna processing, is shown in Figure 2(f). The product of this distribution of clutter power vs angle with the NFMRAD receive antenna pattern represents the distribution of clutter power that is ultimately present in the NFMRAD system, and is shown in Figure 2(g). The integral of the clutter distribution shown in Figure 2(g) is a measure of the total clutter power in the NFMRAD system.

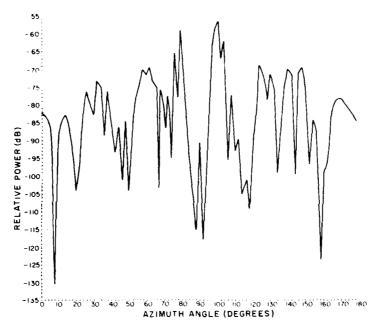
Signal-to-Clutter in AMTI Radars, pp. 15-21, AFCRI-TR-74-0577, AD



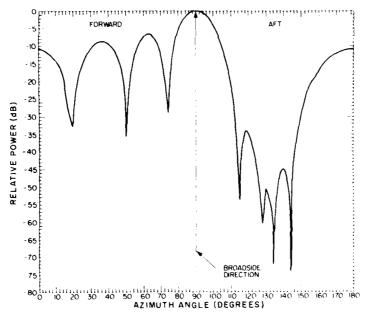
(f) Clutter Power vs Azimuth After Filtering but Before NFMRAD Processing

Figure 2. NFMRAD Antenna Patterns, Filter Power Transfer Functions, and Clutter Distributions (Cont.)

Figure 2(h) shows the composite antenna pattern (product of the antenna transmit pattern with the NFMRAD receive pattern). Note that the composite filter transfer function, Figure 2(d), and the composite antenna pattern, Figure 2(h), are complementary in that the composite filter transfer function has a reject region in the angular range where the composite antenna pattern has a mainlobe, and vice versa.



(g) Clutter Power vs Azimuth After Filtering and NFMRAD Processing



(h) Two Way NFMRAD Antenna Pattern

Figure 2. NFMRAD Antenna Patterns, Filter Power Transfer Functions, and Clutter Distributions (Cont.)

2.2 Experimental Radar System

A simplified block diagram of the experimental NFMRAD system is shown in Figure 3. A low-power N-band transmitter is shown in conjunction with an eight-channel coherent receiver. An eight-element linear receive array feeds the RF front end of the eight-channel coherent receiver. Inphase and quadrature signals for each channel are generated at the output of the receiver. The receiver output signals are converted to a digital format and transferred into an array processor. The array processor forms the receive antenna pattern and filters the radar data. Filtered data is transferred into the host minicomputer where it is stored and displayed. Detection processing takes place in the minicomputer, and detection outputs are also available for display on a CRT. Filtered data is stored on magnetic tape for more sophisticated off-line detection processing, to be performed on a CDC 6600.

The experimental radar system uses conventional AMTI processing as a basis for performance comparison. Figure 4 depicts a block diagram of the total NEMRAD AMTI experimental radar system. The experimental system implemented incorporates two forms of radar processing, NEMRAD and AMTI. The two radar processing algorithms use common data as input; however, the NEMRAD algorithm differs from the AMTI algorithm in that the antenna patterns synthesized in processing are different. AMTI processing forms an antenna pattern by uniformly weighting each receive channel, while NEMRAD antenna pattern synthesis weights each channel so as to form a clutter notch in the receive pattern. Sidelebe clutter falling outside the NEMRAD antenna pattern clutter notch is not in the bandpass of the NEMRAD Doppler filter. Antenna beam-forming coefficients are a function of the Doppler filter bandpass center frequency, therefore, to detect a wide range of target velocities, several Doppler velocity filters are needed, with each filter requiring a separate antenna pattern and clutter notch. The NEMRAD and AMTI Deppler velocity filters that follow the antenna pattern processing are identical.

The block diagram of the NFMRAD system shown in Figure 3 depicts a low-power monopulse transmitter operating at 9.410 GHz. The experimental transmit pattern shown in Figure 16 indicates an azimuth beamwidth of 18°. The experimental transmit elevation pattern of Figure 17 indicates a 3-dB elevation beamwidth of 12°. The transmit horn shown in Figures 5(a) and 5(b) was placed in an anechoic chamber for the pattern measurements.

The eight-element receive array shown in Figures 5(c) and 5(d) feeds the RF front end of the eight-channel coherent receiver. A theoretical and experimental single-element pattern is shown in Figure 20. The measurements were made in an anechoic chamber, and the pattern is indicative of a waveguide opening into free space.

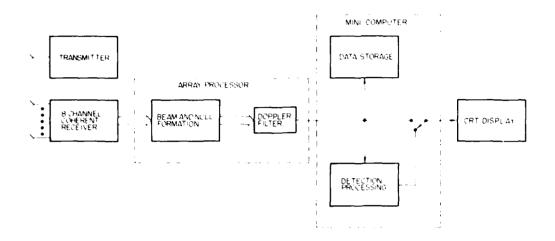


Figure 3. Simplified NFMRAD System

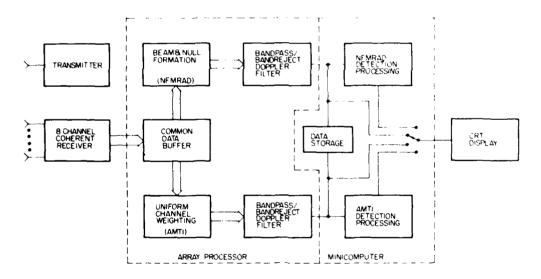
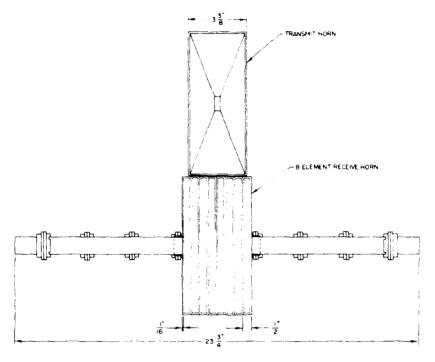


Figure 4. NFMRAD AMTI Experimental Radar System



(a) Transmit and Receive Array (Front View)

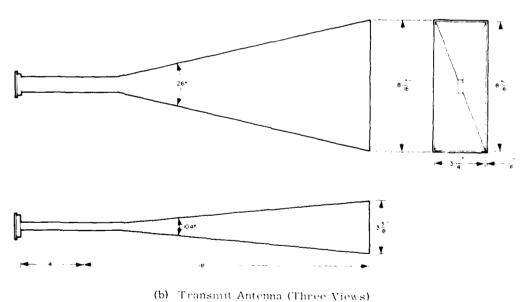
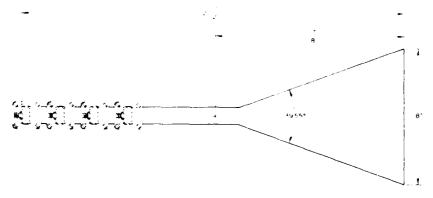
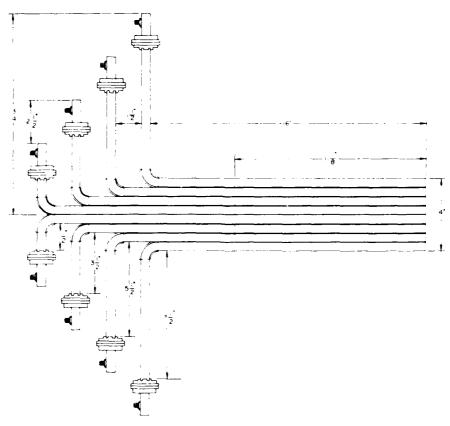


Figure 5. NFMRAD-AMTI Transmit and Receive Antennas



(c) Eight-Element Receive Array (Side View)



(d) Eight-Element Receive Array (Top View)

Figure 5. NFMRAD/AMTI Transmit and Receive Antennas (Cont.)

Figure 4 or a - NEMBAD and AMII real-space been transitionally rather perating across the first base. The array processor forms the receive rottern and offers the right flat abet be transferring the data into the historium mauter. The cornial and experimental AMTI and NI MRAD two successions are shown in Figures 40 and 41. The two sway patterns are discussed in Scott ins 7.1 and 7.2. The Denries tilter is a all smooth bands to and Lawings a liber. The Depoles filter characterists as shown in Ligure (2 and is discussed in Section 7.4. Filter design is reviewed in Appendix of A and B. The function of the Decoder filter London storing in its manufactor of factor of extern, while the Lordon's trementarial consix nd directly with the NI MRAD clutter in tch location in a court. The experiental melar system implements a single NFMRAD clutter in televisione objects spending Doppler filter. In addition to the NEMRAD pattern and filter, one uniformaly-weighted AMTI pattern as synthesized, and an identical Daspler (iller is also implemented in the radar array processor. Following to palses the coherent processing interval), the NEMRAD and AMTI Deppler filters produce ne veltage amplitude per range cell.

filtered NEMRAD and AMTI data is transferred into a high-special mass in puter for further processing, recording, and display. Detection processing is implemented in real time for both NEMRAD and AMTI data. Detection utput data or filtered voltage magnitude data may be displayed on the CRT. NEMRAD or AMTI detections or voltage amplitude may be displayed as a function of range cell on the CRT. Filtered NEMRAD and AMTI voltage magnitudes are recorded on magnetic tape in the format shown in Table 12 for off-line detection processing on a CDC 6600. Detection processing is also performed by the less municomputer. This processing compares each filtered voltage amplitude with a programmable threshold voltage. Detection processing results are not recorded.

Table 1 summarizes system characteristics, some of which were discussed above.

Table 1. NFMRAD AMTI System Characteristics Summary

Experimental Operation

Limited broadside search (selectable search range)

Real-time antenna pattern synthesis, Doppler filtering, and detection processing achieved in radar van

Filtered data recorded for off-line additional detection processing on a CDC 6600

Operational Frequency

9.410 GHz

和"我们,我们们就把我身满身的,我们只要不断的。" 电电影 化电影 化二氯甲酚 医二氯甲酚 化二氯甲酚

Wilde Beralds	
$A_{\alpha}(1) + a_{\alpha}(0) = A_{\alpha}(0) = a_{\alpha}(0)$	
$\lim_{t\to\infty} A(t) = \lim_{t\to\infty} A(t) = \lim_{t$	gang berganak permanan kecamatan dan bermalah bermalah bermalah bermalah bermalah bermalah bermalah bermalah b Bermalah bermalah be
American (S.)	$\begin{array}{lll} 4, 2 & + & -4, 412 & +, \\ 40, 4 & + & 41, 13 & +, \\ \end{array}$
Penancietics	\mathbf{H}_{i} (\mathbf{H}_{i}
Arc. uti Tralipsker Bermwelth	* A.V
Flexation Hall power Bearwidth	42
Beam Direction	IN mark between his con-
Transcitter	
HI pulse length	z 2 ste us
PRU	1804 pales s
Months of the second	
peak	22.5 W
overage.	11 toW
Receive Amenna (Figure 5) Eight H-pl	ane sectional filtras in linear array
Aperiare Size	
composito	3,875 \ 7,875 in. (9,84 \ 20,0 cm)
single element	0.375 \ 7.875 in. (0.953 \ 20.0 cm)
P darization	Horizontal
Azzbuth Bearwidth	
composue	22°
single element	134 ^(*)
Elevation Beamwidth	12 [°]
Receiver	
Minimum Detectable Signal	-95 dBm
Noise Figure	11 dB
RF Bandwidth	4 GHz
IF Bandwidth	16 MHz
Full Word Dynamic Range (8-bit manti	ssa with 3-bit base 2 exponent)
Theoretical (no RF noise)	90 dB
Experimental	≈ 66 dB

Table 1. NFMRAD/AMTI System Characteristics Summary (Cont.)

A/D Conversion

Number of Range Cells 16

Sampling Rate 4 MHz (266 ns per range cell)

Interval per Range Cell 131 ft (40 m) 8-bit Conversion Rate 10 MHz

RF Noise Level as a Function of Receiver Sensitivity

IF Attenuation	Number of Ma Consumed by	
dB	Average	
	Value	Case
0	4	5
6	3	4
12	2	3
18	1	2
24	0	1
30	0	0
36	0	0
49	Λ	0

Switching noise on the A/D boards consumes one mantissa bit, independent of IF attenuation. A combination of RF and switching noise yields the following:

IF Attenuation	Number of Mantissa Bits Consumed by RF and Switching Noise		
$\mathrm{d}\mathbf{B}$		Worst	
	Value	Case	
0	4	5	
6	3	4	
12	2	3	
18	1	2	
24	1	1	
30	1	1	
36	1	1	
42	1	1	

Array Processor

6 asyncronous microprocessors

32-bit word

3 memory buses

Performs real-time beam formation and Doppler filtering for NFMRAD and AMTI processing $\,$

1 Doppler filter implemented

3 dB Doppler filter passband -238, 6 Hz to -401, 5 Hz (diverging case)

Angular sector of clutter in 105.1° to 116° (diverging case)

Doppler filter passband

Table 1. NFMRAD/AMTI System Characteristics Summary (Cont.)

Minicomputer

Memory

32 K interleaved core

4 K bipolar

Cycle Time

100 ns

Word Length

16 bits

Performs real-time detection processing, data storage and

display functions

Recorded Data Display (Table 12)

Filtered NFMRAD and AMTI data recorded voltage amplitude or detection output as a

function of range cell

2.3 Theoretical Investigations Relative to the NFMRAD Experiment

2.3.1 THE NFMRAD EXPERIMENT

The following parameters and specifications are pertinent to the NFMRAD truck experiment:

Radar Van and Target Parameters

Truck velocity = 32.7 mph (14.6 m/s)

Target velocity = 34.4 mph (15.4 m/s)

Target velocity relative to truck = 11.2 mph diverging (5.02 m/s)

Target bearing relative to truck = 90° (constantly broadside)

Target Doppler Frequency = -315 Hz (diverging case)

Angle between truck track and target track = 190

Angle at which clutter return has target Doppler frequency = 110.12° (diverging case)

The layout of the tracks for the radar van and the target is shown in Figure 6. This is a constant-bearing diverging case and ideally results in constant relative velocity and therefore constant target Doppler. However, experimental errors in truck and target velocities and in relative bearing will be present. As the experiments are performed using just one Doppler filter, it is necessary that the filter passband be wide enough to accommodate the anticipated experimental errors.

A constant-bearing converging experiment is generated by reversing the directions of the target velocity and truck velocity. For this case, the target Doppler frequency changes sign to +315 Hz, and the Doppler filter is designed with its passband centered on this frequency.

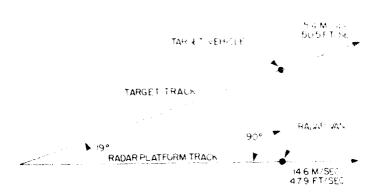


Figure 6. Radar Van and Target Tracks for NEMRAD Experiment (Diverging Case)

2.3.2 OPTIMIZATION OF THE PILITERS

In order to determine the proper FTR filter residens for opticion system in informance, various widths and magnitudes of passband and stopbands were considered. For each case aded filter (that is, bandpass filter combined with a bands of filter), an optimum receive pattern was determined and a figure of ment obtained for the performance of the systems. For each system, the figure of ment obtained for the performance of the received power from the target to the fotal is converted to the ratio of the received power from the target to the fotal is converted elutter power. In order to compare systems using inferent transmittening to decrease patterns, as well as different filters, the figure of them two an employed to the obtained from a system transmitting and receiving as a target of the first of the obtained filtering. Thus the figure of the takes in a cosmost the convergence of the convergence of any system over that of the elementary rate once system.

The investigation showed that two fifter elements is the time segment of the following on the figure of monit. One is the width of the riber massband, which will be a test sharpness of collect from bandpass to bendst a. As could be expected, the reserve the filter passband the higher the ingular to come, in a willy processive NULLED asystem, reducing the willth of the individual filter massband increases the time of filters required, and this increases cost and any dexity. Further an expect continue there are other considerations. There is no enough two with the reserve of the filter must be large enough more than one as a fed site, so the most farm the filter must be large enough to accommodate the news in target Decolor fuelt continue case chosen for the truck experiment, the relative target velocity is small, and this results in the clutter angular sector associated with the passband of the Doboler filter being close to the angular sector associated with the antenna mainbeaus. If

the cascaded filter does not have a rapid rolloff in the region between these sectors, the figure of merit will be reduced.

Generally, it was found that discriminations greater than about 40 dB for bandstop of bandpass (1900) and improve the figure of merit. This is due in part to the noise produced on reception by the analog-to-digital converter because of truncation. Analysis of the experimental system to be used in the truck predicts that if theoretical nulls of the order of -55 dB were desired in the optimum receive pattern, truncation in the AD converters would result in nulls only of magnitude -48 to -50 dB. The effect of the truncation is therefore equivalent to a noise source in the receiver system at a level 48 to 50 dB below the peak of the optimum (NFMRAD) pattern.

Taking into account the effect of the A-D truncation noise on the optimum receive pattern, the figures of merit for many different cascaded pairs of FIR filters were computed and compared. Bandwidth considerations, based primarily on expected errors in relative velocity in the truck experiment, indicated that case eading a BP33-2-1 bandpass filter with a BS33-14-1 bandstop filter was the best compromise solution (that is, high figure of merit together with adequate bandwidth).

2.3.3 COMPARISON WITH OTHER SYSTEMS

NFMRAD was compared with systems using Chebyshev and uniform array transmit and receive patterns with and without filters. In all cases the antenna apertures used were equivalent to those as specified for the truck experiment. Comparisons were made for targets located broadside to the truck and moving at various radial velocities in the interval -11.2 mph to -32.7 mph (-5.02 m/s). Figure 7 shows the improvement of NFMRAD over systems using uniform array transmit and receive patterns with and without filters. The caseaded FIR filters used for this analysis were composed of a BP33-3-2 bandpass filter and a BS33-14-1 bandstop filter. Figure 8 shows the improvement of NFMRAD over systems using -40 dB Chebyshev patterns for both transmit and receive with and without filters. The filters used here were a BP33-2-1 bandpass and a BS33-13-1 bandstop.

Without filters, the performance of both the uniform array system and the Chebyshev array system are far inferior to NFMRAD. Even with filters, the uniform array system performance is 35 dB or more below NFMRAD over most of the clutter frequency range that was considered. The Chebyshev array system performance with filters is at least 8 dB below NFMRAD except for clutter frequencies in a range corresponding to low radial velocities relative to the ground where NFMRAD improvement was 20 to 35 dB. For a given aperture size, the composite Chebyshev pattern (the product of the transmit and receive patterns) has a broader mainlobe than the composite NFMRAD pattern, and for targets with

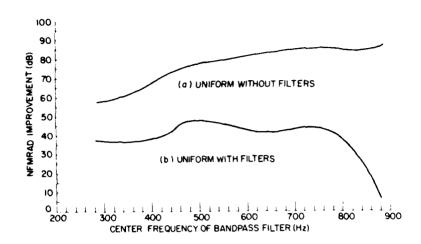


Figure 7. Improvement of NFMRAD System Over a System Using Uniform Patterns on Both Transmit and Receive (a) Without Filters, (b) With Filters. Filters were BP-33-3-2 and BS-33-14-1

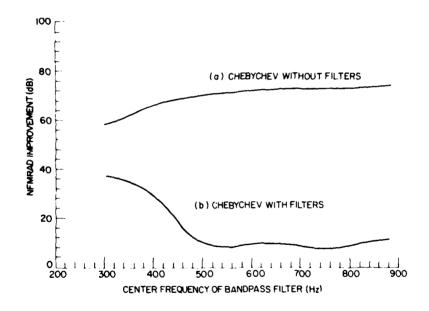


Figure 8. Improvement of NFMRAD System Over a System Using Chebyshev Array Patterns on Both Transmit and Receive (a) Without Filters, (b) With Filters. Filters were BP-33-2-1 and BS-33-13-1

radial velocities close to the radial velocity of the local ground latter of some broadening deteriorates the performance consciently. For the Chebydry make system with filters, the performance improves as the difference between the cold is velocity of the target and that of the local ground clutter decreases.

3. NEMRAD RE HARDWARE

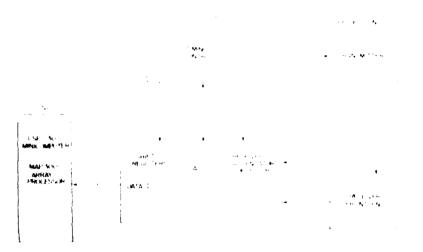
NEMRAD is a "proof-of-concept" system, and the objective was the despectal construction of a radar capable of performing the postulated tunits as will the greatest economy. This economy involved simplicity in design at maintain in our tary cost in the addressing of the program objective. A unique and sephisticated experimental tool is the product of this "economic" consideration.

NFMRAD was created in order to experimentally investigate and evaluate the use of antenna pattern null filtering to reduce Doppler clutter. As a result, NFMRAD performance capabilities are limited in extent. NFMRAD, as a prost-of-concept design, is not a fully operational side-looking, stand-off, a rhoune moving target indicator radar design based on the antenna null-filtering concept.

The principle performance characteristics of NFMRAD are highlighted here. As a side-looking Airborne Moving Target Indicator (AMTI) radar. NFMRAD does not possess the performance capability of angular scanning (azimuth or elevation). NFMRAD responds to targets in its main beam and is capable of nulling Doupler clutter received through one antenna sidelobe. This is possible since the NFMRAD possesses a multichannel receiver design. However, the antenna null is developed through digital signal processing of information from the eight receive channels. The NFMRAD also performs conventional Dopoler filter processing. However, here again only one Doppler filter of experimental interest is implemented, and, as with the antenna null formation, it is created through the digital processing of the eight-channel receiver information. These performance capabilities and limitations are a direct result of the intended purpose of the NFMRAD hardware design.

The NFMRAD may be subdivided into three major functional subsystems: the RF system, containing the transmitter and the receiver mixing preamplification stage; the Signal Conditioning section, consisting of the intermediate frequency amplifiers, the gain control, detectors, sample and hold circuits, analog-te-digital converters, output, timing, and control logic; and the Signal Processor, consisting of a high-speed array processor slaved to a host CSP-30 minicomputer. Figure 9 illustrates this simple functional subdivision of NFMRAD.

Discussion of the NEMRAD RF hardware design and operation will encompass the RF section and portions of the Signal Conditioning section critical to the proper functioning of the NEMRAD RF design. Remaining topics dealing with the digital hardware will be developed in Section 4.

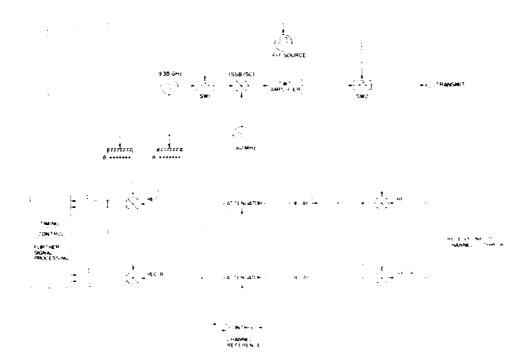


Laurence MARRAD System Among the Albertage of

Althous a pulse Depole of any Unit uses one of very setting of the constitution of the transmitter some estate configuration of NEVRAD and of the constitutions are at signal consents because the received because offers the CEAR of the constitution of earlier and subscriptly selecting the could the CEAR of the constitution of the constitution of the conserved signal of the fault that the GHE transmitters are to develop a on-AHP H signal above, a phase due to turn interest of the constitution of the conserved signal vector. In this restrict, it is not at the transmitted and phase of the target signal vector, in this restrict, it is not constituted to the conservation of the conservation of the conservation of change of the phase of the target signal vector is preserve for rich essenting.

This receives configuration, ted by an eight-element to eight on all location channels. This receives configuration, ted by an eight-element to eight-element on antenna, allows null placement in the figural processing of the eight-element receives intermation. Each receive element evid vs. an in attack government is system, referenced to channel 1. This gain control approach was implemented provide the receiver with a broad linear dynamic control.

Referring to Figure 10, the pulsed vaveters a confidation of the scalar desired through the action of macrovave pin dode sautoles. These because or state to before the transmitter mixing stage and after the transmitter to a linear relationary matter that the samplifier stage (IWTA). The pin dode sautole trigger miles are staged and synchronized to produce a periodic wavetorm of the festived miles of the first extransmitter antenna as color ated with the receiver have an axy and scalar, staged high-gain, sectorial horn. Figure 10 as a simplified schematic of the transmitter design. Note that delays are provided pair to the outer at a contrast context of the color.



and the second of the second o

The second of the second of the eight of the

3.6 Louismittee

The second of the control o

en de la composition La composition de la La composition de la Frequency Stability: 10,0025 percent

Temperature Range: 32 to 140°F (0 to 60°C)

Harmonies: -60 dBc (mminum)

Sub-Harmonics: -52 dBc (-45 dBc minimum)

Spurious: +60 dBc minimum Output Impedance: 50 Ω

The secondary source (a 50-MHz crystal-controlled oscillator (Greenway, model number Y-313B 50)) specifications are as follows:

Frequency Stability: ±0,000 percent

Temperature Range: 32 to 140°F (0 to 60°C)

Output Power: 800 nW (mammum)

Harmonies and Sub-Harmonies: -20 dBc (minumum)

Cutout Impedance: 30 92

Power to rethest, 30-GHz source passes through a soull directional couplest Cardy so delimination 4015C-65. Power to be the soulle of the directional couplest is no visited to the coxer are application stage of the receiver. This stand to wer, it is the queries of the content of the CMHz serves as the LOCar the cight receiver shounds. The amount of the coxiderations as divided, and one-half the reverse directed the nation eight was power by some title eight research detects in stages. The first path of the content of the sould be sourced as the content of the content.

JAPAN GENERALISEN SELECARRILER

The second of the first tenting to the confidence of the confidence of the confidence of the second of the second

en de la companya de la co The mixing products of the 9.35 GHz and 60 MHz are free to propagate from both waveguide ports of this device. The 60-MHz residual is attenuated by the cutoff characteristics of the waveguide. However, the sum and difference signals, as well as the original 5.35 GHz, are within the passband of the waveguide.

Power consisting of reflected 9.35-GHz signal and the various mixing product propagate down the waveguide in the direction of the -6 dB directional coupler out-put port. The directivity of this directional coupler is specified at 15 dB. This enables the coupling of mixing product power into the LO signal path to the receiver. This squrious signal power consists of the sum, difference, original 9.35 GHz, and the intermodulation products. The presence of these mixing products in the LO path to the receiver mixing preamplification stages would desensitize the receiver by raising the mixing preamplification noise floor; that is, effectively "jamming" the receiver front end. In order to avoid this difficulty, an isolator and the first pin diode modulator have been placed between the -6 dB directional coupler and the orthomode mixer. An understanding of the mechanism involved may be obtained through examination of two distinct cases: diode switch "off" condition and diode switch "off" condition.

First consider the diode switch "off" condition. During this condition the pin diode switch provides -45 dB of nondirectional attenuation. This effectively attenuates the 9.35 GHz power (a maximum of 750 mW to a level of -16 dBm) available at the orthomode mixer to a level below that required to effect mixing (2-mW manimum required signal power). Hence, these mixing products cannot be generated by the "turn on" of the mixer by the 9.35-GHz signal power during this condition.

Given the possibility of sufficient signal current available for mixer turnon from the 50-MH; source, sufficient reverse signal attenuation exists to prevent the over desensitivation. The mixed signal would be at a level below the maximum to see autent to easured in this case at 20 mW). But for sake of argument, choose the level of 20 mW. This signal would traverse -45 dB of attenuation in the diode set the -67 dH; of directional attenuation in an isolator preceding the switch, a country of -1 odB of his clivity available in the -6 dB directional coupler, as the 64 to not each to a power division (-9 dB channel). This would give the 125 dB to red each some fact of the diode switch, then a maximum the 10 dB of the country is a present at the first mixing stage of each receiver that the 11 decrease of the 1 of the receiver.

The result of the same is in the the covered each it of the assent autenna) during first the second of the each in assessment in the encern. This is true since little or the second of the new control of the each actually exists at the control of the each of

Next consider the circumstances during the discussive of our countries. During this period is system operation, range turing his tot vet starts 4, 15. We received signals are of nonterest at this time. Hence, it care the distinct that the avoid receiver from end desensitization during to inscriss; profise a mantish. It is important to note here that the 457 dH is dar in discipations any reflectors of morder to protect the prices 9.35-GHz source from a terrial durance. It say event, the power in the reflection path passes through a name up at 32 dH. It reduces any feedback signal to a maximum of 462 dH, as signal in terms the content of the first mixing stage of each receiver channel. Given the absence of these trivers, this Le signal level is insufficient to the tist had maximum.

The bussed 9.35-GHz CW signal is mixed with the b0-wHz CW arrive to consum, difference, and 9.35-GHz bulsed signals. A second state of its latter (-24 dB) prevents any power reflected from the upper suddence in action of the interfecting back to the enther of conxecutant revolution, source as their consistency than The five-pole butterwe the response waveguage their selects the mass of the band pelsed signal at 44 GHz). The b0-MHz separate to fithe proving the period of the filter passband characteristic (0.4). Who PW centered at 0.41 GHz, which could be bandwidth of 39.5 MHz) severely attendates all their frequency was a factor of the mixer output.

1.1.3 TRANSMIT PULSE FORMATION

The desired transmit pulse characteristics are a more itim up to a transmit value of the number of the series of the series of the order of the orde

The first modulates the primary course signed thus generating the discussion of the provides fit feedback suppression during the internal of a provide second switch serves two functions as well. It backs the relatively of the discussion power generated by the TWTA during the interpulse pointed, and also resiming the RF pulse.

The first diode switch is a Howlett-Packard wodel 33142A, and the resulting model 33222A. The model 33142A possesses SMA type RT ports and SMC water port, while the model 33222A possesses N-type RT ports with a BNC composition. Both switches are of compact physical design.

The diple switch is an absorption type and employs RF diples somning the RF path. A large negative going pulse applied to the switch control port is the commod signal for switch turnon. In the absence of control signal bias, the shupting in desprovide a low-impedance path to ground. During this condition (shunting diples biased on by the RF signal) no more than -4 , dB of incident RF power is available at the RF output port. In this state the switch is in the "off" condition. With the

negative going control pulse applied, the shunting diodes are bassed off, and in a dent RF power is available at the RF arput part for the duration of the central pulse. Insertion has at the switch during the "on" condition is specified to be less than 1 dB. Figure 11 chartrates the basic electrical structure of the pin diode switch.

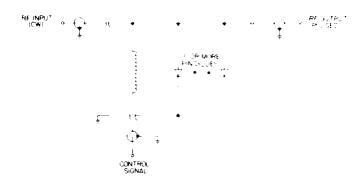


Figure 11. Typical Microwave PIN Drode Switch (Adapted from Hewlett-Packard Application Note, Fast Microwave Switch-SPST Series 33140 and 33640)

An RF pulse produced from the action of Model 33222A will possess rise and fall times no greater than 10 ns. Model 33142A will typically produce an RF pulse with a rise time of 5 ns and a fall time of 7 ns. Switch turn "on" or "off" is a function of control voltage threshold. Actual turn "on" or "off" times are a function of the switching characteristics of the diodes shunting the RF path. Once the negative going control pulse amplitude in fact falls below or rises above the negative control voltage threshold, the switch will turn on or off, according to the characteristic switching time of the switch diodes. Switch model 33142A is capable of absorbing 2 W of CW power in the off mode. Switch model 33222A, at the output of the TWTA, is capable of absorbing 2 W of CW power and sustaining a 75 W peak power at a maximum pulse width of one ms and 0,001 duty cycle.

Both switches are driven by a TTL compatible switch driver (device number DH0035G). The main band trigger is provided to integrated logic circuitry (TTL) which drives the switch driver of the first microwave diode switch. From the same main bang trigger source, the main bang trigger to the second diode switch is first supplied to an SN74123 (TTL retriggerable menostable multivibration). This device delays and reshapes the main bang trigger. The output of the SN74123 TTL device is also supplied to integrated logic circuitry (TTL) which drives the switch driver of the second racrowave purified switch.

Referring to Figure 12, the first dode switch precedes the orthomode mixer and the second diode switch follows the TWT amplifier. As a result, a finite and significant delay exists in the propagation of the RF pulse from the first diode switch to the second diode switch. To compensate for this propagation delay, the firing of the second switch driver is delayed through the action of the SN74123 TTL device. The rising edge of the main bang trigger latches the first stage of the SN74123 on. External RC timing circuitry is adjusted to yield a first-stage intime of 300 ns, equal to the propagation delay from first to the second switch. At the down clock of the first SN74123 stage, the second stage is clocked on for the predetermined period of 266 ns. The output of this stage is used to drive the second microwave pin diode switch driver. The microwave switch is turned on at precisely the time the RF pulse generated by the first switch has risen to its maximum amplitude, and remains on for 266 ns. This action permits opening of the second switch when a stable RF pulse is incident at its inour port and reshapes the wide RF pulse to desired pulse width.

The RF pulse generated by the first diode switch is wider than that desired for transmission. This is a result of the filtering action of the waveguide filter that eliminates the higher frequency components of the RF pulse. To combat this problem, the main bang trigger, as it originates from the Signal Processing Sectioncard nest board number 1 (System Timing I), is 320 ns wide. As a result, the RF pulse generated by the first microwave diode switch is 320 ns wide with rise and fall times less than 10 ns. The RF signal bandwidth is theoretically 400 MHz wide at this stage of transmission pulse formation. However, the waveguide filter bandpass is only 9.41 MHz wide. Consequently, the RF pulse incident at the input to the TWT amplifier is 320 ns wide, with rise and fall times of approximately 100 ns each. The 320 ns wide main bang trigger is delayed 100 ns by the 74123 devices first stage, which in turn fires the 74123 device second stage for the desired pulse period of 266 ns. The firing of the second stage of this TTL device enables the capturing of the degraded RF pulse (when it is present at the second switch), and reshapes the RF pulse to the desired transmit pulse characteristics. The RF pulse, incident at the transmit antenna input, has a slightly rounded reak and is 266 ns wide, with a rise time of approximately 6 ns and fall time of approximately 8 ns.

This reshaping process theoretically produces a final transmit pulse with leading and trailing edge "porches." However, these perches are of duration less than 30 ns and are no greater than 0.6 mW in intensity. These perches were not detectable during system bench testing using a linear detector of 30 mV/MW sensitivity. Figure 12 below illustrates the pulse firing sequence discussed above.

The rise and fall time of the switch driver output pulse is between 4 to 6 ns. This switching time is characteristic of the switch driver and independent of input pulse rise and fall time. In addition, the negative amplitude of the control pulse is

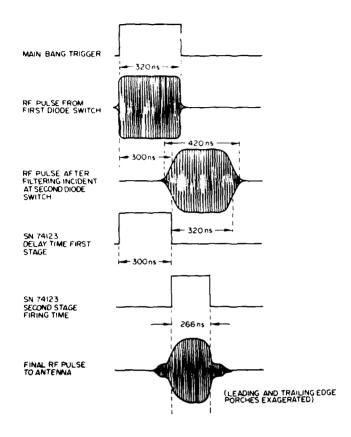


Figure 12. Timing Diagram: Transmit Pulse Formation

far larger than the voltage necessary for diode switch turnon. This insures precise and reliable operation of the diode switches. Figure 13 is a schematic of the microwave diode switch firing circuitry. The quad-Nand gate and inverter (TTI, devices) driving the switch driver add minor delays in the firing of the switch drivers. These minor delays have been compensated for in the design of the firing circuitry.

The second switch also attenuates noise generated by the TWTA during the interpulse period. The characteristics of the Hughes X1277H TWTA are such that 1 mW of white noise is continuously generated across its bandwidth, in the absence of input signal. With the second switch turned off during the interpulse period, white noise is reduced to a level of at least -45 dBm. This, combined with the -65 dB coupling figure from transmit to receive antennas, prevents subsequent jamming of the receiver during the interpulse period.

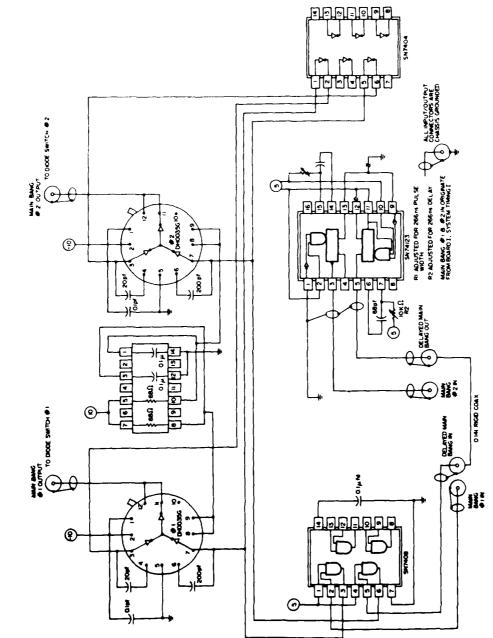


Figure 13. Diode Switch Firing Circuitry (Adapted From Hewlett-Packard Application Note, Fast Microwave Switch-SPST Series 33140 and 33640)

5.1.4 TRAVELING WAVE TUBE AMPLIFICATION

The filtered pulsed 6.41-GHZ signal must be amplified before transmission. Insertion losses through components between the orthonode mixer and the amplification stage yield a final peak signal power of 5 mW maximum incident at the amplifier input. The maximum safe permissible driving power for this TWT amplifier (Hughes, model X1277II) is 0.6 mW. This may be achieved by adjusting the variable attenuator (adjustment located on the transmitter rack front panel) to a setting of -9.2 dB. With 0.6 mW of drive power, the TWT amplifier output power is 22.5 W.

Continuously variable transmitter power is available in two power ranges. In the low range (0-5 mW), the TWTA is switched out of the circuit by two manual waveguide switches, one preceding and one following the TWTA. During low-range operation, the variable attenuator, preceding the TWTA, affords continuous adjustment of transmit power passing through the parallel waveguide transmission path. With the TWTA into the circuit, the same variable attenuator is used to continuously vary transmit output power from 1 mW to 22.5 W through variation of TWTA input power. Figure 14 is the measured gain characteristic of this particular TWTA. In order to protect the TWTA from reflected power, a -16 dB isolator has been installed between the amplifier output and the waveguide switch following the amplifier. This protects the TWTA during manual waveguide switch operation and during the second microwave pin diode switch off time.

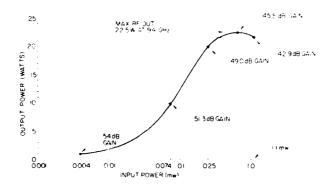


Figure 14. TWTA Gain Characteristic

3.1.5 TRANSMIT ANTENNA

The transmit radiator is a simple sectorial horn situated directly above the receive horn array and polarized in the horizontal direction (H-plane vertical). The horn aperture has an E-plane dimension of 3.3 in. (8.3 cm) and an H-plane

dimension of 8.3 in. (21.2 cm). The H-plane taper length is 18.7 in. (47.5 cm), with an E-plane taper length of 19.5 in. (49.5 cm). These dimensions yield a theoretical gain of approximately 20.3 dB. Figure 15 illustrates the transmit horn.

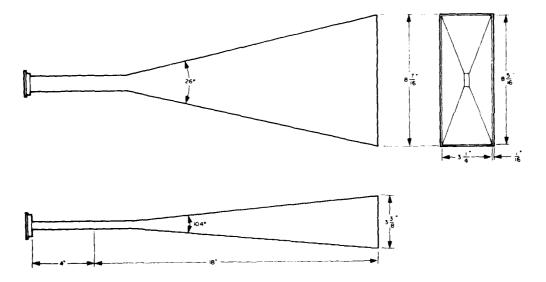


Figure 15. Transmitter Horn

Given the above horn aperture dimensions and uniform aperture excitation in the E-plane and cosine aperture excitation in the H-plane (TE₀₁ mode excitation of waveguide feeding a flared horn), the theoretical azimuth 3-dB beamwidth is approximately 19.3°, and the theoretical elevation 3-dB beamwidth is 10.3°. The theoretical azimuth mainlobe beamwidth is approximately 44°, and the theoretical elevation main lobe beamwidth is approximately 25.8°. It is the azimuth directivity pattern which is of interest here, although the elevation directivity pattern determines the multipath characteristics of the system. Figure 16 compares the theoretical and experimental transmit directivity patterns, while Figure 17 illustrates the experimental elevation directivity pattern.

It is important to note that coupling between the transmit horn aperture and the aperture of any given receive antenna element aperture (located directly below the transmit horn) is approximately -65 dB. This coupling of transmitted power into the receive antenna element apertures results in the characteristic main band video at the start of range timing.

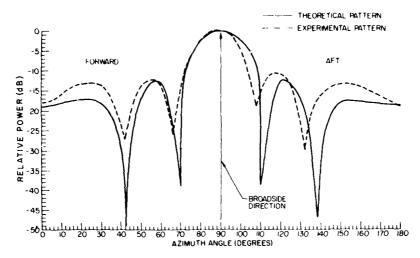


Figure 16. Theoretical and Experimental Transmit Horn Azimuth Power Patterns

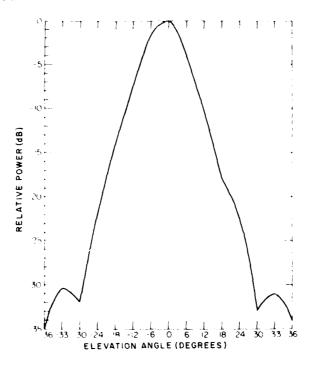


Figure 17. Experimental Transmit Horn Elevation Power Pattern

3.1.3 DIAGNOSTIC FACILITIES

Two continuously variable output power ranges may be selected; 0-5 mW, cr. 1 mW to 22.5 W. in addition, facilities have been provided for the synthesis of a Doppler offset frequency. The imjection of this synthetic Doppler signal into the transmitter mixing process enables efficient diagnostic testing of the receiver hardware and software. The Doppler frequency is that of a target moving away from the radar platform at a speed of approximately 11.5 mph (5.14 m/s) (or Doppler frequency of -325 ftz). The signal is created by the single sideband suppressed carrier mixing of 325 Hz with 60 MHz prior to the orthomode mixing of 50 MHz with 9.35 GHz. The 50 MHz and 325 Hz undergo phase cancellation mixing and the subsequent selection of the first lower sideband of this single sideband mixing process. Phase cancellation mixing is the only effective single sideband suppressed carrier mixing technique available. The frequency separation of the first upper and lower sidebands from the carrier (325 Hz) renders the design of the necessary sideband filter very difficult (if not impossible) for this application.

Figure 18 illustrates the Doppler target simulator. Note that the schematic illustrates the selection of the first upper sideband. Selection of the first lower sideband is accomplished through the interchange of the GL ports of the Hewlett-Packard Balanced mixers shown in the offset signal generator section of the Doppler generator schematic. A simple Wein Bridge audio oscillator and amplifier comprise the 325-Hz simulated Doppler signal source. The power supplied to the orthomode mixer is the same (19.3 dBm) whether it is a pure 60-MHz sinusoid or a sinusoidal 60-MHz plus Doppler sinusoid; thus, the signal level at the receiver is invariant to the selection of either mode.

Selection of the injected Doppler is accomplished by a switch provided on the front panel of the RF assembly (Transmitter Receiver Rack). With the radar platform stationary, the operator may select the injection of Doppler into the transmitter signal; thus, a Doppler target moving at the velocity of interest (-11,5 mph, -5.14 m/s) is synthesized. The signal may be directed at a convenient stationary radar target for operational check of the receiver hardware and receiver operating software, rather than attempting the simulation of this Doppler target through appropriate motion of either the radar platform and or radar target. The operation of the receiver, with respect to range, may be checked through the appropriate selection of either the low- or high-power ranges of the transmitter. This may be done with or without the synthesized Doppler target and the use of an appropriate stationary radar target.

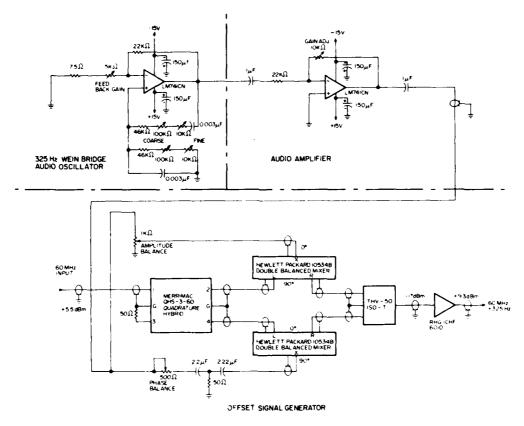


Figure 18. Doppler Target Simulator

3.1.7 SUMMARY OF TRANSMITTER SPECIFICATIONS

a. Frequency Sources

1. Primary Frequency Source (crystal controlled)

Frequency: 9.35 GHz ± 0.0025 percent

Power: 250 mW min to 1 W max, (typically 350 mW)

Harmonics: -45 dBc (min), (typically -65 dBc)

Spurious: -60 dBc (min)
Supply: +28 V dc at 1A
Unit is convection cooled

2. Secondary Frequency Source (crystal controlled)

Frequency: 60 MHz ± 0,005 percent

Power: 800 mW (min) (typically 950 mW)

Harmonics: -20 dBe (min)

Supply: (28 V do : * persent Regulation

Unit is convection cooled

3. Offset Doppler Test Source

Wein Bridge Audio Oscillator

Frequency: 325 Hz, less than 1 percent distortion

Amplitude: typically 5, 8 V peak to peak

Supply: ±15 V de

- Pulse Characteristics (Pulse Generation, Tff. Controlled)
 - Pulse Generated by First Microwave PIN Diode Switch

Frequency: 9.35 GHz

Prf: 1531 Hz

Pulse Width: 320 ns Pulse Rise Time: 5 ns

Pulse Fall Time: 7 ns

Pulse Characteristics after Filtering

Frequency: 9.41 GHz

Prf 1831 Hz

Pulse Width: 320 ns Pulse Rise Time: 100 ns Pulse Fall Time: 100 ns

Pulse Characteristics after Amplification and Action of Second

Microwave PIN Diode Switch

Frequency: 9,41 GHz

Prf: 1831 Hz

Pulse Width: 266 ns Pulse Rise Time: 6 ns Pulse Fall Time: 8 ns

Leading and Trailing edge porches no greater than 30 ns in duration and at least -36 dB below pulse peak power.

- Transmitter Emission Characteristics
 - 1. Signal (Pulsed CW)

Frequency: 9.41 GHz

Prf: 1831 Hz

Pulse Width: 266 ns Pulse Rise Time: 6 ns

Pulse Fall Time: 8 ns

Occupied Bandwidth: 60 MHz (approx.)

Maximum Peak Power: 22.5 W

Duty Cycle: 0.04 percent Spurious: -40 dBc minimum

- The state of the Arthurst
 - 4.00 910 110
 - 116 3 3 3 4 10.
 - $-A \sim arr + 1 < c$
 - This carry to, at
- has Some Power Supplied to Reserve to and a true Processor.
 - 1. Some Place Sumfled to Reserver Viser Present here they
 - Trequency: 9, as GH
 - Powers as IB to buy to SelGP as uncertained
 - 2. Source Power Supplied is Reterence to Land Q Mixers
 - Frequency: 60 MHz
 - Power: #3 dR below 50 MHz source output
- e. Synthesized Doppler Lorget
 - Lower sideband or phasized for significant transfer swing at -11, erob. (**, 14 m/s) relative to radac plat* m
 - Suppression of any anted signal components below this following sideford: Upper Sidebund: -20, 8 dB
 - Carrier: -20 dB
- f. Schematic of NEMRAD Transporter Subsyster (Figure 19)

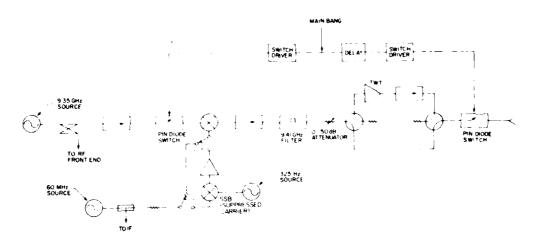


Figure 19. NFMRAD Transmitter Subsystem

3.2 Receives

PROPERTY OF STRAIN

The second of th

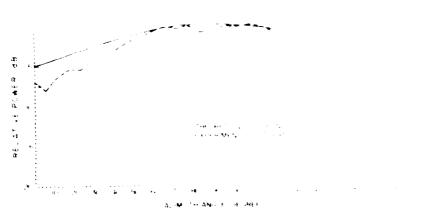


Figure 20. Theoretical and fixture contains a contained by Element Durectivity Pattern

Section 1997 (1997) in the Control of the Section of the Section 1997 (1997) and the Section 1997 (1997).

(a) the transfer to describe and are attracted to a sure for the control of the estimation of the development is as follows:



to the server of the voltage of Single Reserver

$$1 \leq t \text{ Notices} \qquad t \leq \underline{t} + \operatorname{P}(\underline{t+\underline{t}}) \text{ At } \mathbf{G}(t) \text{ or } \mathbf{H}(\mathbf{B}_t) = 0$$

Assuming uniform aperture excitation, the receive array produces an azimuth 3-dB beamwidth of approximately 16° . The calculated eight-element azimuth directivity pattern and the experimental pattern are illustrated in Figure 22. The eight-element directivity pattern was calculated using the principle of antenna pattern multiplication. The relationship for the single-element pattern was multiplied, point for point, with the equivalent value of a pattern produced by eight equally spaced point source radiators. The normalized relationship or array factor for eight equally spaced point sources is as follows:

$$E = \frac{\sin (n_5 - 2)}{n \sin (c - 2)}$$

where

n no, of elements

$$d_p \cos \theta + \delta$$

δ 0 for uniformly excited point sources,

 θ is measured from the normal to the array face and

$$dr = \frac{2\Pi}{\lambda_{co}} d$$
 $\lambda_{co} = 3.188 cm$

with d=1.27 cm, the element spacing (center to center of the receive elements). Each value of ${}^{\dagger}E^{\dagger}$ achieved for a given θ is multiplied for the same value of ${}^{\dagger}E_{\theta}$ achieved for the single-element pattern to yield ${}^{\dagger}E^{\dagger}$ or the composite amplitude pattern. The ${}^{\dagger}E^{\dagger}$ is squared and the log to base 10 taken for development of the eight-element azimuth directivity (power) pattern. Note that all pattern valculations are normalized and referenced to 0 dB.

The above calculations yield a close approximation to the nature of the eightelement pattern. The correction of phase and amplitude errors, element by element, is reference to the first channel receive element. This calibration is
accomplished in the signal processing of the raw radar information with the target
and radar platform stationary. The calibration is performed on a daily basis,
before and after a field testing sessions (refer to Pre-Initialization ranine, software and field testing sections of this report).

Polarized in the horizontal direction (E-plane parallel to ground), the receive array is situated directly below the transmit horn. As a result of this configuration, energy from the transmit horn couples into each receive element at a level 45 dB below the peak transmit power. This results in the detection of main bang video at the beginning of range timing.

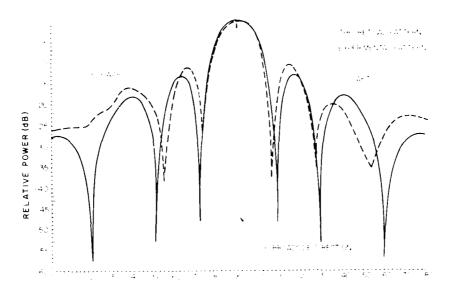
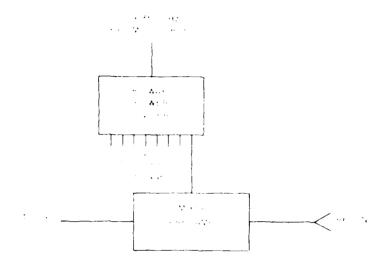


Figure 22. Theoretical and Experimental Azimuth Power Pattern for Receiver Eight-Element Array

3.2.2 RECEIVER FRONT END

Referring to the schematic in Figure 23, the received 9.41-GHz signal is mixed with the 9.35-GHz LO signal to produce a 60-MHz intermediate frequency (IF). The IF signal is then amplified. These two steps are accomplished in one unit (RHG Model MDM 8-12-12A mixer preamplifier). The LO power is derived from the primary (9.35 GHz) transmitter signal source. Power from this primary source is coupled at a level 6 dB below its output power. This coupled power is once again divided, eight ways (through a Merrimax eight way power divider, Model Number PDM 82-10C), and one each of the eight power divider outputs is supplied to the mixing stage of each of the eight receiver mixer preamplifiers. Typically, the LO power available to each of the receiver front end mixers is 11 mW or 10.4 dBm. The mixer preamp requires 3 to 18 dBm of LO power to effect dependable mixing, and an LO injection level is excess of 23 dBm will cause damage to the double balanced mixer. Intermodulation products of signal and LO mixing are suppressed a minimum of 20 dB below that of the 60-MHz IF signal.

The RF bandwidth of the mixer'preamp is 4 GHz, centered at 10 GHz. The H bandwidth is typically 16 MHz, centered at 60 MHz. The noise figure of the mixer'preamp is typically 11 dB. Mixer'preamp RF to FF gain is specified to be 20 dB minimum. With these specifications, the front-end signal sensitivity is



i

Figure 23. Receiver Front End

approximately -95 dBm per channel. This results mean approximately 1.4×10^{-8} W m² minimum incident signal power requirement per receiver channel for signal detection.

7, 2, 3 RECEIVER GAIN CONTROL

With the exception of channel 1, each HT signal passes through a verieble attenuator (0-15 dB, Morchaus Model ARM-D that is used that in the pair the channel. The signal in channel 1 is divided into the paths. One is smoother that log amplifier whose output is ultimately used to automatically charted the rank of all channels to insure linear operation over the complete range of expected input signals. The other forms the input for a linear receive channel that is, channel 1). The variable attenuators in channels 2 through 8 enable balancing of these channels with respect to channel 1. Compensation of the element signals for dissimilar array elements is accomplished in the signal processing. This calibration processing as accomplished daily to establish an antenna pattern measurement baseline, as well as to compensate for changes in receiver component operating characters is ties.

The division of power in channel 1 enables the realization of an unorthodox gain control system. Unlike conventional AGC, the NUMRAD stepped gain control provides a broad but linear dynamic range. This is achieved through a feed-forward control approach. The signal derived from the logarithmic amplifier in channel 1 is amplitude sampled and converted to a 4-bit digital code. The digital amplitude

information is transformed in combinatorial logic into a 3-bit toggling code to control programmable attenuators in each of the eight linear receive channels.

Sufficient time for switching and settling of the attenuators is provided by delaying the H sign at 0.59 μs with a long RG-58 coaxial cable. With a delay of 1.6 ns ift (5.25 ns m), 360 ft (109.7 m) of RG-58 provides the necessary 0.59 μs delay. However, a considerable insertion loss is associated with this 360 ft (109.7 m) coaxial delay line. To compensate for the loss, the signal is preamplified prior to insertion in the delay line.

In addition to toggling the switchable attenuators, the 3-bit switching code is processed and provided to the systems logic interface. This information carries real-time values of received signal level. In this fashion, the order of magnitude of the received signal amplitudes are preserved for later adjustment of the digitized linear channel outputs.

The amplification of the received signal for gain control is accomplished through a logarithmic amplifier. The signal is amplified and the logarithmic value of the signal level is sampled and converted to the 4-bit digital amplitide code. This enables the use of a 4-bit analog-to-digital converter for the first step in generation of the 3-bit attenuator switching commands. The use of linear amplification would require the use of an analog-to-digital converter of much greater than 4 bits of dynamic range. Unfortunately, the required conversion speeds constrain this portion of the design to A/D converters of 8-bits capacity or less. The choice of a 4-bit A/D converter also simplifies the design of conversion logic for the generation of attenuator switching commands as well as the digital amplitude information for later digital processing of the received signals.

Amplifiers following and preceding the switchable attenuators in each channel serve as isolation amplifiers. The attenuators, during switching, are mismatched to the $50-\Omega$ delay lines. In order to isolate reflected spurious power during attenuator switching, a stage of IF amplification has been inserted prior to the attenuators. In addition, a stage of IF amplification following the attenuator isolates the mismatch from the input of the I and Q mixers in each channel. These amplifiers also compensate for component insertion losses throughout the receiver system, as well as provide the required system gain.

Without the influence of this gain control system, the dynamic range of the receiver (per channel basis) would be only 48 dB. This is derived from the 8 bits of A/D conversion capacity for either the Lor Q sides of the eight channels. Each toggling of a bit in the A/D converters corresponds to a doubling in signal level. Hence, 8 bits of conversion multiplied by 6 dB of signal dynamic range per bit yields 48 dB of dynamic range.

The a fors extend this dynamic range by 42 dB for a total linear dynamic range of 90 db. — e attenuation occurs at the rate of 6 dB per step or 6 dB per bit change on the switching command code. This operation is illustrated in Table 2.

Table 2. IF Attenuation as a Lunction of Base 2 Exponent

Total Attenuation (dB)	Steps Set (dB)	Base 2 Exponent (IF attenuated switching code)
()	nohe	000
ti	6	001
12	12	010
18	12 & 6	011
24	24	100
30	24 & 6	101
36	24 & 12	110
42	24 x 12 x 6	111

When the signal power present at the input to the mixer preamps approaches -53 dBm, the operation of the switchab, cattenuators is automatically initiated. At a level of -5 dBm of power incident on the input to the mixer preamps, the receiver will begin to saturate. It is important to note that the 90-dB dynamic range assumes a noise level such that no A D conversion bits are set by noise rather than the signal of interest. The total dynamic range is linear as coposed to logarithmic fencountered with feedback control, AGC). This enables the signal processing that forms the NEMRAD and Doppler filters to be implemented.

3.2.4 IF BANDPASS CHARACTERISTICS AND DETICATION OF MOVING TARGUTS

The three IF amplifiers serve various functions with regard to the receiver gain control system. In addition, their cascaded bandpass characteristics determine the overall IF bandpass characteristic. The composite IF bandpass is contered at 60 MHz with a 3-dB bandpash is with of 8 MHz and a redloff of 40 dB ber decade.

The receiver IF bandwidth has been chosen to approximate the reciproral of the pulse width (that is, $2\times 1/266$ ns ≈ 7.5 MHz), which in turn approximates the performance of a matched filter. This filter characteristic only crudely approximates a matched filter characteristic (that is, the IF bandwidth characteristic passes only those signal components within 4 MHz of the 60-MHz IF). Many of the signal frequency components are attenuated, resulting in pulse spreading. This would cause two consecutive pulses that are very close in time to everlap or become indistinguishable as two unique pulses. This does not pose a problem with respect to range determination, since the range of any given target is a function of the associated target pulse position within a given range bin. This dictates the range

accuracy of the radar. This is opposed to continuous range determination referenced to the leading edge of a received pulse. Hence, he need exists to preserve exact pulse characteristics to enable separation of oulses, since pulse positions in time are of importance only with respect to their occurrence in a given range leng. Consequently, the HF bandpass characteristic is sufficiently broad to preserve the gross nature of a received pulse and yet sufficiently narrow to band limit noise that is, the maximization of SNR is tantamount to the preservation of exact pulse shape and the avoidance of interpulse overlap or interference).

Information carried by the received pulses (per channel) encompasses not only position information (with respect to any given range bin) but return signal instantaneous phase information as well. The division of radar range into range bins, and the timing of returned pulses with respect to these range bins, enables the extraction of target range information. However, phase discrimination of the returned signal, with respect to the transmit signal, is accomplished for the extraction of instantaneous target signal phase information. This later phase information when compiled to form a time history of phase differences for a target of interest, constitutes information concerning the Doppler frequency of the target of interest and hence the target's radial velocity with respect to the NEMRAD platform.

The IF signal undergoes quadrature mixing with the 60-MHz reference from the transmitter. This quadrature mixing yields signal magnitudes proportional to the rectangular components of the signal vector. One product of quadrature - ixing is proportional to the magnitude of the real component of the signal vector, so in the other product is proportional to the magnitude of the imaginary component of same signal vector. In addition, the positive or negative nature of the real imaginary parts of the signal are determined. Hence, the quadratur mixing of the II signal and 60-MHz reference results in information regarding not only the amplitude of the received signal but knowledge of its complex component magnitude. as well. Later processing of the component magnitudes, on a per pulse backs. yields the instantaneous phase difference with respect to the transmitted somal. Compilation of a time history of these phase differences enables measurement of the time rate of change of received signal phase. This is the definition of frequency and is the Doppler frequency of the target. The positiveness or negativeness of complex component magnitude yields information on the positiveness or negativeness of the phase difference. With the time history of positive or negative phase differences, the sign of the target Doppler may be determined with successively increasing negative phase differences indicating a target with relative velocity diverging from the radar, and a time history of successively increasing positive phase differences indicating an approaching target.

The data processing of the target signal vector components not only yields torget Doppler information but also enables the appropriate processing of each channel

output, carrying information on the same target, in order to form the receive antenna pattern null. This is covered in greater detail in Section 5.4.2 of this report.

The IF signal, after the attenuator post amplification stage, is power divided and inserted at the G-X ports of two Hewlett-Packard Double Balanced Mixers (MDL 10534B). A 60-MHz reference signal from the transmitter secondary signal source is power divided through a Merrimac Quadrature Hybrid (Model QHS3-20). This 60-MHz reference signal is typically of 500-mW power level, yielding approximately 50 mW, after eight-way power division, of reference signal power into each of the eight quadrature hybrids. In the quadrature hybrid, the 60-MHz reference signal is power divided. One portion is inserted directly into the R-G port of one of the model 10534B double balanced mixers. The other portion of the 60-MHz reference is phase delayed by 90° and provided to the R-G port of the remaining model 10534B double balanced mixer.

The portion of the IF signal mixed with the unshifted 60-MHz reference produces a signal in phase with the 60-MHz reference and with magnitude proportional to the magnitude of the inphase component of the signal vector. This is designated as the "I" component of the signal vector and is represented as the real component of the signal vector in phase with the reference. The portion of the IF signal mixed with the phase-delayed 60-MHz reference signal produces an output in quadrature with the 60-MHz reference and with magnitude proportional to the quadrature component of the signal vector. This signal is designated as the Q component of the signal vector in quadrature phase relationship with respect to the reference signal. Figure 24 illustrates this I and Q signal relationship with respect to the 60-MHz reference vector.

Referring to Figure 24, a time history of consecutive I and Q values, indicating a change in Φ such that each new Φ value is successively greater than the last and changing in the positive direction, would indicate a positive target Doppler or target motion on a radial path away from the NFMRAD platform. The converse is true for Φ changing in the negative or clockwise direction.

There is conversion loss associated with the mixing process. In addition, the only mixing products of interest are the sum and difference frequencies. The original input mixing frequencies and the intermodulation mixing products are of no interest. To overcome these difficulties, both I and Q sides of each channel possess amplification and filtering of the quadrature detection output. Filtering is accomplished by virtue of the frequency response characteristics of components following the quadrature mixers. The wideband amplifier (Datel Model AM-193R) following the mixers compensates for conversion loss in the mixing process. The gain of this amplifier is set to equal the conversion loss of the power division and

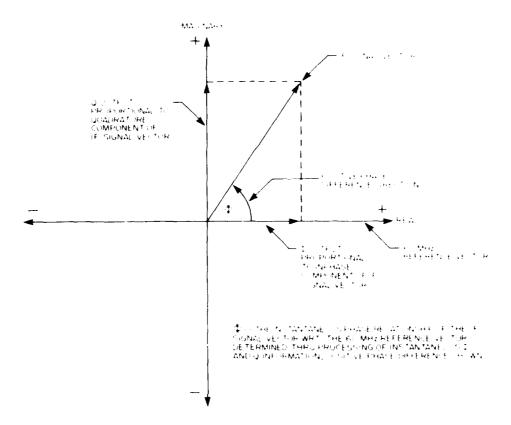


Figure 24. Diagram of I and Q Outputs with Respect to Reference Signal Vector

mixing process (typically 8.1 dB). The 3-dB bandwidth of this device is also established by the chosen gain setting. Gain and bandwidth of anatomistics of this device are coupled. By the selection of the wideband another cannot 8.1 dB, the amplifiers 3-dB bandwidth is set at roughly 10 MHz. This not only compensates for conversion losses but also affords attenuation of all frequency mixing components above 10 MHz.

Further attenuation of unwanted high-frequency reixing products below 10 MHz is accomplished during the amplitude sampling of the amplitude I and Q signals. The response time of the sample and hold device (Datel digh Speed Sar ple and Hold, Model SHM-UID is such that the highest sinusoidal signal frequency that can be accurately quantized is 5 MHz (that is, a maximum sampling rate of 10 VHz [minimum required Nyquist rate to accurately sample a a-MHz sinusoid]). As a result, the 3-dB bandwidth of this device is 5 MHz; thus, additional attenuation of mixing products above 10 MHz is afforded, as well as attenuation of mixing products.

between 5 and 10 MHz. Any remaining products of mixing above \rightarrow MHz are present as noise riding the sampled signal.

The 10-MHz sampling rate is sufficiently fast in order to sample a signal of 2-MHz bandwidth. The signal bandwidth results from a pulse train of roughly 2 KHz prf, with each pulse carrying information of approximately 1-KHz bandwidth (1 KHz equals one-half the unfolded Doppler spectral bandwidth. This bandpass is sufficiently broad to preserve the approximate character of each pulse (1 266 ns - 3.8 MHz). This later characteristic minimizes amplitude error generated from off-peak sampling of individual pulses.

The sample signal for both I and Q channels of each of the eight receive channels is converted to an 8-bit amplitude code on a pulse-to-pulse basis (Datel A D Converter Model VH8-B2). The analog-to-digital converter possesses a maximum conversion rate of 10 MHz (5-MHz conversion bandwidth), again providing sufficient conversion speed for a signal of 2-MHz bandwidth. This digital amplitude order for the eight I and Q vairs is sent in parallel to the Radar Data Buffer for eventual transfer into the array processor.

3.2.5 SUMMARY OF RECEIVER SPECIFICATIONS

- a. Frequency: 9,41 GHz
- b. Antenna
 - 1. Eight sectorial horns flared in the H-plane only, horizontally polarized, forming an eight-element receive array
 - 2. Array 3-dB Beamwidth Elevation (H-plane): 8° Azimuth (E-plane): 16°
 - 3. Gain

Array: 20.0 dB (approx.) Element: 11.1 dB (approx.)

- c. Front End (Per Channel Basis)
 - LO Source: 9.35 GHz supplied from transmatter, typically 11-mW power level
 - 2. RF Bandwidth: 4 GHz (centered at 10 GHz)
 - 3. Maximum RF Signal Power: +23 dBin
 - 4. Minimum Discernable Signal: -9 : dDm
 -). IF Bandwidth: 16 MHz
 - 6. RF to IF Gain: 20 dB
- d. II Section (Per Channel Basis)
 - H. Bandwidth: 8 MHz centered at IF frequency with 40 dB per decicle relloff.
 - 2. H. Frequenex: 50 MHz
 - 3, H. Gaung endB (approx.)

- e. Signal Detector (Per Channel Basis)
 - 1. Quadrature Detector
 - 2. Reference: 50 MHz from transmitter at typical power level of 50 mW
- f. Composite Characteristics (Per Channel Basis)
 - 1. Dynamic Range: 48 dB (without gain control)
 - 2. Dynamic Range With Gain Control: 90 dB (no noise environment)
 - Gain Control: Referenced to channel 1, gain settings in 6-dB increments with fully automatic operation
 - 4. Detected Signal Bandwidth: 2-MHz (approx.)
 - . Doppler Bandwidth: 2 KHz (approx.) centered at 0 Doppler frequency
 - 6. Signal information (on per pulse basis) transferred to System Digital Logic Interface, 1 and Q from each channel (relative amplitude only, order of magnitude information obtained from gain control circuitry)
 - Amplitude Word: 8 bits
 - Order of Magnitude Word: 4 bits (base 2 notation)
 - 7. Timing and Control: Digital (TTL) origin See Section 4 of report for complete discussion
- g. Pattern Null Formation, Doppler Filtering Processing, and Target Detection accomplished in Digital Signal Processing of Digitized 1 and Q Information (See Section 5 of this report)
- h. Schematic of NEMRAD RF Receiver Hardware, Figure 25°

4. RECEIVER DIGITAL HARDWARE

Receiver digital hardware is tasked with the analog-te-digital conversion of f and Q detector outputs. Digitally formatted data is temporarily stored in mantissa and exponent buffers, but ultimately transferred to an array processor in which bear, formation and Doppler filtering takes place. Digital hardware utilized to convert the outputs of the Land Q receiver to a format appropriate for input to an array processor will be discussed in the following sections.

A functional description of receiver digital hardware will be presented to yield insight into the tasks required of each digital system. An input output approach will be used for explanation throughout the digital receiver hardware discussion, since a review of hardware design techniques is beyond the scope of this report.

Reference to Figure 26 shows that the receiver automatic gain control hardware establishes a base 2 exponent which is ultimately transferred to the array processor. Expectally, the logarithm of channel 1 HE signal establishes the signal attenuation

thermold allustrated showing gain control circuitry, channels 2 through 8 signlar outh exception of property of balancing attenuator after mixer/preamp and absence a possess by second log cutters are platfor with 4-bit A. D. conversion circuitry.

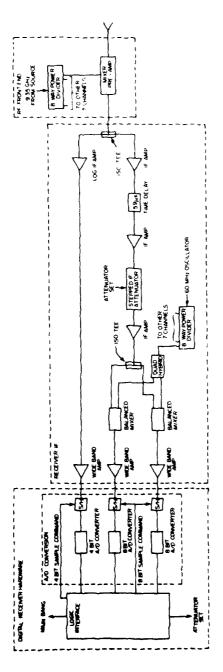


Figure 25. NRMRAD Receiver Subsystem

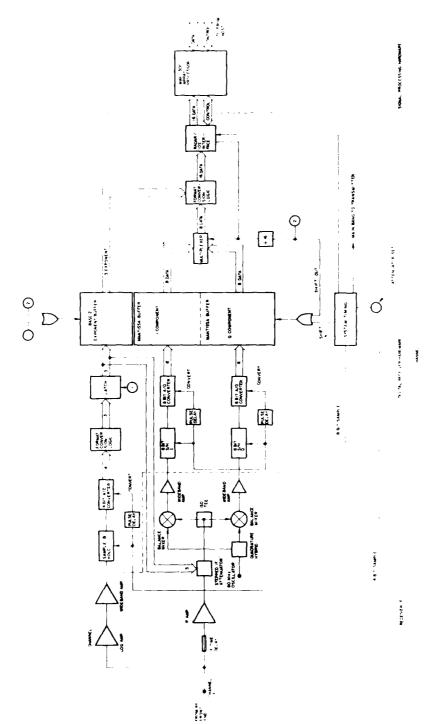


Figure 26. Receiver Realization. The receiver consists of eight I and Q channels. Channel 1 is shown with the log amplifier voltage scaling circuitry. Each receiver channel uses common scaling circuitry; that is, Channel 1 IF is used to determine the base 2 exponent for all eight channels. Seven of the I and Q receiver channels are not shown.

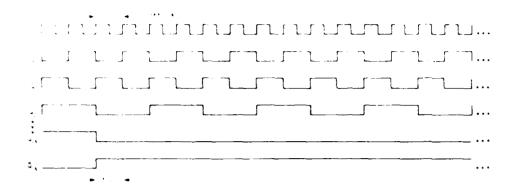
numediately preceding the modestine and transport. The rest If attenuator may be characterized a conversion of the money tred lines which establish attenuation in the Hospins' radii. After the available are 0, 6, 12, ..., 36, 42 dB. Sauta able it would be voltage scaling mechanism installed in the H signal patience of the conhas been derived. Scaling information contained within the trace in the contained control lines serves as the 3-bit base 2 exponent. For example, 2012 the conswitched into the IF signal path in Figure 26, the II voltage would be halve by the halved again; therefore the scaling factor must be $4(2^2)$. If $(kex)se_1 \le 24 \le H$. attenuation, the scaling factor is 2^4 . With three control lines, the maximum is 1/22 exponent obtainable is 7, corresponding to 42 dB IF attenuation; minimum (1 attenuation of 0 dB; corresponding to 2° or a scale factor of unity. Scaled () as Qanalog components are input to wide-band amplifiers seen in Figure 25. Then sampled for analog-to-digital (A D) conversion. Timing of sequential events and as analog sample and pulse transmission are under control of system to the transmission are ware. A D conversion is initiated upon sample and hold output stabilization. The A D converter digital output plus 3-bit base 2 exponent are temporarily steps in mantissa and base 2 exponent buffers. When data buffers are filled, the Manti-Arithmetic Processor (MAP) array processor is informed of data availability viinterface control logic. Under array processor control, the data is suitiple to it from radar temporary storage through data conditioning logic into MAP for any for beam formation and Doppler processing.

The functional hardware discussion in the next section reviews system theory, sample and hold circuits, analog-te-digital conversion, radam data buffers, formal conversion logic, and radam processor interface.

4.1 NEMRAD [AMTI] System Timing

NUMRAD (AMTI) system timing circuitry, shown in Figure 26, sequences beriodic transmitter and receiver functions (for exacuple, pulse transmission and madog receiver signal sampling). The system timing circuitry consists 1 in 10-24H clock oscillator, synchronous bin cy counters, and sense logic for detecting counters outputs.

The transmit pulse command (MAIN BANG), SAMPLII occurrands for the 4- and 8-bit analog-to-digital conventors (ADC), the radar buffer memory shift in (SHH FIN) occurreds, the AFTENIATOR SHF command, and the radar buffer load (RADBUTELID) command are derived from outputs of the binary counter string, VID-MHZ clock output is divided by 2^{13} , producing binary counter outputs Q_1, Q_2, \ldots, Q_{13} and $\overline{Q}_1, \overline{Q}_2, \ldots, \overline{Q}_{13}$, in addition to the original co. 7-ns clock pulse (CP) shows in Figure 27.



Ligare 27. An age Stend Bandy Counter Options

Let to the outside of the norm Quantum spaces to be not a Q_1, Q_2, \ldots, Q_{11} of them time as a district of time to the outside the form of expression of the outside of the expression of the expression of the outside of Q_1, \ldots, Q_{1n} of the outside of the expression of the ex

Event for
$$e=(\Delta t)\sum_{i=1}^{l+1}Q_{i}z^{l+1}=Q_{13}-2^{l+2}(\cos t,7\cos -27\cos s)$$
 .

The includes are derived from and locked to the moder $1 \leftarrow aHe(1)$ is $s_1, t_0 \leftarrow 1$. The $1 \leftarrow aHe(1)$ is sufficient specifically self-additional synchronized with the 60-AdHe self-additional synchroneusly with the radar $1 \leftarrow aHH$ system to $s_1, s_2 \leftarrow 1$. Later. The $1 \leftarrow aHE$ clocks associated primarily with system to $s_2, s_3 \leftarrow 1$ sampling events.

Typic dly, a tuning command sequence would appear similar to Table 7. Turang signals referenced in Table 3 are defined in Table 4.

Table %. Timing Corverand Sequence Sixteen range cells are implemented in hardware; however, only three cells are shown in Table 3

100			•			to the control of the second	
	ંપ પ	47	٠.	${\bf w}_{\rm t}$	Carpo Co. 1	in the contract	E Car Con
1					1 1 1 1 1 1 1 1 1	•	†
1	100		11	1			1
i	0.00	t	1		•		i
					The Albert At Albertain		
· ;	I a second					11 1 1 1 1 1 1 1 1 1 1 1 1 1 1 1 1 1 1	I
	1 6			•			
1							: I
	1				1.1 1.2 1.2 1.6 1.6	$= (2.453443) \text{NeV} \times 4.000 \text{M}_{\odot}$	
	1 1						[144] ND
	. 1				i		
	6 1					of LowLot AND	Late Alice Advanced a
i 1.	, (1	:	+1	ŧ	1990 Block		
1	1 ve 1	1	1	1			1
	$_{i}$ ≈ 1						
	1						11 1 1 1 1 1 Sec. (1)
1	1 1 0					1.1.11.11.11 (N	'
	1 -						
10	1)
	1 1 11						
i	1 0						self-shirle in
1	1 1 0						
	1	1	1	1			
1.24	1 : 1	11	0	0			
1.7	1 1	į,	0	1	1		
1.3	1 1	()	1	11			' -
	1 1		1				
	1 1			D			į .
1.29	1 1						٠.
(1	1 1		į,		1		
	4	•		•		1	l j

Table 4. Syste . Wir ibn Shennle

Command Name			
AIAIN BANG	Line teans dividisc		
4-by SAMPLE	Sample logarithm of hamel I link stand		
8-bit SAMPUH	Synchronicus sample of eight land Q detector outputs		
CONVERT	Begin analog-to-digital conversion		
END OF CONVERT	find a analog-ro-digital conversion.		
ATTINUATOR SUT	Set III signal attenuators		
SITETAN	Shift mantissa into burfer		
SHIFT CUT	Shift montisse and exponent to confirmities place:		

4.2 Ultra High Speed Sample and Hold

Dated ultrashigh speed Saundone i Hi Ti (skill)— rules can be the analog of all Q wideband amplitions upper a drope to large a success of the C-br of can. The Skill module will need is charm to med by account a success of the respective of the skill module will med is charm to med by account a second construction at the suggests of the 20 ps with the sking medality of the success of the 4.1. Accountilly, the samples of the system through them to seem of the second condition of the value and so leading to the first open of the second condition of the sample of the sample of the Skill model of the sample of the Skill model of the sample of the Skill of the strong of the Skill of the Skill of the sample of the Skill of the sample of the Skill of the Skill of the sample of the Skill of the Skill of the sample o

4.3 Ultra High Speed Analog to Digital Converter

Datel ultra-bigh-speed UI series 8-bit ADC's were utilized our objects of the r S&H end of upout to an 8-bit bivert for S&H binary for stars define in Table 1. ADC-UI series are capable of a-bit conversion at 10 MHz. The XIMBAD CYCLU 200, 8 us a represell dictates a minimum conversion wite of approximate by UIII 200, 8 us a represell dictates a minimum conversion wite of approximate by UIII 200, 8 us a represellation S&H output stabilitation, CONVERT are considerations. A UIII and ADC ECONVERT (FCO) pulse is generated under Datel ADC

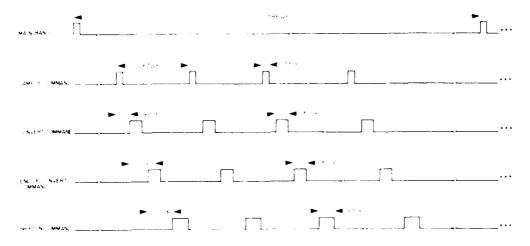


Figure 28. ADC Board Finning Signals

control. The EGC command is a TTH compatible 30 as positive going pulse. Let rising and falling edges are used to latch ADC sutput data in TTH buffer registers until SHIFT IN strobes output data into the Mantissa Buffer described by Section 4.4.1. Eight channels, one I and one Q component per channel, require to 8-bit ADC's. Eight-bit SAMPLE command rising edge initiates synchronous S&H and ADC cycles for the A-D conversion hardware shown in Figure 28.

4.4 Radar Data Buffer

Two 8-bit mantissas (I and Q components), in conjunction with a 3-bit exponent, define the amplitude and phase of one channel range sample. Each channel is divided into 16 range samples separated in space by 131 ft (40 m). The cantissal storage buffer is loaded under control of radar system thang a country discussed in Section 4.1. Following the lapse of a selectable range counter training interval (referenced to t = 0 of Section 4.1), system timing circuitry dictates the region where range samples will be taken. Sixteen sample and hold modules synchronously respond to the master timing 8-bit SAMPLE command. Following crebic sampling, a CONVERT command is issued to 16 A D units. At the conclusion of A D conversion, eight data channels consisting of two 8-bit words per channel are ready for loading into the radar mantissa buffer. One 3-bit positive base 2 exponent is stored per range sample in base 2 exponent storage buffer. Data representing one range sample over eight channels consists of 16 8-bit words stored in inverted offset binary format (defined in Section 4.5.1), plus one positive 3-bit base 2 exponent. Eight digital I components, plus eight digital Q components, are

and a series of the second second

synchronously loaded in parallel into the mantissa buffer under the control of the master tuning circuitry. The base 2 exponent is loaded in parallel prior to the loading of the mantissa buffer (one 3-bit exponent per range bin). The mantissa and exponent buffers are raplemented with TTL shift registers; therefore the first range bin loaded per channel will be the first range bin shifted out when unleaded into the array or wesser.

A diagram, denoting the parallel loading of the radar data buffer is shown in Figure 29. The data load commands, hereafter referred to as SHIFT IN commands are generated by the radar system timing. The buffers are completely filled following the 16th SHIFT IN command.

Data is multiplexed out of the mantissa buffer in a serial string of 256-8-bit words. The unload buffer commands or SHFT OUT commands are under software control of the array processor (MAP-300) Input Output Scroll (IOS) board. The IOS board is the input output interface used to pass radar data to the array processor memory. Data contained in the mantissa buffer is read out by component, channel, and finally range bin. The pecking order of the data multiplexer is depicted in Table 5. The multiplexer strobes 16 words from one range bin and recycles with a SHFT OUT command to advance shift register data forward toward the multiplexer in Figure 29.

Table 5. Mantissa Buffer Data Multiplexer Pecking Order

Position in Serial Word Train	Signal Component Description (8-Bits Wide at Output of Mantissa Buffer)
1	Channel 1, I Component, Range Bin 1
2	Channel 1, Q Component, Range Bin 1
3	Channel 2, 4 Component, Range Bin 1
4	Channel 2, Q Component, Range Bin 1
•	•
•	•
14	Channel 7, Q Component, Range Bin 1
1.5	Channel 8, I Component, Range Bin 1
1.6	Channel 8, Q Component, Range Bin 1
17	Channel 1, I Component, Range Bin 2
	•
•	•
2.5	Channel 8, 1 Component, Range Bin 16
25.	Channel 8, Q Component, Range Bin 16

MULTINEST HOLES

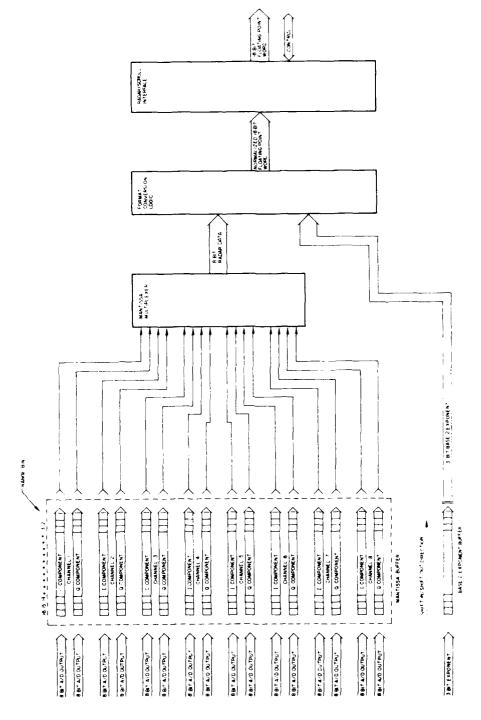


Figure 29. Mantissa and Exponent Shift Register Buffer with 8-Bit Wide Data Multiplexer. SHRT IN communds error from the radar master timing. SBET OVT commands originate from the array processor ICS interface

The output data train is combined with a 3-bit base 2 exponent and directed through format conversion hardware to insure radar data format compatibility with that of the array processor. Details of the format conversion hardware are discussed in Section 4.5.

4.4.1 MANTISSA BUFFER

Radar digital data is stored in shift register memory during the interpulse period until the radar initiates an array processor input cycle. The shift register memory may be visualized as a data matrix built of 8-bit word elements. The eight-channel receiver outputs an inphase and quadrature analog component per channel. Sixteen analog range samples are taken at 267-ns intervals; therefore, the data matrix is organized by row with regard to range cells and by column with respect to channels. A data matrix is loaded into shift register memory following every transmitted pulse. An I and Q 8-bit word is loaded for 8 channels and 16 range cells, generating a matrix of 16 range cell rows and 8 complex channel columns (256 8-bit words). The mantissa buffer shown in Figure 30 obtains input data from Datel 8-bit A/D converters. The output from the data buffer is directed into an array processor via Format Conversion Logic.

Mantissa Buffer								
	Col	umn 1	Col	umn 2		Col	umn 8	
		nnel 1 Quadrature		nnel 2 Quadrature			nnel 8 Quadrature	
ROW 1 RANGE BIN 1	8 bit	8 bit	8 bit	8 bit		8 bit	8 bit	
ROW 2 RANGE BIN 2	8 bit	8 bit	8 bit	8 bit		8 bit	8 bit	
		· ·		• •			· ·	
ROW 16 RANGE BIN 16	8 bit	8 bit	8 bit	8 bit		8 bit	8 bit	

Figure 30. Radar Receiver Mantissa Buffer (256 8-Bit Words)

4, 4, 2 BASE 2 EXPONENT BUTTER

Each of 16 range bins is associated with one positive 3-bit exponent that charactorizes the effective gain of 6 channels. The 3-bit expenent may vary mon, range byn to range bin if the stepped attenuators are in the automatic mode of speciation. If the step attenuators are operated in the manual mode, the 3-bit exponent will stay constant for 16 range bins. The exponent is stored in a shift register array 3 bits wide and 10 range bins deep. The array input comes from conversion logic following the 4-bit A/D converter sampling the log of channel 1 lF when in automatic operation. The logarithm of the channel 1 H signal is provided by an analog logarithmic amplifier. Channel 1 IF signal is split using an Isotee or power splitter. Half of channel 1 IF signal power is used as input to the logarithmic amplifier. The log amplifier output ultimately determines the IF signal attenuation required for eight channels. The remainder of channel 1 IF signal power is time delayed by utilizing coax cable. Channels 2 through 8 HF signal power is attenuated by 3 dB and delayed in a fashion identical to channel 1. The log amplifier output is sampled and converted to a 4-bit word. The 4-bit A D output is converted to a 3-bit IF attenuator control word, which establishes the IF signal attenuation required in all eight channels and the base 2 exponent as a function of range bin. Establishing the necessary IF attenuation requires time for A D conversion, 3-bit conversion, and attenuator setting and stabilization. Channels I through 8 are delayed for the time required to establish the appropriate IF signal attenuation. While in manual openition, the 4-bit A D cauput is bypassed, and the 3-bit exponent is hardwired in and loaded following each 4-bit SAMPLE command,

4.5 Data Format Conversion Logic

Format conversion hardware transforms the 8-bit A D output and 3-bit lesse 2 exponent into a normalized 16-bit floating point data word. The 16-bit floating noint format is compatible with the input requirements of the CSPI MAP array processor. Format conversion logic follows the output of the radae dat, buffer multiplexer in Figure 26. Radae data is transferred from the mantisss and exponent buffers through data conditioning (format conversion) logic and into the array processor. Data format conversion could have been implemented in array processor software; however, due to the process speed requirements of our real-time operating environment, format conversion was necessarily mademented in hardware.

4.). A ANALOG-LO-DIGITAL CONVERTER (INPUT AND CATPLET SPECIFICATIONS)

- a. Input voltage same to 8-bit Datel brocke mountainly g-to-digital convector ranges from -1.27 V to -1.28 V. Digital output coding for Datel model ADC-CH series is referenced as inverted offset Umary, as defined in Table 5.
 - b. From Table 6, A D input sensitivity is (0.0 mV per bit.
- c. The A-D converters used perform an 8-bit conversion in 0.1 μs (10-MHz conversion rate).

Table 6. Datel ADC Output Format

Analog	(-1)	11 [5]						,
Input Voltage For - polarity (volts)	7 N S D	10		103 4			1	0 1 5
-1.27	1	1	1	1	1	1	1	1
-0.54	1	1	()	()	()	()	()	0
0,00	1	()	0	0	()	()	0	0
1.27	0	()	0	0	0	Ü	()	1
1,28	0	0	0	0	0	O	()	0

4. 5. 2 S-BIT INVERTED OFFSET BINARY FORMAT CONVERSION TO 8-BIT SIGN MAGNITUDE FORMAT

The first stage of format conversion following the ADC output is dedicated to transfarming the ADC output of sign reagnitude format. If bit 7 is sensed to be set, the 8-bit data word is transferred directly through the first section of digital logic without modification. However, if bit 7 is not set, the conversion logic nerforms a 2's complement operation on bits 0 through 6 with one exception. It bits 1 through 7 are not set, bit 7 remains unchanged while bits 0 through 5 are set.

Table 7 defines logical input and output states for the first stage of formal conversion circuitry. Equation (1) relates the A-D anput voltage to sign magnitude binary components $\mathbf{m}_7,\ \mathbf{m}_6,\ \dots,\ \mathbf{m}_0$ before combination with base 2 exponent.

Table 7. Sign Magnitude Format

Analog Input Voltage	Format Conversion Input	Format Conversion First Stage Output
(volts)	$\begin{array}{cccccccccccccccccccccccccccccccccccc$	Sign Magnitude bit position 7
-1.270	1 1 1 1 1 1 1 1	1 1 1 1 1 1 1
-0.640	1 1 0 0 0 0 0 0	1 1 0 0 0 0 0 0
-0.010	1 0 0 0 0 0 0 1	1 0 0 0 0 0 0 1
0.000	1 0 0 0 0 0 0 0	1 0 0 0 0 0 0 0
+0.010	0 1 1 1 1 1 1 1	0 0 0 0 0 0 0 1
+0.640	0 1 0 0 0 0 0 0	0 1 0 0 0 0 0 0
+1.270	0 0 0 0 0 0 0 1	0 1 1 1 1 1 1 1
+1.280	0 0 0 0 0 0 0 0	0 1 1 1 1 1 1 1

$$V^{\text{smag}} = (-1)^{m_7} (10 \text{ mV}) \sum_{i=0}^{6} 2^{i} m_i$$
 (1)

where

$$\begin{array}{ll} v^{smag} & \quad \text{input voltage to 8-bit A/D} \\ \\ m_6, m_5, \dots m_0 & \quad \text{binary data bits} \\ \\ m_7 & \quad \text{sign bit} \end{array}.$$

4.5.3 8-BIT SIGN/MAGNITUDE MANTISSA WITH POSITIVE 3-BIT BASE 2 EXPONENT CONVERSION TO 16-BIT FLOATING POINT FORMAT WITH BASE 16 EXPONENT

The 12-bit radar data word is defined as shown in Table 8 following the combination of sign/magnitude format and positive base 2 exponent. The A-D input voltage expressed (as seen at output of sign magnitude format conversion logic after combination with base 2 exponent) in terms defined by Table 8 is seen by Eq. (2).

The second of th

F 7." - 2	***			- · t	in P	12 (T1 H			-		
11	10			7			:			1	()
8 + G ×	A × B						; ;	7::37	- C - E		1.5.1
VI.;	W _{ci}	VI,	M_{4}	Mg	W.,	\\\\\\\\\\\\\\\\\\\\\\\\\\\\\\\\\\\\\\	U ₀			1	Σ_0
$s_{\rm M}$	Mantissa							¹ N		oner	:1

$$v^{\mathrm{siningx}} = \frac{(4x_2 \cdot 2x_1 \cdot x_0)}{v^{\mathrm{sining}}}$$

$$v^{smingx} = (\sim i)^{\frac{S}{min}} (10 \text{ mV}) e^{\frac{(4s_2 + 2s_4 + s_6)}{2} \sum_{i=0}^{d} z^{i_i} s_{i_i}}$$
(2)

Abere

 S_{cc} Sign bit of mantissa.

 $S_{\zeta}=8$ ign bit of base 2 exponent (always positive or $S_{\zeta}=0$)

 $v_{\rm eq}, v_{\rm eq}, \ldots v_{\rm 0}$. binary contissabits

 $\mathbf{x}_2, \mathbf{x}_1, \mathbf{x}_0$ exponent bits

Bit positions are defined in Table 8.

The radar data word of Table 8, following conversion to a fasher floating point word, is defined as shown in Table 9 and Eq. (3). Hematica CO yields the relief ADC input voltage as seen by the MAP.

$$\nabla^{MAP} = (-1)^{\frac{N}{2}} h^{-1} e^{(NP)} - \sum_{k=1}^{3} -\frac{\Pi_{k}}{16^{\frac{1}{2}}}$$
(1.3)

where

 $\mathrm{exp}\ \mathrm{is}\ \mathrm{derived}\ \mathrm{from}\ \mathrm{S}_{\mathrm{e}^{+}}\ \mathrm{e}_{2^{+}}\ \mathrm{e}_{1^{+}}\ \mathrm{e}_{0^{+}}$

 $S_{_{\mathrm{C}}}$ is the sign of the base 16 exponent.

If $\exp \left(0, (S_{ij} = 0) \right)$ then

$$\exp - 4e_2 + 2e_1 + e_0$$

If $\exp < 0$, $(S_0 - 1)$ then e_2 , e_1 , and e_0 are in 2's complement form. Perform 2's complement operation on e_2 , e_1 , and e_0 , yielding e_2^t , e_1^t , and e_0^t ; then

$$\exp{-(4e_2^t + 2e_1^t + e_0^t)}$$
,

H1, 42 Hex digits converted to base 10.

H31 Hex digit with LSB deleted converted to base 10.

Bit position for arguments of Eq. (3) are defined in Table 9.

Table 9. MAP Base 16 Floating Point Half-Word Format

[Bit	. Po	sitio	on .		-				
	1.5	14	13	12	1 1	10	3,	8	7	6	5	4	3	2	1	0
	SIGZ	M S B		S						L S B	S I G N	M S B		L S B		
1	h ₁₁	h ₁₀	\mathbf{h}_{9}	h ₈	h ₇	h_{g}	h ₅ .	h ₄	h_3	h_2	h ₁	^h o	\mathbf{e}_3	\mathbf{e}_2	· 1	.0
	$s_{ m h}$	$\mathbf{S_h}$ $\mathbf{H_1}$ $\mathbf{H_2}$ $\mathbf{H_3}$							S _e Exponent							
Ī	Hex Mantissa									se l						

Equation (3) relates the voltage observed by the MAP to the hex components identified by Table 9.

Equation (2) is not equivalent to Eq. (3). The MAP defined voltage, \mathbf{V}^{MAP} differs from $\mathbf{V}^{\text{Smagx}}$ by a constant multiplier.

$$v^{\rm strangx} = (10 \, \mathrm{er} \, \mathrm{V}) (2^7) v^{\rm MAP}$$

$$v^{smagx} = (10 \text{ mV})(2^7)(-1)^{\frac{S}{h}} 16^{\exp(-\frac{3}{h})} = \sum_{k=1}^{3} \frac{H_k}{16^k}$$
.

Equation (4) allows one to predict the A'D output utilizing Table 9. MAP has voltage representation, and the IF attenuator settings \mathbf{x}_2 , \mathbf{x}_1 , and \mathbf{x}_0 . Equation (4) allows the conversion of MAP base 16 data to A'D input voltage.

$$V^{\text{smag}} = (-1)^{\frac{8}{10}} \left(2^{7}\right) \frac{(10 \text{ mV})(16^{\text{exp}})}{(4x_{2}^{+2}x_{1}^{+x}x_{0}^{-})} \sum_{k=1}^{3} \frac{\Pi_{k}}{16^{k}} . \tag{4}$$

Equation (4) is useful when relating A/D voltage input observations to MAP voltage observations used in processing. Equation (4) may also be used to insure A/D linear operation by insuring that the input voltage specifications are never exceeded.

4.5.4 NORMALIZATION OF 16-BIT FLOATING POINT WORD

The 16-bit data word is normalized in hardware to insure $\rm HI \times 0$ (unless $\rm HI$). H2, and H3† 0). If hex shifts are required for normalization, the base 16 exponent is decremented accordingly.

4.6 Input/Output Scroll (IOS) Interface

Discussion of the IOS interface will be developed primarily around data and control interface hardware. An event timing diagram is presented with references to RADAR ICS handshake control signals. Interface test hardware is presented in addition to detailed discussion regarding real-time data status indication. Data transfer rates realized are presented, and the data double buffering input scheme implemented is discussed. Radar data is transferred from the radar data storage buffer through format conversion logic and into an array processor under control of the array processor interface board (IOS).

4. 6. 1 16-BIT NORMALIZED FLOATING POINT WORD TRANSFER FROM RADAR TO TOS INTERFACE

Real-time radar operational constraints require all signal processing and data transfers be completed within one interpreter eriod. Data transfer rates must be high to insure maximum signal processing in \sim 2. The radar IOS interface and conversion logic realize a 16-bit MAT of word—ansfer in approximately 0.30 μ s; 120 μ s is needed for 32-bit MAP full word transfer (* 154 μ s to transfer 128 MAP full words, * 546 μ s per interpulse period).

4.6.2 RADAR MAP-300 IOS INTERFACE CONTROL AND TIMING SIGNALS (Figure 34, Table 10)

The array processor (IOS interface) informs the radar that the IOS processor has started via signal IOSRUN. Following activation of IOSRUN, the IOS interface informs the radar that processing is complete and the IoS is waiting for data, wir-PALSE control signal. The radar responds to the processor data request following the filling of the radar mantissa and exponent buffer discussed in Section 4.4. When the mantissa and exponent buffers are filled with new data, the radiac inforces the processor that data is ready by issuing the interface control signal CLRPAUSL. The PAUSE signal and CLRPAUSE signals insure that the data transfers are synchronized and new data is transferred. PAUSE is active until cleared by racher. that is, the array processor must complete all processing and data transfers within one interpulse period, and must wait until radar data is ready. The IOS then requests data, utilizing the leading edge of control signal ICSIN. Data input request is acknowledged by radar, utilizing control signal IOSACK, and the data is transferred (in handshake fashion) on the trailing edge of IOSIN. A total of 128 complex word transfers takes place in 154 μs , then processing is initiated. Three control lines were used to monitor radar data integrity and insure that the MAP did no drop a pulse by missing a data matrix, or transfer data as the radar data buffer was being updated.

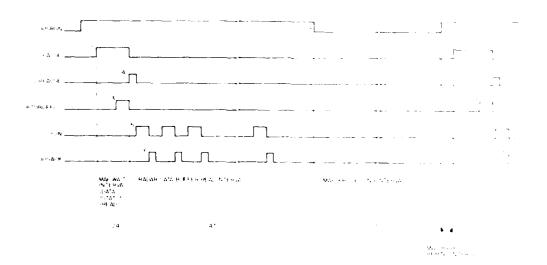


Figure 31. Radar IoS interface Control and Timing Signals. Only the most sugnificant control and timing signals are shown. Active signal levels shown the concentrately reflect interface. Positive logic was used for discussion purposes.

Table 10. Radar ICS Interface Control and Tuning Signals Active interface logic levels are not necessarily as shown

Edge Number	Name	Classification	Message
I	ICSRUN	MAP IOS interface control	Scroll is running
2	PAUSE	MAP IOS interface control	MAP waiting for data
3	RADBUFFLD	Radar timing	Radar mantissa and exponent buffers start load cycle.
4	CLRPAUSE	Radar interface control	Falling edge of RAD-BUFFLD indicates buffer load complete. This event triggers CTRPAUSE implying new data available.
	IOSIN	MAP IOS interface control	Leading edge of IOSIN requests data transfer from radar.
1	IOSACK	Radar interface control	Leading edge of IOSACK acknowledges data request causing data transfer on trailing edge of IOSIN.
7) IOSRUN	MAP IOS interface control	Radar to MAP data transfer complete, scroll is halted,

4, 6, 3 DATA STATUS INDICATOR

Three data status lines are provided under radar control to indicate data integrity. NFMRAD Doppler processing requires a constant time lapse from data group to data group; therefore, the loss of one pulse data group during a coherent processing interval is intolerable. If the array processor requires more than one interpulse period for beam formation and Doppler filter processing, invalid data will be transferred into the MAP. The radar is tasked with monitoring data integrity and reporting data status to MAP. Radar interface logic monitors transfer control signals and internal timing commands to determine data status. If the IoS requires more than 546 µs between data requests, the radar hardware writes over data stored in the radar buffer.

New radar data may become available at the ADC output as the MAP transfers data under IOS centrel. In this situation, new data would be shifted in the mantissa

The configuration of the state of the state of the configuration of the state of th

ber retre is 8 obertage starts curring, data is said to be a did be now, the divided for retre is 8 obertage starts curring, data is said to be a did be now, the divided cossing interval. Read reduced the GRADBULLEDD generates the CLUPAUSI signal, which is readly could ask the iGS of and start data traducer of the ics were in a software wait been that is, PAUSI ACTIVID. When a CLUPAUSI is issued and PAUSI is not active, the CLUPAUSI onlike is ignored in the loss the expression, the IGS is not aware that new data has been backered and retreated it, raised. Later, the Scroll starts running and activities the PAUSI signal. The PAUSI is not be cleared until the right buffer is once again tilled out to CLUPAUSI and crated. At least one data pulse will be lost under this activity. An even of the ature is referred to as a process observal out it.

If radar data becomes available after the ics interpretable of the IOS has exerted PAUSE, the MAP is short to be basedy before. The CLRPAUSE is issued before PAUSE is active, the return of the mass of the PAUSE rats until the next melan buffer local torract CLRPAUSE rats.

4.7 Receiver Simulator Hardware

Receiver situation has increased speed and for the pure secretice. As interface hardware and software diagnostics. Unprocessed to a perceive a terroved from the ReS data input next. Simulate head of a tag of replace to receiver data at the ReS input port to interchanging the latest case into the secretic board 10, with the receiver simulator card Ofigure 60 a latest in the latest of Figure 32.

The receiver simulater card provides a time invariant has an extension as Interface. Typically, the data matrix may be characterized by 12m or dexidence of a 15 cause cell voltage magnitudes are small compared to me to a prince of a 15 total cells. Every phase angle command within the samulated fater stars of 4 confidence and phase tremposed by fivery range cell signed as a particle and phase from pulse to pulse; however, the cell with relativery large or 5-time may be moved to any of the 15 cells by the use of a series of an togethe switches munifored 6 through 4 shown to figure 34. Voltage to approach a within the simulated data matrix may be altered, and are determined by the one 15-time beader chires a united in the simulated and the si



Compared to the entry of the con-

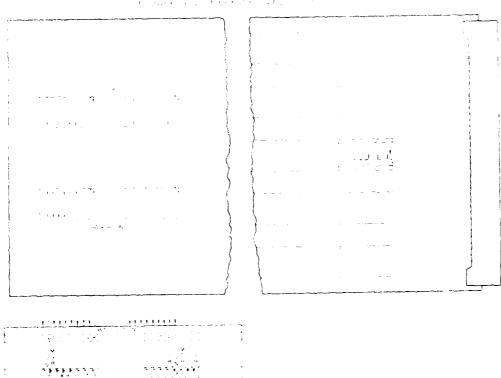


Figure 1. The constraint of the constraint of X by a constitution of the first X with a X particle of the constraint of the constraint of X with the constraint of X and X particle of X and X and X are X and X and X are X and X and X are X and X are X and X are X and X are X and X are X and X and X and X are X and X and X and X are X and X and X are X and X and X

N OF MENT A

It will be a serious each bloom to single relatively convent base a matricle, which is contained to only be managed of the Ir. The new of the two besides a state of the remaining Localls. A header of the remaining Localls. A header of the remaining Localls. A header of the remaining Localls and the series of the remaining Localls. The header only bit configuration is shown at Lotte of a continuous test that the two at the defined in Table 9. One header note two the magnitude of both Lami Q of appearing therefore, the entire key trage magnitude absence by the MAP counts \$2 times the data as mins defined by the header himpary. The function of each figural count base is settined in Table 11.

Table 11. Digital Consut Bossi Function Deputing

B and	
:	28.26 (10.00) I
	System Transport
	Crome Int - F. Winter Control of Server
1	Charmel I district of the
	Cromel 2 Months of this
	Chromod J. Maintess - Practic
-	Chemel 4 diediss - Partic
33	Channels (So Want ass. Market ever
٠.	Chaire - About ass Dayle
; c	Champel Memoss Purper
1;	Charact Tallettiss., Parter
: .:	Channel Willowissa Burner
14	dentissa Sign wagning in Lagrant Carrier of ma
	History to 8 internal
· i	Buse to Format Conversion
100	of the Errorst offer PCS (fest Courte)

5. SYSTEM SOFTWARE

System processing functions are inches ented in the CSP-30 time of public and MAP-300 array processor. CSP-50 and MAP-300 array processor. CSP-50 and MAP-300 arrayess is sist operators of the maintenance fields. Maintenance and real-time operational wadmark inclination sectors.

The Computer Signal Processer (CSP) came consider a a velicity commonities 32 k or interleaved core memory contained granus the qualities e. It will be 1000% suid-state memory overlay the fower core sectors in our ry. Periodemic excitation and sufficient tendence at the fower law of the engaged in support of CSP-30 operation and sufficient tendence entail indicative the series, fine periode, a tendence and containing containing containing a restrict the containing and the Containing Section 11 to 1000 and 11 to

Six now easy, as we will the MAP for a control of the six of the s

5.4 CSP-30 MAP 300 System Initialization Software

The prime section of a restriction of the test of channel 1. A state nary reflect in is classed to a place of the eight selection receive array to factor in the fellow. A prime wave currents as any elimentest on the receive array to factor in the factor of the P. A prime wave currents as any elimentest on the receive areas of. There are estimates of a ninels 2 to begin a corresponding to the factor of commel 1. Commel normal, when that as the reference to channel 1. Commel normal, when that as the relationship in the form of complex multipliers. These gain and phase connector is particle as a section and invariant layout for system initial ration is described as a section 1.2.4.

During the course of system initialization, the MAP processor is tasked with averaging 64 pulse returns. After 64 pulses are averaged by the MAP, the largest voltage magnitude from channel 1 is chosen from the group of 16 range bins. The range cell containing the largest voltage amplitude is the range cell containing the stationary reflector used for channel 2 through 8 normalization. The range cell containing the reflector is first determined, and then the eight complex average voltages chosen from the range cell containing the reflector are transferred to the host minicomputer.

These averaged voltages represent a planewave parallel to the lace of the eight-element receive array. This voltage data is used by CS2-30 software to calculate an amplitude and phase correction factor. The software correction factors are normalized to channel 1 (that is, the remaining seven channels are normalized in phase and amplitude to channel 1). Once the CSP-30 receives the eight-element voltage array, the CSP-30 software calculates antenna weight correction factors normalized to channel 1. The eight-element receive array scattering matrix and the average voltage array transferred to the host by the MAP are used to determine the antenna weight correction factors.

CSP-30 software modifies AMTI and XFMRAD beam-forming coefficients: reflect system channel gain and phase variations, and then transfers the modified beam-forming coefficients and the Doppler filter coefficients to the MAP processor. The CSP-30 function during initialization is to supply the MAP with corrected beam-forming coefficients and Doppler filter coefficients (Doppler coefficients are not officient initialization).

5.2 CSP 30/MAP 300 Real-Time Operation

In real-time operation, the MAP-300 APU's are responsible for AMTI and NEMRAD beam-formation calculations. Typically, a beam-forming calculation, the a single range cell would involve eight complex multiplications and a summation at complex products over eight channels. The APU's are also tasked with Depoter filter implementation. Two identical Doppler filters are implemented within the MAP; one filter as for NEMRAD and one as for AMTI processing. To implement a complex cut a challeful filter over one range cell requires do pulse acturns, to complex multiplications and a cumulative sum for a single range cell.

The IOS is responsible for transfer of receiver data from the wider into MAP was serve. The HIM is tasked with the transfer of processed radar data transfer MAP was a winto CSP-40 memory.

A supercry of MAP residetime functions inductes this groun of six MAP processes is turked with NEMRADJAMITE because in atom, NEMRADJAMITE because in atom, NEMRADJAMITE because in a transfer from the radar and into the CSP-30.

CSP-30 real-time processing functions consist of detection processing, processed data recording, and driving a CRT display. Under real-time operating conditions, the CSP-30 signal processor is almost exclusively utilized to record processed NFMRAD and AMTI voltage magnitudes, and data batch status. Processed data is recorded to cartriffle tape for more sophisticated detection processing at a later time. Detection processing is discussed in detail in Section 6.2.4.

5.3 Maintenance Software

Maintenance software consists of a group of programs designed to aid in receiver hardware troubleshooting and diagnosis. Using the array processor in conjunction with the host minicomputer and line printer, hardware diagnosis software is used to insure that the eight-channel receiver is operational. If a problem is detected, maintenance software is used as a troubleshooting tool.

MAP maintenance software consists of a straightforward transfer of receiver data from the receiver into the host minicomputer. MAP-300 maintenance software transfers one 128 complex word array of radar data into a block of MAP memory, then the HIM transfers the entire block of unprocessed data into CSP-30 memory. During system maintenance, the MAP serves only as a receiver data funnel. No numerical processing responsibilities are placed on the MAP during the maintenance mode of operation.

CSP-30 maintenance software consists of several programs. Che program entitled MDS (Minimum Detectable Signal) is written to run with the receiver in a maintenance configuration. The function of this software is the generation of an L'O transfer characteristic for each receiver channel. Typically, low-power RLCW is coupled into each channel of the RL front end. The RL energy phase and power level is under control of external test hardware (phase shifter and wave guide attenuator). Data is collected over a range of input power levels from approximately -100 dBm to -10 dBm. At the conclusion of the test, eight LO curves are produced, relating receiver input power to output power or voltage.

A second maintenance routine, entitled BITCHECK, was written to gain insight into receiver operation with constant power input. Generally, the receiver input may be RF CW at constant phase and power, or noise. Independent samples are taken and compiled over an extended period of time, and whistogram is produced showing the number of observations as a function of the output voltage magnatude. An example of this routine operation is as follows: With no signal present, only noise is present at the output of the receiver. By noting her match ADC dynamic cance is consumed by the system noise, the dynamic cance lost due to noise may be determined.

5.4 MAP Software

Repeating the MAP architecture for use in Section 3.4 discussion, there are six processors within the MAP-300, all of which operate asynchronously: the host interface module (HIM) for communication between the CSP-40 host machine and the MAP-300, the LO scroll (IOS) for communication between the made and the MAP-300, the central signal processing unit (CSPU) for overseeing the entire obtained controlling the other processors, the two arithmetric processing units (SPU) which run in parallel, and the addresser processing scroll (APS) which or vides a stream of input and output addresses for the APU. The various processors of loaded with the necessary programs, started by the CSPU, and their statuses are parted to the CSPU by the setting or clearing of days.

CALL MAP INSTALLIZADON

The system initialization function and unrose is discussed in Section 5.4.1 reviews MAP processor activity when the system initialization response system in the regram is executed.

initially, the host signals initialization phode to the LAP-300 many personal recontaining a 11. The CSPU reros a 512-30 rd black of mean ry on host one bit 8-2 which will be used for numerical summation. The CSPU mentionistic 103 200 mader-to-MAP data transfer program, loads the API with a data averaging personal, and loads the APS with the corresponding addressing program.

For 64 times, the CSPU turns on the icS, whith for the radar to transfer hit. (the IOS program turns off the IoS at the end of the transfer), turns on the APS which in turn starts the APU, and whits for an APU done fing to be set. This operation divides each data element by 64, and sums there for 64 pulses. This complex voltage averaging process takes place with the radar and reflector startionary. The reflector signal is large when compared to the signals is as the remaining 15 range cells. The phase and amplitude of the stationary target of the signal are averaged for 64 pulses. The receiver channels are to be to relationary target and gain and phase to channel 1. This average phase and ampritude data are average, the basis for receiver channel normalization.

Next, the CSPU loads the APU with a vector-rangingude program and the APS with the proper addressing program. The APS is turned an which stars the APS.

The CSPI waits for the API dene flag to be set, at which there have to 1 32-bit vector magnitudes on Memory Bus-2 from the next location 250 to 23 HeV. The 16 vector magnitudes are calculated from the average complex voltage. The lected over the range cells of channel 1. The following MAP task determine the range cell with the targest voltage magnitude, and declares this range central termination the stationary initialization target.

The CSPU loads the APU with a program to determine which range his of the radar data contains the greatest magnitude, and next leads the APS with the addressing program. The APS is started and the CSPU waits for the APU done flag to be set (it was necessary to introduce additional timing delay to allow time for the result to be placed in memory).

The CSPU loads the HIM with a program to transfer eight I and Q voltages to the CSP-30 host. The host uses this average voltage data to normalize the gain and phase of channels 2 through 8 to channel 1. A complex normalization factor is calculated in the host by using the eight-element receiver array scattering matrix and the average voltage array transferred from the MAP. The normalization factors are used to modify the AMTI and NEMBAD beam-forming coefficients resident in CSP-30 core memory.

The CSPU loads the HIM with a program to transfer the modified NEMRAD beam-forming coefficients, or antenna weights (eight complex factors), the modified AMTI antenna weights (eight complex factors), the XEMRAD filter coefficients (65 complex factors), and the AMTI filter coefficients (65 complex factors) from the host to the MAP. The CSPU waits for a host ready flag to be set to allow the host machine to compute these quantities and place them in the correct host mentagory area. When the CSPU senses that the host is ready, it starts the HIM progressor, and the antenna weights are placed in identical memory areas on MAP. Memory Bus-2 and Bus-3. The filter coefficients are placed on MAP Memory Bus-1. After the data has been transferred to the MAP, the CSPU loads the progressors for real-time processing and then waits for another host ready signal before proceeding. This completes system initialization.

3.4.2 MAP REALSTEME PROCESSING

Assuming that the MAP has performed system initialization and is varing to the host, all that is necessary to begin real-time processing is to the host one all that is necessary to begin real-time processing has begun, the host one ally had the MAP with an I/O reset, otherwise the MAP runs indefinitely, synchologically the availability of rador data.

If the MAP has been imited by an I-C reset from the host, but not consecuted down, its inemory is not disturbed and real-time processing context and context in having to go through system initialization by sending the MAP of the context and ing a non-ber greater than 11.7

The APU program multiplies eight counters received voltages at V and come for 1 by the NI MEAD antennal tender. On Januar management of a agencies bornents. The corr plex resultant (I) A resultant place to alterdise to the corresponding to

Beam formation and Doppler filtering is repeated for AMII processing, use, a dentical radar data, identical Doppler filter coefficients, and AMII antenda weights. The API and APS run continuously for a block of too, adar pulses (i) they should finish calculating before more fata is available, they so in xisting loops).

$$B_{n,\,n} = \sum_{i=1}^{\mathcal{B}} \mathbf{X}_i + \mathbf{A}_{i,\,n,\,n}$$

$$C_{n} = \sum_{p=1}^{n/2} \gamma_{p} + D_{n, p}$$

- No Began forming coefficients wight complex entenne weights)
- A Complex receiver voltage from radar whita complex voltages (1 rom) birs not outset
- B. Synthesis count are pattern (1% complex voltages necessalise)
- Deputer Char so therent (65 cer, ob x weights)
- 1 I'h autenna element teight-element receive annevi.
- n Nth range bin (10 range bins)
- n P^{TF} ender bulse (4 saulse Coherent Precessing Interval (CPI))
- C. Doppler tilter output (one complex voltage per range bin per CPD

After a conditionless, the APL and APS are turned off, switched to the concilex vector-reagnitude program, and turned back on. Following each coherent processing interval, the magnitude of the 16 output filter veltages is calculated and transferred to the host for storage and display.

The radic data interest the ALAP as 16-bu floating point numbers. All calculations are performed using 32 bits, and the final vector magnitudes are converted to 16-bit floating point format on MAP mericov Bus-2. The HEM program to a term 16 NEMBAD vector magnitudes, 16 AMED vector magnitudes, a worst magnitudes, and are zero, and and Costatus word (a total of 34 lesbit words) to the host model in after processing to radia data pulses. The CSPU makes actors to see if the host machine takes the data, but proceeds to set up for the next blook, it is not as it.

The LO status word sent to the host contains into cata or ancerning the left transfer. The status word indicates data validity with a series of data condition cades. There are three separate invalid data codes possible. They are:

- a. Radar data became available during IOS read (data the IOS read was invalid because as the IOS read data from the radar data buffer, the radar data buffer was being written over with new data).
- b. The IOS was running a few microseconds behind the radar (in this case one pulse of radar data was dropped).
- e. Radar data becomes available while the MAP was processing and before the IOS started running (at least one pulse of radar data was dropped). If no data status error or combination of errors occurred during the CPL the CPL is said to be valid. For the purpose of definition, the CPL output combined with the status word is referred to as a batch.

In order for MAP processing to keep up with the radar data, it was necess to employ a double buffering input scheme and to have a very effortent APL forgram. Some of the specific features which were necessary \$416.00

- a. The IOS is turned on and the radar data, when ready, is transferred to MAP Memory Bus-2.
 - b. The APU-APS is readied to process data on Bus- a
- As soon as the data has been transferred, the R-S turns itself off and the CSPI sets a flag to break the API out of an idling books of process that data.
- d. The ICS is switched to Memory Bus-2 and enabled, writing for the next bulse of data which will becur before the API has timished processing Bus-2 data.
- c. After the data has been transferred to Memory Bus-2 and the Ios turns—ft, the CSPU sets a flag to switch the APU to process Bus-2 data. If the APU has in a finished Bus-3 data, it continues to process Bus-3 data until it does thash, at which time it immediately begins to process Bus-2 data. If the APU has tunshed Bus-3 data before Bus-2 data is ready, it sets in an idling be obtained for the flag to switch it to Bus-2 data. The IoS is readied after setting the APU Bus-2 data to transfer radar data to Bus-3. The CSPU obsers an APU flag to change that its APU has timished with the data on a particular memory bus before allowing the IoS to overwrite that data with another oulse of table data.
- Let this notifine continues until be obtained in the first rays becomes $(e^{-1}e^{-1})$. The resistants word as CRM with a removing Leading "ICSLAT" that is editioned the regimning of each to-make blood tablewing each ratio for the resistance of the ansatz. ICSLAT" is part of the rate sent to the rast.
- At the end of the recombines, the ADI and APS are threned in. The CSPI sets a flag to indemnate vector rangentudes, thems in the APS and API, then you for the APU to perform the calculations. As soon as the APU is a set, the CSPI enables the ICC to transfer made data to Alemony Bussian Course with HIV processes to transfer results to the host reaching. If then also some input necessary summing locations and turns on the APS and the API (years or a granted)

flag was cleared by the APU before turning off) to process another 65 pulses of radar data.

5.4.3 MAP SOFTWARE TEST MODE

If the host sends the MAP a mode word less than zero, the CSPU executes a test program that does everything the real-time program does except for the radar-to-MAP data transfers. The MAP Bus-2 and Bus-3 memory locations used for radar data are filled instead with simulated test data from the host machine. The MAP performs all calculations on this test data. The MAP is now synchronized by the data coming from the host machine and will run at a much slower rate.

The host machine is tasked with simulating the radar data matrix and transferring the test data to the MAP for beam formation and filter processing. In the Software Test Operating Mode, the MAP looks to the host for radar data, independent of the operational status of the radar. The simulated test data is generated based on simple target and clutter models. The host calculates a new test matrix on a simulated pulse-to-pulse basis. The host first calculates a test matrix, then transfers the simulated data into the MAP. As the MAP is processing simulated test data, the host also processes the simulated test data in a fashion identical to the MAP. When the host has completed processing of the test data, the MAP transfers processed results back to the host. The host then compares both sets of results and reports any significant errors to the operator. The next sequential simulated data pulse is calculated by the host and transferred to the MAP, and the test process repeats until halted by the operator.

The Software Test Mode of Operation allows a check of the digital processing software and hardware independent of the operational status of the radar.

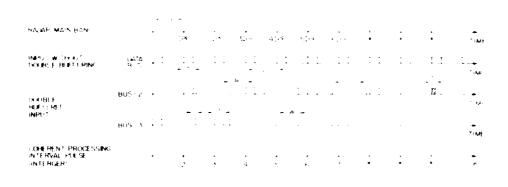
5.5 MAP-300 Double Buffered Input

In a rigorous real-time radar operation, the time required to transfer the radar data plus the time required to process the data must be less than one interpulse period. This constraint may be loosened somewhat by implementing a double buffer input scheme.

Radar data is double buffered at the input of the MAP-300. Double buffering allows additional time for processing during the radar interpulse period. As 2011 be shown, double buffering allows the processing time to extend this ugh the data transfer interval and extend beyond one interpulse period. Real-time software requires a few interposeconds more than the interpulse period to consider the processing of one data buffe; therefore, this allitical processing time is a secretari.

Radian data is loaded into two separate highers located on two data busises, specifically 2 and 3. Cdd-numbered bulses been based and a core taked into be enably on Physic, and even-numbered bulses between based at 1.15, 32. Data can be concluded by the

there is a Bus-2 as data from memory Bus-3 is actively processed; therefore, and decrease of double buffering is that data transfers and data processing proceed at the accusive. The data transfer interval appears transparent to the MAP artistical upon process. The data transfer interval appears transparent to the MAP artistical upon process as executed to be extended by and one interpulse period. There is a superiod of executed by and one interpulse period. There is a superiod of executed by and one interpulse period. There is a superiod of executed by and eventually data will be content very and the entire executed by and eventually data will be content very and the executed by a superiod of executed by a superiod of executed by the execut



Trace 1. Death Buttered input to ans

The double furthermic scheduler is noticed at follows, to othe recovers in $x \in \mathcal{C}$ and a social in these coeffs by tructive side effects (even though the recovers in two communities and see that one internal separated). The arccessing scheduler wides a consider a gressingly of bound the data truit rate; have very the dath buttern.

input scheme provides the additional time necessary to complete interpulse processing for 65 pulses, while not dropping pulses due to APU execution speed frontations.

To quantitatively determine the additional available processing time due to double buffering the input data, refer to Figure 34. The time available for real-time processing (p) without double buffering equals the interpulse period (IPP) minus the time required to transfer one pulse of radar data (T), or

$$p \le IPP-T$$
 . (5)

The additional processing time per pulse due to the double buffering input schene may be found by the use of Figure 34. From the double buffered input trains fiagram in Figure 34.

$$2IPP - T + W + P + B$$
.

Also note

W (n-1)1

P IPP+1.

To insure that MAP memory is not destroyed, constrain B > 0.

IPP - T -
$$(n-1)L - L > 0$$
,

Solving for the lag time (L) beyond one interpulse period (IPP), the processing $-\alpha$ extend:

$$L \leq \frac{\mathrm{IPP} - \mathrm{T}}{\mathrm{n}} \quad .$$

Letting a equal the number of pulses contained within one CPI yields

$$1 \sim \frac{(PP - T)}{CPT} \quad . \tag{1}$$

Therefore, the time allexed for processing with louble buttering a

$$P \leftarrow (PP + \frac{PP - 1}{CP}). \tag{79}$$

Subtracting the available processing time without double buffering from the processing time available with double buffering yields (Eq. (7) minus Eq. (5)) Eq. (8).

Let

Δt Additional process time due to double buffering

$$\Delta t < P - p - T + \frac{IPP - T}{CPI}$$

$$\Delta t < T + \frac{p}{CPI} . \tag{3}$$

The processing time gained by double buffering made real-time possible using the MAP-300. Double buffering allowed the processing time to be expanded by the distributionsfer interval plus a fraction of the processing time available without double buffering (p). The fraction of p decreases as the CPI increases. The limit of the processing improvement as the CPI approaches infinity is T.

For the NEMRAD(AMTI) processing application:

CPI 65

IPP - 546 μs

T 154 μs .

Therefore

$$\Delta t = 154 \pm (546 - 154) 65 - 160 \,\mu s$$
.

With 546 μs between pulses, up to 552 μs may be used for data processing with a 55-pulse CPL

6. FIELD INSTALLATION AND TESTS

Section 5.1 documents the common entrused in experimental testing and the complex comboxed to commute making and test common on the codule accuration. Section 5.1.1 from a situation instablishing a T. let make. The result test meality, consider another, and registered components respectively. Section 5.1.5. The coherent make target used in the maxing target experiments is shoused in Section 5.1.5. A bare eight target alignment tochmune to insure accurate his sister target nesticing a place are sented, and in computation with a description of the reasons.

Section 5.2 reviews the four phases of field testing. Section 5.2.1 discusses the method used to measure two-way antenna patterns. Section 5.2.2 discusses the method used to measure the Donaler filter characteristics. Section 5.2.4 discusses 5.2.4 review the M. HEMD on experiment on rewriting a true product of an account of medical filters.

6.1 Experimental Set Up.

$= \sum_{i=1}^{n} \sum_{j=1}^{n} \sum_{j=1}^{n} \sum_{j=1}^{n} \sum_{i=1}^{n} \sum_{j=1}^{n} \sum_{i=1}^{n} \sum_{j=1}^{n} \sum_$

White Applications is a substitution of the control of the control

The content of the co

. The first of the second contract of the t

from a some the utility of the transfer of the conflicture are sent on the following of the conflicture of t

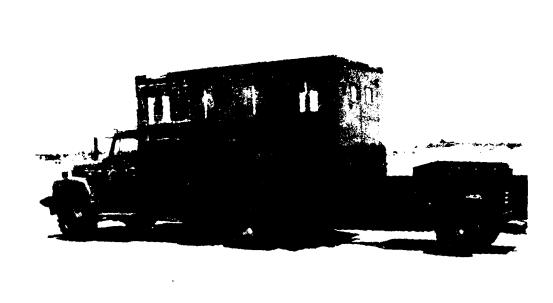
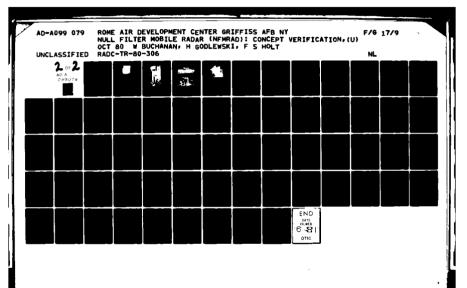


Figure 35. Radar Van Installation with Generator



Figure 3). Racher Laurier out payant class to a record



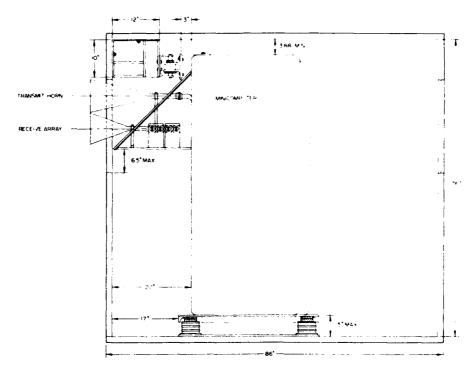


Figure 37. Radar Equipment Layout (End View of Van)

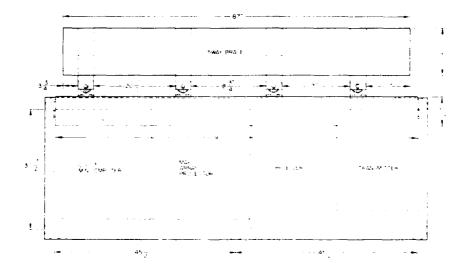


Figure 38. Floating Radar Platform with Shocks and Sway Brace" (Top View)



Figure 39. Base Plate Shocks

6.1.3 ENHANCED RADAR TARGETS

6.1.3.1 Pickup Corner Reflector Combination Target

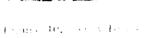
The enhanced radar target utilized in moving target experiments described in Section 6.2.4 consisted of a large corner reflector mounted on the passenger side of a six-passenger pickup (see Figure 42). The corner reflector is depicted in Figure 43. A technician riding in the radar target vehicle insured that the target vehicle was positioned broadside to the radar van as the two vehicles traverse taxiways "Raytheon" and "Whiskey" shown in Figure 48. This was accomplished by the use of a boresight mounted adjacent to the large target corner reflector. A spotlight mounted above the radar van receive array served as an optical alignment aid for use with the boresight.

6.1.3.2 Flat Plate Reflector

The 12-in, (30,5-cm) square flat metal plate shown in Figure 44 was tripod mounted and used for system initialization. An optical alignment procedure insured broadside flat plate positioning. A light source held adjacent to the rifle scope seen in Figure 44 was used to insure broadside flat plate alignment relative to the receive array face. The experimental layout for system initialization is similar to that shown in Figure 45. Approximately 293 ft (89,3 m) from the radar van, a series of metal plates canted skyward were dispersed to break up the specular multipath component. Figure 45 shows the flat plate 450 ft (137 m) away from the radar







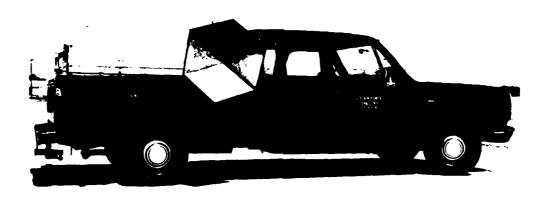


Figure 41. Remote Test Usculity

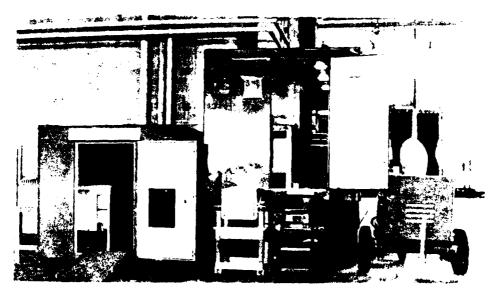


Figure 42. Enhanced Radar Target

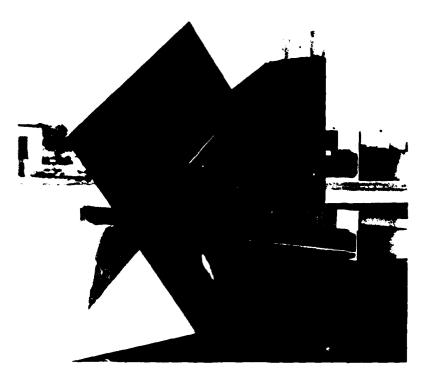


Figure 43. Corner Reflector

van used as a target for two-way antenna pattern measurements or for system initialization. Typically, the flat plate or corner reflector (Section 6. 1. 3. 1) would be used as a stationary target for antenna pattern measurements or system initialization. Due to the fact that the corner reflector provided a substantially larger radar cross section over a broader beamwidth, the corner reflector was used as a target most often.

6.2 Field Tests

NFMRAD {AMTI} field testing was divided into four separate phases. Phase 1 of field testing yielded two-way antenna patterns for the experimental radar system. Phase 2 consisted of experimentally verifying Doppler filter performance. A Doppler filter transfer characteristic was obtained with the radar position held constant measuring radar performance for converging and diverging targets traversing the radar main beam. In phase 3, target detection the shold voltages were determined. After target detection thresholds were established, phase 4 involved

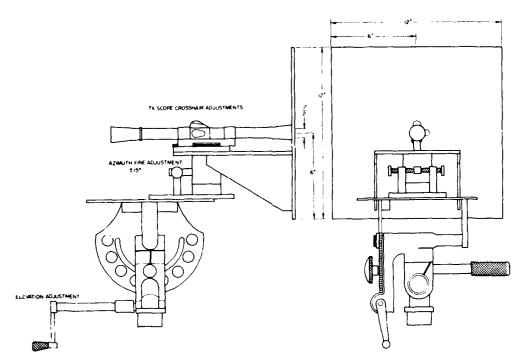


Figure 44. Flat Plate Reflector

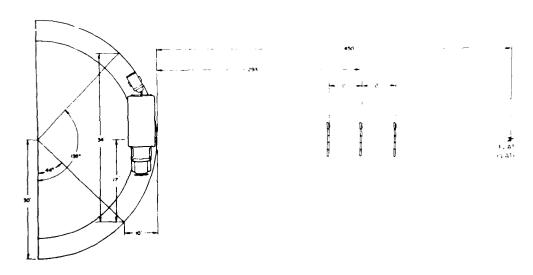


Figure 45. Field Site Used for Antenna Pattern Measurements (Top View)

moving target data collection in an effort to establish the probability of detection (P_d) for NFMRAD processing and conventional AMTI processing.

The discussion that follows will clarify the experimental details involved with generation of the data described above. Conditions in which the experimental antenna patterns, filter characteristics, target thresholds, and $P_{\vec{d}}$ curves were obtained will be discussed.

5.2.1 MEASUREMENT OF TWO-WAY ANTENNA PATTERNS

 10.7 ± 0.0 , the second phase of the data was the generation of the antenna patterns shows that

Several arrays as the measurement techniques were tried before a final scheme was adopted for antenn, pattern generation. Initially, with the radar van stationary, a flat plate reflector was moved in azimuth at constant range. Pattern data was accumulated and stored on tape. Typically, the target was moved 2^{Ω} in azimuth, realigned optically with respect to the radar van receive array, and pattern data was recorded on tape. The cycle would repeat from 0^{Ω} to 180^{Ω} bearing angle. An antenna pattern measurement consumed 4 hours; therefore, the measurement scheme was modified. The modified measurement scheme involved moving the receive array with respect to a stationary passive flat plate or corner reflector.

The modified scheme involved displacing the radar van in azimuth and holding the reflector stationary. Figures 45 and 46 depict the experimental layout utilized when transmit/receive patterns were measured. The van and receive array would advance 2^0 in azimuth and stop, pattern data was recorded on magnetic tape, the truck would then be positioned forward 2^0 , and the cycle repeated. This modified antenna pattern measurement scheme was not without drawbacks, however.

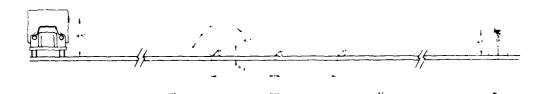


Figure 46. Field Site Used for Antenna Pattern Measurements (Side View)

There was concern the van would move outside the beamwidth of the stationary reflector. A second concern was multipath interference due to the low reflector and receiver array height. The terrain over which pattern data was collected was not flat, which lead to concern over vertical beam deflection as two-way patterns were measured. When advancing the van over unlevel concrete, the reflector

height would stay constant; however, as the truck advanced through arc, the relative height and tilt of the antenna array face with respect to the stationary reflector surface would vary slightly. The reflector illumination would vary due to multipath lobes formed in the beam; therefore, the pattern measured would typically be a composite of an antenna pattern generated primarily by radar azimuthal position but modulated by radar vertical displacement. The passive reflector was located at a range of approximately 450 ft (137 m). The van was driven in a tight turning arc. The radar van was displaced radially approximately 10 ft (3 m) from the reflector as data was collected over azimuth bearing angles of 44° through 136°. The receive array displacement parallel to the reflector was approximately ±17 ft (±5.2 m) referenced to broadside of the reflector. Every 80 of arc, the flat plate was optically aligned and the multipath reflector wall repositioned. Flat plate height relative to the ground was 4.5 ft (1.37 m). Height of the receive/transmit antenna array was 8,5 ft (2,57 m). (When using the corner reflector shown in Figure 43 for making pattern measurements, it was not necessary to adjust reflector position as the radar van advaced through arc. The reflected power variation due to the van displacement was less than 1 dB.) The illuminated multipath patch of earth was masked as seen in Figure 45. The earth surface between the radar van and target was not prefectly flat, which presented a problem when trying to accurately ascertain the ground patch significantly contributing to multipath interference. A shotgun approach was adopted and a large ground patch was masked, using long metal reflectors canted skyward and X-band absorber material.

Single-element patterns were measured for each of the eight-receiver channels. Two-way patterns, measured as described above, were obtained by uniformly weighting each receive channel and summing over the eight-element array to form one composite pattern (hereafter referred to as the AMTI pattern). Finally, each receive channel was weighted to form the NFMRAD pattern. Theoretical and experimental patterns are presented in Sections 7.1 and 7.2. Patterns previously discussed in Section 6.2.1 are referenced in Chapter 7 as AMTI and NFMRAD.

Typically, antenna patterns were measured using common real-time operating software with modified antenna weights and Doppler filter coefficients. For example, to measure an antenna pattern for channel 1, the following software modifications are required. Channel 1 antenna weight is set to 1+j0; weights for channels 2 through 8 are set to 0+j0. Doppler filter coefficients are modified to form a depass filter, or all 65 filter coefficients are uniformly weighted to 1.65+j0. The resulting software zeros channels 2 through 8 receiver data and sums the weighted receiver data over all eight channels. After 65 pulses, an average channel 1 receiver output is generated for use as data in channel 1 single-element antenna pattern.

Similarly, to generate an AMTI antenna pattern, antenna weights in each channel are set to 1/8+j0. Doppler filter coefficients are uniformly weighted to form a dc pass filter just as in the single-element pattern.

One additional concern is the requirement for the eight-receiver channel I O characteristics to appear uniform in phase and amplitude from channel to channel; all phase path lengths and gains must be uniform channel to channel. In practice, this constraint is not realized; therefore, the receiver channels are normalized in to insure channel uniformity before each series of measurements. The channel weight correction is a software normalization of channels 2 through 8 to channel 1. Before data is collected for processing, a channel normalization takes place within the software. Specifically, the gain and phase of all receiver channels are normalized to channel 1. A correction factor for each channel is calculated based on receiver response to an incident planewave parallel to the eight-element array aperture. The correction factor assures channel to channel uniformity by modifying each channel weight approximately, and assumes linear time invariant receiver operation. Before radar data is collected for processing, the channel normalization procedure is performed.

A flat plate or corner reflector is used as the signal source in the normalization procedure. A reflector is set normal to the receiver array and aligned optically. A multipath wall is constructed over an appropriate ground patch. Data is accumulated to determine gain and phase differences of each channel, and then the channels are normalized to channel 1. Antenna weights are modified by the appropriate correction factors, and the normalization procedure is complete.

To calculate an antenna patter, generally several (5 to 15) records of data were obtained per azimuth bearing angle. For the purpose of system term definition, one record consists of 60 data by tches. One data batch is output following the processing of 65 received pulses over which the coherent processing interval extends. Every data batch contains processed data resulting from two radar processing techniques operating on a common radar data base. In the case of normal real-time radar operation, NFMRAD and AMTI processing would be implemented; consequently, the batch output would consist of NFMRAD and AMTI processed data. In addition to processed output data, the data batch also contains a batch status work indicator. This status word is an indication of data validity (that is, did the MAP processing stay ahead of the radar or was data lost over the 65-pulse coherent processing interval?). If a data pulse was dropped or written over, or if the MAP ran "barely behind" the radar during the coherent processing interval, the status word indicates the integrity of each processing interval. Every data batch is written to cartrifile tape in groups of 60. Sixty batches make up a record. In normal radar operation, one data batch consists of 16 NFMRAD range bin words (one voltage magnitude per range bin, no phase information) followed by 16 AMTI

range bin magnitudes. The final word in the data batch serial string is the status word. Table 12 depicts the contents of one tape record during normal real-time radar operation. Generally, several records were averaged per bearing angle or velocity to obtain an antenna pattern or Doppler filter characteristic. A record is constructed of 1980 words or 60 batches, and is defined for normal radar operation as shown in Table 12.

Table 12. Tape Record Obtained during normal real-time radar operation

NFMRAD voltage magnitude, range bin 1, batch 1 NFMRAD voltage magnitude, range bin 2, batch 1 NFMRAD voltage magnitude, range bin 16, batch 1 voltage magnitude, range bin 1, batch 1 voltage magnitude, range bin 2, batch 1 AMTI AMIT AMITI voltage magnitude, range bin 16, batch 1 STATUS word indicator 65 pulse interval, batch 1 NFMRAD voltage magnitude, range bin 1, batch 2 AMTI voltage magnitude, range bin 16, batch 2 STATUS word indicator 65 pulse interval, batch 2 NFMRAD voltage magnitude, range bin 1, batch 3 AMTI voltage magnitude, range bin 16, batch 60 STATUS word indicator 65 pulse interval, batch 60

6.2.2 MEASUREMENT OF DOPPLUR FILTER CHARACTERISTICS

Measurements were made in an effort to verify digital Doppler filter performance. Theoretical filter characteristic is shown in Section 7.3, Figure 52. For a radar moving platform speed of 32 mph (14.3 m/s), the 3 dB bandpass velocities extend from 7.75 mph (3.47 m/s) diverging through 14 mph (6.25 m/s) diverging, with a peak centered around 11.25 mph (5.03 m/s). Bandreject velocities extend from approximately 4 mph (1.79 m/s) converging to 4 mph (1.79 m/s).

Experimental Doppler filter charm teristics were obtained by a country shall represent the response to meeting target signed returns with 12 of the red of the red of the region of the approximately 32 mph (14.3 m/s) of the region of the region directions. Typically, several records of data were taken or them making target centered in radar main beam. Figure 47 indicates the experimental layout used when measuring the radar Doppler filter characteristic.

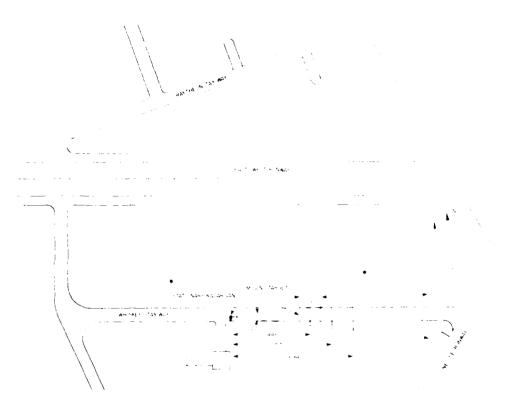


Figure 47. Field Site Used for Measurement of Doppler Filter Characteristic (Top View)

One record extends over 60 coherent processing intervals (65 pulses per interval). An average of 1 pulse is lost when a batch output is transferred from the MAP-300 to CPS-30 minicomputer for tape storage. Approximately 3960 pulses are transmitted during one record at a pul of 1831; therefore, approximately 2, 16 s expire during the accumulation of one record. The problem of multipath was not addressed when measuring Depoler filter data. The change in target beight relative to the malar was also assumed to be negligible (due to the short distance traveled over one record and the apparent flatness of the surface traversed).

Each experimental becommon in Figure 32 was averaged over many batche to obtain the enaracteristic shown. Lach point on the experimental curve comessents an average over many coherent processing intervals with the number of CPPs per data point a function of the target velocity. I give 47 indicates the approximate range and sampling interval over which but was secure whitea of this fifter characteristic. The stationary radial recorded withing target data as the target traversed through the rent in shown.

The target veincle was a SIX-messenger and him trues and common effect of the target size of the trues and reflecter was seen as the cribe of severe text of merchang velocities. The times was viewed to be the analysis in the other texts of merchang velocities; as a consequence of experimental necessity, the solution of memory as as section to diverging velocities in the other time true is as section to the engineerace. The interest of as section to diverge the methan of the common true of the engineerace.

The first the expertment of the contents of the first security of the first the mutualization of the contents of the first the mutualization of the contents of the first the first the first security of the first the first security of the first th

... ARGET DETECTION THRESHOLD VOLTAGE DETERMINATION

are composeen in Figure 45 indicates the Raythe mand Whiston tixes which are seen the image rate for determining target threshold to trages as a P_{α} data.

thresholds as a function of false plants rates for use in calculations. P_d cure. A large data base was a flected for use in leteraturing NFARAD (AACTI) tag. NFARAD (AACTI) tag. (CPa) (V, (Pa))).

taxis by Winskey at 32 mph (14.3 m/s) with no moving target vehicle present. The contradiction of the term of the first properties to the term of the first properties of of the first proper

Channel normalization was carried out in controlled repeatable hashion room the extent of the testing. Data collected was assumed to be spatially related but holevel from pass 1 down taxiway Whiskey through the final pass down William taxiway taken days later. Threshold data collection on taxiway Whiskey was to see it

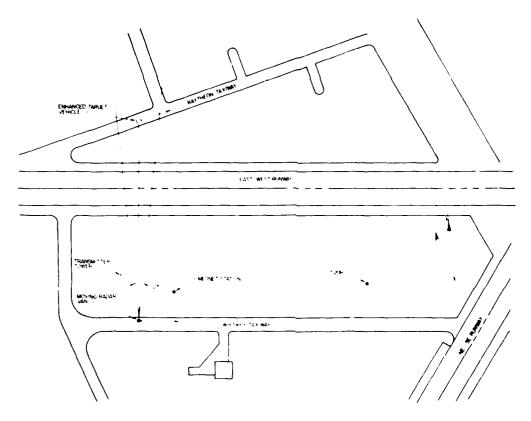


Figure 48. Field Site Used to Determine NFMRAD {AMTI} Thresheld Voltages and NFMRAD {AMTI} $\rm P_d$ Curves (Top View)

only if the radar van had reached v_o before passing the transmitter tower shown in Figure 48. Typically, 10 records were accumulated per pass down taxiway Whiskey. The pass length extended for 1015 ft (309, 4 m) and took approximately 22 s. Due to the reughness of the taxiway runway intersection, data collection was terminated before the intersection. The effort to obtain data starting position repeatability was driven by the need to have data from pass to pass related on a batch-to-batch, record-to-record basis (that is, batch 1, record 1, of pass 1 was measured overlooking the same terrain as batch 1, record 1 of pass 2). This constraint was imposed by the analysis method employed when calculating target thresholds and $P_{\rm d}$ curves.

Samples were gathered in an effort to obtain a data base with sufficient information to insure false alarm rates as low as 1 in 24 K. Approximately 2.4×10^5 samples were collected for the threshold data base.

Three separate analyses for determining target thresholds were implemented. Each scheme utilized a common data base for threshold calculation. The receiver detection threshold voltage is chosen to achieve the desired false alarm probability, P_{fa} . The false alarm probability of method 1 and method 2 may vary as the receiver gain and noise level drift; however, for analysis, the system was assumed time invariant. Method 3 utilizes a constant false alarm rate (CFAR) average; therefore, uniform drift in receiver gain and noise levels are of little consequence to the detection process (drift does affect system performance by causing channels to not be uniform).

Method 1 involved compiling, sorting, and tabulating range bin voltage data, and forming a histogram. Histograms were necessary for AMTI and NFMRAD data; therefore, two separate histograms were formed and separate thresholds were obtained. All range bins were lumped into one common data group, yielding a histogram containing 16-R-B-P samples where R total number of records per pass, B total number of batches per record, and P total number of data collection passes. There are 960 NFMRAD (AMTI) voltage magnitudes contained within one record after lumping every NFMRAD {AMTI} range sample together. A single pass down taxiway Whiskey yields 9600 NFMRAD [AMTI] voltage samples, assuming 10 valid records. To achieve false alarm rates of 1 in 10^6 , 1050 data collection passes are required. Clearly, so many Whiskey data runs is outside practical limits. A total of 105 passes are required to obtain sufficient data to insure false alarm rates of 1 in 10⁵. This figure was determined to be beyond tolerable hardware limits; therefore, in the interest of all concerned, 25 passes were run to develop the voltage threshold data base. 240 K samples were collected, yielding a false alarm rate of 1 in 24 K. The data contained within this data base is filtered radar data; each batch represents one coherent processing interval. One might argue that since each voltage magnitude represents a weighted summation of 65 voltages, the false alarm rate should be 1 in 1,56 \ 10⁶ instead of 1 in 24 K.

Target thresholds are determined for NFMRAD {AMTI} by selecting voltages with magnitudes sufficiently large to realize the desired false alarm rate. Since no target is present, any voltage above the threshold voltage chosen should be considered a false alarm. Typically, NFMRAD {AMTI} voltage thresholds, NFMRAD AMTI $V_t = (P_{fa}) \; \{V_t \, (P_{fa})\}, \; \text{are specified given a probability of false alarm } P_{fa}; \; \text{for example, a NFMRAD false alarm rate of 1 in 10}^6 \; \text{yields a threshold voltage written NFMRAD as } V_t = (10^{-6}).$

The second method implemented for threshold selection is a modified version of the first. Data is grouped on a range bin basis, forming 16 histograms for NEMRAD and 16 histograms for AMTL. Sixteen threshold voltages are chosen for

NFMRAD {AMTI} detection processing, resulting in one threshold voltage per range bin. The threshold selection scheme is similar to that described earlier. The significant difference in this scheme is the reduction is relative size of available threshold data base. The gain of method 2 is a spatially localized threshold level. Thresholds derived from method 2 are referenced using a κ index, for example, range bin 2, NFMRAD probability of false alarm, $P_{in} = 10^{-3}$, may be written as

$$\frac{\mathrm{NFMRAD}}{\mathrm{V}_{\pm(k)}^{-}(\mathrm{P}_{\mathrm{fi}})} = \frac{\mathrm{NFMRAD}}{\mathrm{V}_{\pm(2)}^{-} - (10^{-3})} \; .$$

Method 3 employs a form of CFAR average. For a given NLMRAD (AMT1) data batch, 16 samples are averaged and multiplied by a constant $\sigma^{NLM(1)}$ (σ^{AMT1}), resulting in a batch dependent threshold

$$\begin{array}{ll} \mathrm{NFMRMD} & \mathrm{AMTI} \\ \mathrm{V}_{\mathrm{p}} & (\mathbf{x}, \mathbf{o}) \; \{ \mathrm{V}_{\mathrm{p}} \; (\mathbf{x}, \mathbf{o}) \} \; . \end{array}$$

Separate NEMRAD (AMTI) a values are required. Ledering CEAR averaging, NEMRAD (MIL) detection processing is performed. If the threshold value, $V = (x, p) + V_{\perp}(x, p)$, a false alarm is less than any range bit voltage magnitude, $V_{RB}(k) = (x) + ($

6, 2, 4 NUMRAD (AMTI) P_d DETERMINATION

The map of Figure 48 indicates taxiway Whiskey utilized in Section 6.2.3, Target Detection Threshold Voltage Determination, is also used in Section 5.2.4. Data collected for determining detection probability was gathered by using two moving vehicles. In addition to the radar van traversing taxiway Whiskey, an electromagnetically enhanced target vehicle travels Raytheon taxiway in the direction shown. Radar moving platform velocity, v_o, equals 32 mph (14.3 m/s), as in Section 6.2.3 testing; however, Section 6.2.4 differs from Section 6.2.3 in that an

enhanced target vehicle travels broadsid to the moving radar platform at v_t of 34,6 mph (15,5 m, s) (see Figure 48 for velocity directions). Raytheon taxway 19^0 diverging angle is such that target radial velocity (v_p) is approximately 11,25 mph (5,03 m/s), the center frequency of Doppler filter passband,

Data collection begins after the radar van passes taxiway Whiskey transmitter tower if the moving platform velocity (\mathbf{v}_0) and target radial velocity (\mathbf{v}_p) are achieved before passing transmitter tower and the target vehicle possition is broadside to eight-element receive array mounted on moving platform. The target position was aligned optically with respect to the moving platform eight-element receive array.

Typically, \mathbf{v}_0 was achieved before reaching the transmitter tower. Shortly thereafter, the moving target position was aligned followed by stabilization of v. If v_p was realized before passing the transmitter tower, data collection was initiated and continued until moving platform approached runway 23 of Figure 48. Radio communications were established between the moving radar platform and target vehicle to insure experimental coordination. An optical bore sight alignment technique was implemented it he target vehicle to insure proper broadside target positioning. A bore sight mounted in the target vehicle was used for broadside target alignment in conjunction with a narrow-beam light source mounted on the moving radar platform. An observer riding adjacent to the large corner reflector mounted on the target vehicle monitored broadside target position. Verbal feedback from passenger position monitor to target vehicle driver was utilized in conjunction with radio communications to the moving platform. In summary, verbal and optical feedback coupled with nighttime testing made for a somewhat oscillatory (overshoot/undershoot) target position and velocity control. These experimental errors were due to accuracy limitations of vehicle speedometer readings, coupled with optical and verbal velocity and position control. However, velocity variations of v_r (v_r deviations related to fluctuations in v_t , v_o , and bearing angle θ) fall within the 3-dB Doppler passband characteristic of Figure 52. The theoretical NFMRAD and AMTI patterns of Figures 51 and 50 indicate NFMRAD performance is more sensitive to target position fluctuation at broadside than is AMTI, due to the forward canter of the NFMRAD main beam.

Real-time software used in Section 6, 2, 4 measurements was identical to software used in Section 6, 2, 3; however, the significant difference is the presence of an enhanced moving target traversing Raytheon taxiway broadside to radar moving platform.

Data accumulated pass to pass is again considered to be related batch to batch, record to record (as in Section 6.2.3). Approximately 25 passes were made down taxiway Whiskey, collecting data in Section 6.2.4 testing. Analysis of moving target data base toward the calculation of $P_{\overline{d}}$ values for NFMRAD and AMTI was implemented as described in the following discussion.

Section 6.2.4 data collected traversing taxiway Whiskey was compiled by grouping data batches as a function of taxiway Whiskey position in x, as shown in Figure 49. For purposes of this data analysis discussion, let

P ≈ data collection passes 25

B ≡ data batches per tape record 60

R ≡ records accumulated per data collection pass = 10

K ≈ range bins involved in detection processing

SF = distance scale factor

p ≡ integer data collection pass index where 1 < p < P

b = integer batch index where 1 < b < B

r ≡ integer record index where 1 < r < R

 \overline{x} = normalized Whiskey taxiway position where $0 < \overline{x} < 1$

x = Whiskey taxiway position relative to transmit tower where 0 < x < 81

k = integer , ange bin index

STATWD = data batch status word

 $\frac{\text{NFMRAD}}{V_{f(k)}} = \frac{\text{AMTI}}{\{V_{f(k)}(P_{f_0})\}} \equiv \frac{\text{NFMRAD}}{\{AMTI\}} \text{ threshold voltage as function of } P_{\text{rec}}$

 $P_{fa} = probability | f false alarm$

 $\begin{array}{c|c} \mathrm{NFMRAD}(p) & \mathrm{AMTI}(p) \\ V_{\mathrm{RB}(k)}(x) & \{V_{-}(x)_{-}\} \equiv & \mathrm{NFMRAD} \text{ } \{\mathrm{AMTI}\} \text{ range bin voltage magnitude} \\ & \mathrm{RB}(k) & \text{where } 1 \leq k \leq \mathrm{Kinch} \text{ } 1 \leq p \leq \mathrm{P} \text{ }, \end{array}$

 $\begin{array}{ll} {\rm NFMRAD} & {\rm AMTI} \\ {\rm P_d} & ({\rm x},{\rm P_{fa}}) \end{array} \} \equiv {\rm NFMRAD} \ ({\rm AMTI}) \ {\rm probability} \ {\rm of} \ {\rm detection} \ {\rm as} \\ & {\rm function} \ {\rm of} \ {\rm Whiskey} \ {\rm tax} ({\rm avay} \ {\rm position} \ {\rm and} \ {\rm probability} \ {\rm of} \ {\rm false} \ {\rm ability} \ {\rm of} \ {\rm false} \ {\rm of} \ {\rm false} \ {\rm of} \ {\rm false} \ {\rm of} \ {\rm of}$

 $_{o}^{\mathrm{NFMRAD}}$ $_{\{o}^{\mathrm{AMTI}}\}$ \approx CFAR real coefficients

NFMRAD AMTI $V_{\alpha} = (x, p) \{V_{\alpha} = (x, p)\} \equiv CFAR$ batch dependent voltage threshold

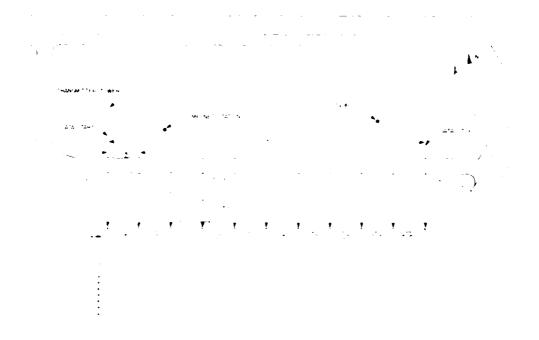


Figure 49. I follow Wheskey Division into Tape Records. Ten tape records are recorded to recover, x_i and x_i ross.

Whose votax as vote of the observable of the first and results are the variable ∇ may be extracted as for the results and reasons.

there bounds are integers such that 1 * b * Bound 1 * c * B

$$\mathbf{y} = -s\mathbf{1}(\overline{S})$$

where x is a feet. Given found r_i establish \overline{x}_i for example, but r(1) record 1 fixes moving platform position on tax x as Whiskey is a chart x to the right of transmitter tower. In other words

$$\overline{x} = \overline{x}(1, 1) = \frac{1}{500}$$

or at $\overline{\mathbf{x}}(1,1)$, 1 300 total taxiway pass has been completed. At b B and r R,

 $\overline{x}(b, v) = \overline{x}(B, R) = \frac{(60)}{(60)} \frac{(10)}{(10)}$

or a $\vec{x}(B, R)$ total taxiway pass has been completed. For any Whiskey position, $\overline{x}(b,r)$, P data batches are used to calculate $P_d(\overline{x})$. The p^{th} batch specified at \overline{x} NFMRAD contains 16 NFMRAD voltage magnitudes, $V_{RB(k)}$, 16 AMTI voltage magnitudes,

 $V_{\mathrm{RB(k)}}$, and 1 batch status word, STATWD. The status word is used only to insure data integrity; STATWD is not used in detection processing. If STATWD indicates batch data is invalid, batch data is not processed. If the pth data batch at x(b, r) is valid, detection processing is performed over K NFMRAD range bins and K AMTI range bins. Three separate detection procedures are implemented in an effort to determine $P_{\overline{d}}(x)$ sensitivity to the detection procedure utilized. Target threshold

voltages, $v_t = (P_{fa})$ and $v_t = (P_{fa})$, established as a function of P_{fa} in Section 6.2.3 testing, are used in detection processing implemented in Section 6.2.4. Three separate detection methods were implemented as follows.

Method 1, described in Section 6, 2, 3 yields $V_t = (P_{fa})$ and $V_t = (P_{fa})$. Given probability of false alarm, P_{fa} , one NFMRAD threshold and one AMTI threshold voltage are produced following method 1 detection threshold analysis,

 $\begin{array}{ccc} & \text{NFMRAD} & \text{AMTI} \\ \text{Method 1 detection processing utilized } V_t & (P_{fa}) \ \{V_t \ (P_{fa})\} \ \text{to ultimately} \end{array}$ calculate P_d $\{P_d^{AMTI}\}$ as a function of moving platform taxiway Whiskey position x(b, r). NFMRAD {ATMI} probability of detection P_d P_d for a specified probability of false alarm P_{fir} at taxiway position x(b,r) may be written as

$$\frac{\text{NFMRAD}}{P_d(\mathbf{x}(\mathbf{b}, \mathbf{r})P_{fa})} = \frac{\text{NFMRAD}}{P_d(\mathbf{x}, P_{fa})} \frac{\text{AMTI}}{\{P_d(\mathbf{x}(\mathbf{b}, \mathbf{r}), P_{fa}) - P_d(\mathbf{x}, P_{fa})\}} = \frac{\text{AMTI}}{P_d(\mathbf{x}, P_{fa})} \left\{ \frac{P_d(\mathbf{x}, P_{fa})}{P_d(\mathbf{x}, P_{fa})} \right\} = \frac{P_d(\mathbf{x}, P_{fa})}{P_d(\mathbf{x}, P_{fa})} \left\{ \frac{P_d(\mathbf{x}, P_{fa})}{P_d(\mathbf{x}, P_{fa})} \right\} = \frac{P_d(\mathbf{x}, P_{fa})}{P_d(\mathbf{x}, P_{fa})} \left\{ \frac{P_d(\mathbf{x}, P_{fa})}{P_d(\mathbf{x}, P_{fa})} \right\} = \frac{P_d(\mathbf{x}, P_{fa})}{P_d(\mathbf{x}, P_{fa})} \left\{ \frac{P_d(\mathbf{x}, P_{fa})}{P_d(\mathbf{x}, P_{fa})} \right\} = \frac{P_d(\mathbf{x}, P_{fa})}{P_d(\mathbf{x}, P_{fa})} \left\{ \frac{P_d(\mathbf{x}, P_{fa})}{P_d(\mathbf{x}, P_{fa})} \right\} = \frac{P_d(\mathbf{x}, P_{fa})}{P_d(\mathbf{x}, P_{fa})} \left\{ \frac{P_d(\mathbf{x}, P_{fa})}{P_d(\mathbf{x}, P_{fa})} \right\} = \frac{P_d(\mathbf{x}, P_{fa})}{P_d(\mathbf{x}, P_{fa})} \left\{ \frac{P_d(\mathbf{x}, P_{fa})}{P_d(\mathbf{x}, P_{fa})} \right\} = \frac{P_d(\mathbf{x}, P_{fa})}{P_d(\mathbf{x}, P_{fa})} \left\{ \frac{P_d(\mathbf{x}, P_{fa})}{P_d(\mathbf{x}, P_{fa})} \right\} = \frac{P_d(\mathbf{x}, P_{fa})}{P_d(\mathbf{x}, P_{fa})} \left\{ \frac{P_d(\mathbf{x}, P_{fa})}{P_d(\mathbf{x}, P_{fa})} \right\} = \frac{P_d(\mathbf{x}, P_{fa})}{P_d(\mathbf{x}, P_{fa})} \left\{ \frac{P_d(\mathbf{x}, P_{fa})}{P_d(\mathbf{x}, P_{fa})} \right\} = \frac{P_d(\mathbf{x}, P_{fa})}{P_d(\mathbf{x}, P_{fa})} \left\{ \frac{P_d(\mathbf{x}, P_{fa})}{P_d(\mathbf{x}, P_{fa})} \right\} = \frac{P_d(\mathbf{x}, P_{fa})}{P_d(\mathbf{x}, P_{fa})} \left\{ \frac{P_d(\mathbf{x}, P_{fa})}{P_d(\mathbf{x}, P_{fa})} \right\} = \frac{P_d(\mathbf{x}, P_{fa})}{P_d(\mathbf{x}, P_{fa})} \left\{ \frac{P_d(\mathbf{x}, P_{fa})}{P_d(\mathbf{x}, P_{fa})} \right\} = \frac{P_d(\mathbf{x}, P_{fa})}{P_d(\mathbf{x}, P_{fa})} \left\{ \frac{P_d(\mathbf{x}, P_{fa})}{P_d(\mathbf{x}, P_{fa})} \right\} = \frac{P_d(\mathbf{x}, P_{fa})}{P_d(\mathbf{x}, P_{fa})} \left\{ \frac{P_d(\mathbf{x}, P_{fa})}{P_d(\mathbf{x}, P_{fa})} \right\} = \frac{P_d(\mathbf{x}, P_{fa})}{P_d(\mathbf{x}, P_{fa})} \left\{ \frac{P_d(\mathbf{x}, P_{fa})}{P_d(\mathbf{x}, P_{fa})} \right\} = \frac{P_d(\mathbf{x}, P_{fa})}{P_d(\mathbf{x}, P_{fa})} \left\{ \frac{P_d(\mathbf{x}, P_{fa})}{P_d(\mathbf{x}, P_{fa})} \right\} = \frac{P_d(\mathbf{x}, P_{fa})}{P_d(\mathbf{x}, P_{fa})} \left\{ \frac{P_d(\mathbf{x}, P_{fa})}{P_d(\mathbf{x}, P_{fa})} \right\} = \frac{P_d(\mathbf{x}, P_{fa})}{P_d(\mathbf{x}, P_{fa})} \left\{ \frac{P_d(\mathbf{x}, P_{fa})}{P_d(\mathbf{x}, P_{fa})} \right\} = \frac{P_d(\mathbf{x}, P_{fa})}{P_d(\mathbf{x}, P_{fa})} \left\{ \frac{P_d(\mathbf{x}, P_{fa})}{P_d(\mathbf{x}, P_{fa})} \right\} = \frac{P_d(\mathbf{x}, P_{fa})}{P_d(\mathbf{x}, P_{fa})} \left\{ \frac{P_d(\mathbf{x}, P_{fa})}{P_d(\mathbf{x}, P_{fa})} \right\} = \frac{P_d(\mathbf{x}, P_{fa})}{P_d(\mathbf{x}, P_{fa})} \left\{ \frac{P_d(\mathbf{x}, P_{fa})}{$$

 $\begin{array}{l} {\rm NFMRAD} \\ {\rm A~typical~analysis~to~evaluate~P_{d}(x,P_{fa})~at~x'=x(b^{i},v')~and~P_{fa}=P_{fa}{}^{i}~follows:} \end{array}$ Given:

 \mathbf{b}^{t} , \mathbf{r}^{t} (establishes taxiway position on Whiskey as \mathbf{x}^{t})

 $P_{f_0}^{-1}$ (establishes probability of false alarm)

 $\mathbf{x}(\mathbf{b}^i, \mathbf{r}^i)$ is equivalent to P data intches collected a \mathbf{x}^i .

 $\begin{array}{l} \mathrm{NFMRAD}(p) & \mathrm{NFMRAD} \\ \mathrm{If} \ V_{\mathbf{RB}(k)}(x^i) & \geq V_t & (P_{\mathrm{fa}}^{-1}) \ \mathrm{for \ any} \ k \ \mathrm{such \ that} \ 1 \leq k \leq K \ \mathrm{and} \ p - 1, \ \mathrm{then \ a} \end{array}$ single target hit is counted.

 $\frac{\mathrm{NFMRAD}(p)}{\mathrm{H}(V_{\mathrm{RB}(k)}(x^i))} < V_{t} - \frac{\mathrm{NFMRAD}}{(P_{\mathrm{fit}})} \text{ for all } k \text{ such that } 1 \leq k \leq K \text{ and } p-1, \text{ then no}$

Pass counter p is incremented and the detection procedure is repeated for $p = 2, 3, 4, \dots P-1, P$. Following detection processing conclusion at $x(b^t, x^t)$, the total number of hits over P basses are totaled. A target is assumed present at \mathbf{x}^{t} P times. Total hit count at \mathbf{x}^{t} is divided by P passes to obtain probability of

determine $P_{ij}(\mathbf{x}^i, \mathbf{P}_{e_i}^{-1})$. Localeunate $P_{ij}(\mathbf{x}^i, \mathbf{P}_{e_j}^{-1})$ from $\overline{\mathbf{x}}$ (6.1) such $\overline{\mathbf{y}}$ (4.19) in Feld constant and \mathbf{x} is varied even the entire Whiskey taxiway in $0 < \mathbf{x} < 81$. A parallel as conclusivithmed to calculate $P_{\mathbf{d}}^{AM}(\mathbf{x}, P_{\mathbf{q}})$.

Method 2. described in Section 5.2.3, yields $V_{t(E)}(P_{\gamma_i}) = (V_{t(E)}(P_{\gamma_i}))$ where 1 * k * K. Given Pag. K threshold voltages are produced for NEMRAD (AMTE).

K 16. In summary, Section 6.2.3 method 2 analysis yields K NFMRAD thresholds and K AMTI thresholds. The results from method 2 analysis yield K NFMRAD (AMTI) P_d curves for a single P_{fa} value; generally, one pair of P_d curves per range bin. Method 2 processing yields K Pd curve pairs, or one NFMRAD AMTI curve pair per range cell for specified $P_{\rm fo}$.

Method 1 detection processing analysis yields one composite NFMRAD AMTI curve pair per Pfa.

 $\begin{array}{c} NFMRAD \\ Method~2~analysis~to~evaluate~P_{d(k)}(x,\,P_{fa})~for~range~cell~1~follows. \end{array} \ Determine$ NFMRAD probability of detection at $x=x^t$, $P_{fa}=P_{fa}^{-1}$, k=1. Obtain $V_{t(1)}(P_{fa}^{-1})$ from method 2 voltage threshold detection at $x=x^t$, $P_{fa}=P_{fa}^{-1}$, k=1. from method 2 voltage threshold detection analysis.

 $\text{If } V_{RB(1)}^{NFMRAD(p)} \simeq V_{t(1)}^{NFMRAD} \text{ where p } -1 \text{, then a target is declared for range}$

cedure stated above is repeated for p = 2, 3, 4, ..., P-1, P. Following P detection calculation decisions, the total number of range bin 1 target hits at x^i , $P_{i_0}^{-1}$ is summed. If target was known to be present in range bin 1, it is assumed present for P taxiway passes. The total number of target hits divided by P yields

NFMRAD

 $P_{d(1)}(x^i,\ P_{fa}^{-i})$. If target was known to be outside range cell 1, all target hits are counted as false alarms, and a P_{fa} curve is calculated.

The total number of samples taken for range cell 1 equals 65 R B P/16. Let total samples taken for k^{th} range cell equal sample tot. To calculate false alarm probability, total false alarm count is divided by sample tot. The procedure outlined above yields P_d or P_f calculated at x^t only. To generate entire curve over x, x must vary over entire taxiway, or from 0 through SF.

Method 3 described in Section 6.2.4 yields σ^{NFMRAD} and σ^{AMTI} given P_{fa} . These σ values are used in implementing a form of CFAR averaging. Typically, σ^{NFMRAD}_{fa} and σ^{AMTI}_{fa} is multiplied by the average of $V_{RB(k)}(x) = V_{RB(k)}(x)$ where $1 \le k \le K$ over P passes. The resultant product is treated as a batch-dependent threshold voltage. To calculate NFMRAD batch-dependent threshold NFMRAD(p) $V_{to}(b, P_{fa})$:

$$\begin{array}{ccc} \text{NFMRAD(p)} & \frac{\alpha \text{NFMRAD}}{K} & \sum_{k=1}^{K} & \text{NFMRAD(p)} \\ v_{t,r}(b, P_{fa}) & \frac{\alpha \text{NFMRAD}}{K} & \sum_{k=1}^{K} & v_{RB(k)}(x) \end{array}$$

where p=1,2,3,...P. The batch-dependent threshold was treated in method 3 detection analysis as in method 1. A single composite curve pair is generated given P_{fg} , and 16 curve pairs are generated in a fashion similar to method 2.

7. EXPERIMENTAL RESULTS AND CONCLUSIONS

7.1 Two-Way Antenna Patterns

7, 1, 1 UNIFORMLY WEIGHTED ANTENNA PATTERN

The antenna pattern shown in Figure 50 was measured as described in Section 6.2.1. Figure 50 depicts the two-way experimental antenna pattern with cross-hatches, and the theoretical pattern with a solid line. Experimental pattern data was collected over bearing angles ranging from 44° to 136° . Experimental error in azimuth resolution was estimated to be less than 2° . The experimental pattern shown is averaged over many tens of data batches, or each crosshatch represents an average of several data records. The theoretical nulls at 68° and 112° were contributed by the transmit pattern; however, the forward null at 68° and the aft null at 112° were not experimentally verified, as seen in Figure 50.

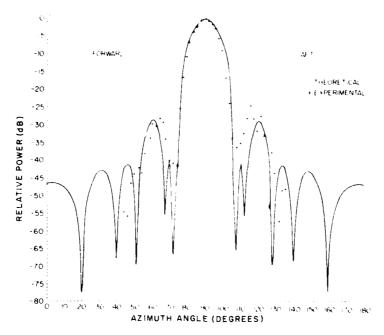


Figure 50. AMT1 Two-Way Azimuth Pattern (Theoretical and Experimental)

7.1.2 NFMRAD ANTENNA PATTERN

The antenna pattern shown in Figure 51 was measured as described in Section 6.2.1. Figure 51, like Figure 50, depicts the experimental two-way antenna pattern with crosshatches, and the theoretical pattern with a solid line.

The experimental NFMRAD pattern shows the most serious problem encountered thus far during field testing. Results indicate the experimental NFMRAD {AMTI} radar is unable to synthesize a broad antenna pattern null. Theoretically, the NFMRAD null should extend from approximately 104° to 118° ; however, this broad null has thus far not been obtained. Narrow -45 dB nulls have been measured; however, they generally are not repeatable. For the NFMRAD processing scheme to realize performance improvement over AMTI processing, the 14° antenna pattern null is essential. A solution to this problem is now being implemented.

The minicomputer software is being modified to include an adaptive beamforming algorithm. Beam-forming coefficients will be dynamically updated and the null will be formed adaptively.

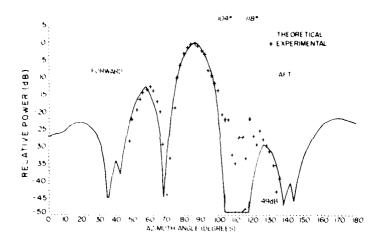


Figure 51. NEMRAP Two-Way Azimuth Pattern (Theoretical and Experimental)

7.2 Doppler Filter Characteristics

The Doppler filter characteristic, shown in Figure 32, was measured as described in Section 6, 2, 2. Experimental filter data was collected over a range of target velocities from 32 mph (14, 3 m/s) converging to 32 mph (14, 3 m/s) diverging. The experimental data outside the bandstop bandpass region of the filter characteristic is approximately 15 dB higher than the theoretical response.

7.3 Threshold Voltage Determination

Data described in Section 6.2.3 was obtained for determining appropriate target thresholds as a function of false alarm rate; however, our inability to realize a broad repeatable antenna null insured the collected data was inadequate to prove the NFMRAD concept.

7.4 Receiver I/O Characteristic

Figure 53 shows a typical receiver I O characteristic. RF power varying from -96 dBm to -26 dBm was fed to each of the eight receiver channels. The receiver output voltage was measured, using the MAP and CSPI processors. This typical characteristic exhibits a linear receiver dynamic range of approximately 64 dP. The receiver theoretical dynamic range (assuming no noise) is 90 dB. As seen in Section 7.5, noise due to the RF front end may consume up to a bits or 30 dB of dynamic range. Generally, 24 dB of receiver dynamic range is consumed by the mean noise voltage.

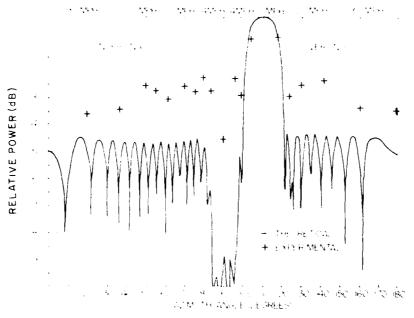


Figure 52. Doppler Filter Characteristic

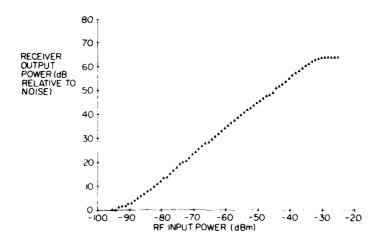


Figure 53. Receiver I/O Characteristic

7.5 Receiver Noise Histogram

Figure 54 is a typical histogram of receiver channel noise. The noise amplitude was calculated for 1000 complex independent voltage samples. One may approximate the number of bits consumed by receiver noise using Figure 54. For worst-case analysis, assume the noise voltage is equal the Q voltage component, and the I voltage component is zero. The mean noise voltage over all eight channels was calculated to be 80 mV. ADC input sensitivity of 10 mV/change of ADC output state; therefore, eight changes of state occur at the output of the ADC. Thus, the mean noise voltage consumes 4 bits of the ADC dynamic range (worst case). From Figure 54, a noise magnitude of 200 mV occurred 10 times out of 1000 samples or 1 percent of the total number of samples. Worst-case analysis of this case yields 20 changes of ADC output state or 5 ADC bits may be consumed by receiver noise (7 mantissa bits total given a constant base 2 exponent).

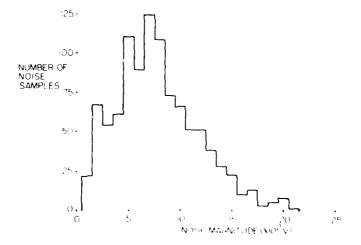


Figure 54. Receiver Noise Histogram

A noise histogram, generated using integer 1 and Q voltage components, will contain voids around 1.5 and 4.5 \times 10 $^{-2}$ V. This apparent problem concerns the histogram generation algorithm and the quantized voltage data, not the statistical nature of the noise data. For an explanation, let n be the noise voltage magnitude or

$$n = \sqrt{I^2 + Q^2}$$

where I and Q are integers. Then the case where $1, i \le n + 2$ and $4, i \le n + 1$ closes not exist for any integer I and Q combination. The discrete nature of the quantized voltage data and the histogram; search and sort algorithm are the causes for the deceiving noise instribution.

7.6 Preliminary Conclusions and Future Direction

Thus far, we have seen that it is extracr unarity difficult to form around (4^{9}) and deep (-40 dB) notches in our receive antenna pattern.

can beam formation approach assumed an accurate knowledge of the recorded array scattering matrix. One explanation of our experimental or line on the one ingoing the broad antenna null may be in the accuracy to which the scattering of the activity as known. Figure 55 shows the sensitivity of null depth to unitarial distributed errors in the scattering matrix. With relatively small errors in the scattering matrix, the null between 104° and 108° rapidly fills. The scattering matrix is suspected because it was measured in an anechoic chamber using the receive array with write transmit from a mean weil. It seems reasonable to assume that the scattering matrix is only be altered a charmac the interactions let then the receive array energy with states of the van the constitutions for each the receive array energy that the states is of the van the constitution between the array and the year spikes of the transmit from a charmac charmac charmac the constitutions.

As the result to be a nestdened is that the channel normalization be accided before it to see thering a strik for the calculation of super prints channel express, in factors. Seathering within empore therefore may partially explain borrole expects would entend by the nad Doppler filter discrepancies.

The immed normalisation procedure seemed reasonable; however, it was not conclusively shown to be adequate. Typically, the correction factors were repeats able to within one or two decimal digits when compared over as long as 4 hours. Generally, after 4 hours of operation, de drift would be sensed at the output of one or course of the receiver channels. The problem was compounded by having 16 i and Q or openents to check and calibrate. Following caribration, channel normalization to the ice.

Liberts are now underway to develop software that will adaptively form the receive actenna battern. The modified system will sample as environment and their adults at an improvegate to optimize the SNR. This work this alternately are particular to adopt by 5 cm, the broad antenna pattern mill require i for NI MEAD reconsisting.

An effort to measure the scattering matrix of the receive construction the radar con its idea being pursued.

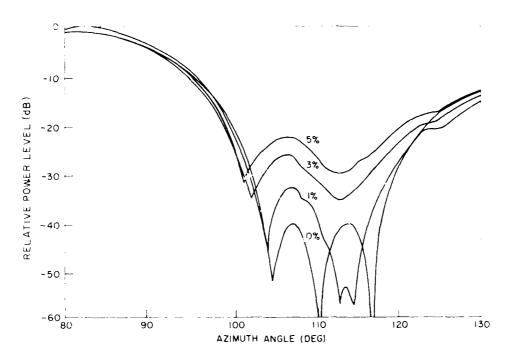


Figure 55. Effect of Uniformly Distributed Error in the Scattering Matrix on the Xull Region of Receive Pattern. Errors indicated are maximum percent error

References

- Goggins, W.B., Jr., Sletten, C.J., and Holt, F.S. (1974) New concepts in AMTI radar: Nulling effect of Doppler filter multiclement horn array, Microwave J. 17(No. 1):29-33.
- 2. Brown, Dr. Gary S., and Curry, William J. (1979) An Analytical Study of Wave Propagation Through Foliage, RADC-TR-79-359.
- 3. Cherry, D.K., and Tseng, F.L. (1965) Gain optimization for arbitrary antenna arrays, IEEE Tr. AP AP-13(No.6):973.
- 4. Drane, C.J., Jr., and McIlvenna, J.F. (1969) <u>Gain Maximization and Controlled Null Placement Simultaneously Achieved in Aerial Array Patterns, AFCRL-69-0257</u>, AD
- Goggins, W.B., Jr., and Schindler, J.K. (1974) Processing for Maximum Signal-to-Clutter in AMTI Radars, pp. 15-21, AFCRL-TR-74-0577, AD
- Collin and Zucker, eds. (1969) <u>Antenna Theory</u>, <u>Part I</u>, McGraw Hill, pp. 621-630.

Appendix A

Complex Recursive Infinite Impulse Response (IIR) Digital Filters

AL FILTER SPECIFICATIONS AND NORMALIZED REAL LOW-PASS FILTER DESIGN

It is desired to design digital filters that have a single passband or a single stopband in the frequency interval $\neg \Pi$ $f_p \le \Omega \le \Pi$ f_p where f_p is the pulse repetition frequency. Except for the special cases where the passbands or the stopbands are centered at de, it will be necessary to use filters whose transfer functions are complex.

For any particular design, the following specifications are needed:

- (1) Passband (or stopband) extend $\omega_1 \leq \omega \leq \omega_2$
- (2) Upper bound on ripple in the passband
- (3) Filter discrimination (ratio of maximum signal power passed to maximum signal power in the reject region)
- (4) Rolloff or rate of transition from the pass regions to the resect regions of the filter
 - (5) Filter response time
 - (6) Sampling period (T = $1/f_0$).

Two methods were used to develop desired HR digital bandpass and bandstep filters. The first method proceeds as fo' --:

Let $0<\omega_1<\omega_2$ be the desired passband (or stopband). Using the design procedures described by Gold and Rader, A1 frequencies $\omega_{A1}^i,~\omega_{A2}^i,~\omega_{A0}^i$ and ω_{AC}^i are defined by the relations

$$\begin{array}{ll} \omega_{A1}^{\prime} & \tan\left\{\frac{\omega_{1}T}{2}\right\} \\ \omega_{A2}^{\prime} & \tan\left\{\frac{\omega_{2}T}{2}\right\} \\ \omega_{A0}^{\prime} & \left\{\frac{\omega_{1}-\omega_{1}}{2}\right\} \\ \omega_{A0}^{\prime} & \left\{\frac{\omega_{1}-\omega_{2}}{2}\right\} \end{array}$$

Based on the specifications of ripple in the passband, discrimination, and roll-off rate, the nomographs described in Christian and Hisemann A2 determine suitable filter types (that is, Butterworth, Chebycheff, or Caver), and for each type the associated voltage transfer loss function, H(S), S= Σ + j Ω that will meet the specifications in a normalized lowpass filter. A plot of a typical power transfer loss function $A(j\Omega)=10\log_{10}|H(j\Omega)|^2$ for a normalized lowpass filter is shown in Figure A1. The quantity A_{max} is the maximum attenuation in the passband and is a measure of the ripple in the passband. A_{min} is the minimum attenuation in the reject region, and hence the difference A_{min} - A_{max} is a measure of the filter discrimination. The frequency $\Omega_{\rm S}$ is related to the rolloff rate and, in particular, the quantity $(\Omega_{\rm S}-1)/2$ is the ratio of the width of the transition region at one edge of the passband to the full width (-1 $\leq \Omega \leq 1$) of the passband. The tables in Christian and Eisenmann A2 specify the voltage transfer loss function A(S) by tabulating the zeros $\Omega_{01},~\Omega_{02},~\ldots$ and poles $\Omega_{>1},~\Omega_{>2},~\ldots$ of H(s) (see Figure A1). The voltage transfer function F(S) for the normalized lowpass filter is given by

$$F(S) = 1/H(S).$$

Filters with a single passband or a single stopband can be generated from the same normalized lowpass filter by means of well known transformations described in the next section.

A1. Gold, B., and Rader (1969) <u>Digital Processing of Signals</u>, McGraw Hill, New York.

A2. Christian and Eisenmann (1966) <u>Filter Design Tables and Graphs</u>, John Wiley and Sons, New York.

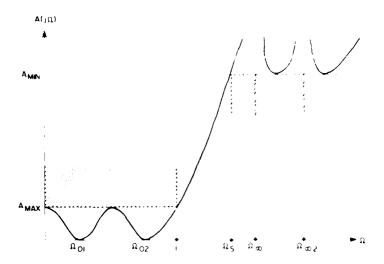


Figure A1. Power Transfer Loss Function for a Cavet C04a Type Filter - ,

A2: TRANSFER FUNCTIONS FOR SINGLE PASSBAND COMPLEX FILTERS

The transformation

$$\mathbf{S} = \frac{\omega_{\mathbf{A}\mathbf{1}}^{\prime} - \omega_{\mathbf{A}\mathbf{2}}^{\prime} + \left(\mathbf{S}^{\prime}\right)^{2}}{\mathbf{S}^{\prime} \left(\omega_{\mathbf{A}\mathbf{2}}^{\prime} - \omega_{\mathbf{A}\mathbf{1}}^{\prime}\right)} \quad , \quad \mathbf{S}^{\prime} = \sigma^{\prime} + \jmath \omega^{\prime}$$

converts the normalized lowpass filter into a baildpass filter with voltage transfer function

$$F_{bp}(S^i) = F\left\{\frac{\omega_{A1}^i \omega_{A2}^i + (S^i)^2}{S^i(\omega_{A2}^i - \omega_{A1}^i)}\right\}$$

and symmetrical passbands

$$0<\omega_{\mathsf{A}1}^{\mathsf{I}}\leq\omega^{\mathsf{I}}\leq\omega_{\mathsf{A}2}^{\mathsf{I}}$$

and

$$-\omega_{A2}^i \le \omega^i \le -\omega_{A1}^i < 0$$

and will be denoted by B and -B respectively.

In carrying out the present design procedure, it will be necessary eventually to identify the roots and poles of $F_{\rm bp}(S^t)$. The voltage transfer function F(S) for the normalized lowpass filter is ordinarily prescribed by means of its roots and poles, and it is advisable to transform this function factor by factor in order to be able to determine the roots and poles of $F_{\rm bp}(S^t)$. Thus each factor $S - S_{\rm c}$ transforms into a rational fraction as follows:

$$S - S_0 = \frac{(S^{\dagger} - r^{\dagger})(S^{\dagger} - r^{\dagger})}{S^{\dagger}}$$

where

$$r^{\pm} = \frac{(\omega_{A2}^{i} - \omega_{A1}^{i})S_{\phi}}{2} = \pm \sqrt{\frac{\left[(\omega_{A2}^{i} - \omega_{A1}^{i})S_{\phi}\right]^{2}}{4}} - \omega_{A1}\omega_{A2}}$$

and

$$p = 0$$
.

Since $F_{bp}(S^i)$ is real on the real axis, its roots and poles will occur in conjugate pairs, and the behavior of the filter in the region $\omega^i>0$ that contains the passband B will be due primarily to those roots and poles that lie in the upper half-plane. Conversely, the behavior of the filter in the region $\omega^i<0$ that contains the passband -B will be due primarily to the roots and poles of $F_{bp}(S^i)$ that lie in the lower half-plane.

Discarding the roots and poles of $F_{\rm bp}(S^{\rm I})$ that lie in the lower half-plane creates a complex voltage transfer function that represents a filter with only the single passband B. Conversely, discarding the roots and poles in the upper half-plane results in a complex voltage transfer function that represents a filter with only the single passband -B.

This method can be used to generate a single passband filter, provided that the passband does not overlap $\omega^t=0$. If $\omega^t=0$ is overlapped and $\omega^t_{\Lambda 2}=-\omega^t_{\Lambda 1}$, then a single real lowpass filter will be sufficient. The case where $\omega=0$ is overlapped and $\omega^t_{\Lambda 2}\neq -\omega^t_{\Lambda 1}$ will be discussed later.

The single passband filter can be normalized in different ways, resulting in several different forms (see Figure A2). The form shown in Figure 2(b) has been normalized to the average value in the passband.

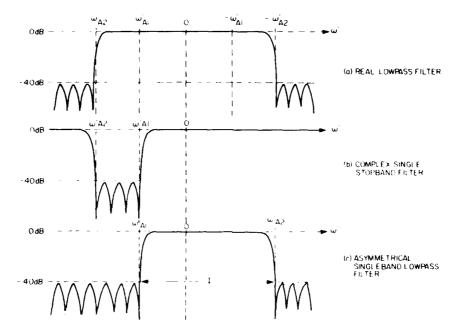


Figure A2. Power Transfer Functions of Filters Used to Realize an Asymmetrical Single-Band Lowpass Filter. Filter (a) caseaded with filter (b) produces filter (c)

A3. TRANSFER FUNCTIONS FOR SINGLE STOPBAND COMPLEX FILTERS

The transformation

$$S = \frac{\Omega_{\mathbf{S}}(\omega_{\mathbf{A}2}^{t} - \omega_{\mathbf{A}1}^{t})\mathbf{S}^{t}}{(\Delta_{\mathbf{A}1}^{t})\omega_{\mathbf{A}2}^{t} + (\mathbf{S}^{t})^{2}}$$

converts the normalized lowpass filter with voltage transfer function F(S) into a bandstop filter with voltage transfer function

$$\Gamma_{\mathbf{bs}}(\mathbf{S}^{0}) = F\left\{ \frac{\Omega_{\mathbf{S}}(C_{A_{1}}^{1}, -C_{A_{1}}^{1})\mathbf{S}^{0}}{\omega_{A1}^{2}(\omega_{A2}^{2} + (\mathbf{S}^{0})^{2})} \right\}$$

and symmetrical stopbands B and -B.

As with the bandpass filters, it is desired to identify the roots and poles of $F_{bs}(S^i)$, and to this end it is advisable to transform the voltage transfer function F(S) factor by factor in order to determine the roots and poles of $F_{bs}(S^i)$. Thus each factor F(S) transforms into a rational fraction as follows:

$$S = S_{o} = \frac{(S^{\dagger} - v^{\dagger})(S^{\dagger} - v^{5})}{(S^{\dagger} - p^{\dagger})(S^{\dagger} - p^{5})}$$

where

$$r^{\pm} = \frac{\Omega_{8}(\omega_{A2}^{r} - \omega_{A1}^{r})}{2S_{o}} \pm \sqrt{\frac{\{\Omega_{8}(\omega_{A2}^{r} - \omega_{A1}^{r})\}^{2}}{\{2S_{o}\}^{2}} - \omega_{A1}^{r}\omega_{A2}^{r}}}$$

$$p^{\pm} = \pm j \sqrt{\omega_{A1}^{\prime} \omega_{A2}^{\prime}} .$$

The zeros and poles of $F_{\rm bs}(S^i)$ will as before occur in conjugate pairs, and the behavior of this filter in the regions $\omega^i \geq 0$ which contains the stopband B is due principally to the roots and poles that lie in the upper half-plane. Also, the behavior of the filter in the region $\omega^i \neq 0$ which contains the stopband -B is due principally to the roots and poles that lie in the lower half-plane.

Discarding the lower half-plane roots and poles in $F_{bs}(S^{i})$ creates a complex voltage transfer function with only the one stopband B_{\star} . Conversely, discarding the roots and poles of $F_{bs}(S^{i})$ that lie in the upper half-plane creates a complex voltage transfer function with only the one stopband -B.

This procedure can be applied as long as the desired stopband does not include $\omega^i=0$. If the desired stopband contains $\omega^i=0$ and the interval is symmetric with respect to $\omega^i=0$, then a real lowstop filter will be the solution. The design of filters for asymmetrical intervals including $\omega^i=0$ is discussed below.

A4. TRANSFER FUNCTIONS FOR SPECIAL CASES

Assume $\omega_2 > 0$, $\omega_1 < 0$ and $\omega_2 > -\omega_1$, then $\omega_{A2}^2 > 0$, $\omega_{A1}^2 > 0$, $\omega_{A2}^2 > -\omega_{A1}^2$ and the interval Ligiven by $\omega_{A1}^2 > \omega_1^2 > \omega_{A2}^2$ is asymmetrical and contains $\omega_1^2 = 0$ (see Figure A260). The transfer function for a complex bandbass outer with bandbass 1 of an beigenerated by multiplying the transfer function for a complex bandbass filter with passband $-\omega_1^2 = \omega_1^2 + \omega_1^2 = \omega_1^2 = 0$ by the transfer function for a complex bands for filter with stopland $-\omega_1^2 = \omega_1^2 + \omega_1^2 = 0$ by the transfer function for a complex bands for filter with stopland $-\omega_1^2 = \omega_1^2 = 0$. The transfer function that with stopland 11 (see Figure A36), the transfer function for a complex for filter with stopland $-\omega_1^2 = \omega_1^2 = 0$. Its transfer function for a complex transfer filter with stopland $-\omega_1^2 = \omega_1^2 = 0$. Its transfer function for a complex transfer filter with stopland $-\omega_1^2 = \omega_1^2 = 0$.

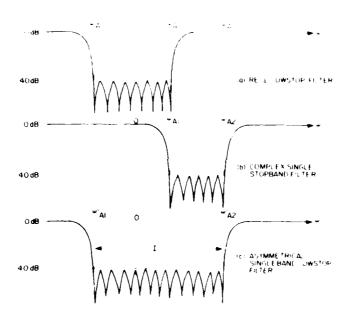


Figure A3. Power Transfer Functions of Filters Used to Realize an Asymmetrical Single-Band Lowston Filter. Filter (a) cascaded with filter (b) produces filter (c).

If $\omega_2 \geq 0$, $\omega_1 \leq 0$, and $\omega_2 \leq -\omega_1$, then $\omega_{A2}^{\dagger} \geq 0$, $\omega_{A1}^{\dagger} = 0$, and $\omega_{A2}^{\dagger} \leq -\omega_{A1}^{\dagger}$ and the interval Ligiven by $\omega_{A1}^{\dagger} \leq \omega^{\dagger} \leq \omega_{A2}^{\dagger}$ is asymmetrical and contains $\omega^{\dagger} = 0$. Proof have similar to those described above can be used to produce transfer functions for complex bandpass or bandstop filters with Las the bassband or stepbard.

A5. DIGITAL FILTER REALIZATION

Whether bandpass or bandstop, each of the voltage transfer functions of the single-band filters created by the methods described above is of the form of a ratio of polynomials in S^t , the coefficients in general, being complex. The generating function G(Z) for producing the digital realization of a given voltage transfer function $F(S^t)$ is obtained by means of the transformation

$$S^1 = \frac{Z - 1}{Z + 1}$$
.

This transformation maps the imaginary axis in the St plane onto the boundary of the unit circle in the Z plane. In particular, it maps the points St $- \iota \omega_{A1}^{\prime}$ and St $- \iota \omega_{A2}^{\prime}$ into the points Z $- e^{i\omega_{1}T}$ and Z $- e^{i\omega_{2}T}$ respectively. Thus

$$G(Z) = \mathbb{P}\left\{\frac{Z+1}{Z+1}\right\}$$

and GCD vill be a ratio of polynomials in Z_{\star} . The coefficients of these polynomials determine recursive forms of digital realizations of $\Gamma(80)$. A4

A6. IMPROVED DESIGN PROCEDURE

An approved design procedure for deriving digital fifter constanting master in for another hand bandpass or bandstep fifters has been fever ped, the first this may eithed, the near of read leavass fifter as selected as before, the terminal process fifter as selected as before, the terminal process fifter as selected as before, the terminal process above physical first and a process process of the constant support of the straint support of the process process of the fifteen participation of the process process of the straint of the constant process of the process of the straint of the constant process of the straint of the of the strain

The first bases of the countries are first, in most that $\frac{1}{4}$ and $\frac{1}{2}$ are considered as $\frac{1}{2}$ and $\frac{1}{2}$ and $\frac{1}{2}$ are considered as $\frac{1}{2}$ and $\frac{1}{2}$ and

where

$$\omega_{\Delta}^{\prime} = \tan \frac{\omega_2 - \omega_1}{4} T$$
.

This produces a voltage transfer function $F_{bp}(S^t)$ for a lowpass filter with passband $-\omega_{\Delta}^{t} \leq \omega^{t} \leq \omega_{\Delta}^{t}.$ The transformation

$$S^{1} = \frac{Z^{1} - 1}{Z^{1} + 1}$$

converts E(S) to a generating function in the 29 plane for a lowbass filter with pi ssband

$$-\frac{\omega_2-\omega_1}{2}+\ldots+\frac{\omega_2-\omega_1}{2}.$$

The transform dues

relates the center of the Loupass filter to the center of the besche Esmajor assisting (with a 2). The generating function is then given by

$$G_{\text{bd}}(\mathcal{O}) = 1 - \left\{ \frac{1}{\frac{1}{n^{\frac{1}{2}}}} + \frac{\frac{2n}{n^{\frac{1}{2}}} - \frac{n}{n^{\frac{1}{2}}} - \frac{n}{n^{\frac{1}{2}}} + \frac{n}{n^{\frac{1}{2}}} - \frac{1}{n^{\frac{1}{2}}}}{\frac{n}{n^{\frac{1}{2}}} - \frac{n}{n^{\frac{1}{2}}} + \frac{n}{n^{\frac{1}{2}}}} \right\} = 1$$

For randstar filters with single of the respective range of the range

 $(\mathcal{A}_{i}, \mathcal{A}_{i}) = (\mathcal{A}_{i}, \mathcal{A}_{i}) = (\mathcal{A}_{i}, \mathcal{A}_{i}, \mathcal{A}_{i}, \mathcal{A}_{i}) = (\mathcal{A}_{i}, \mathcal{A}_{i}, \mathcal{$

$$S^{\dagger} = \frac{Z^{\dagger} - 1}{Z^{\dagger} + 1}$$

and

$$\lim_{z \to -\infty} -j \left\{ \frac{(\omega_2 \cdot \omega_2) T}{2} \right\}$$

as before, shift the Z plane and rotate the stopband of the lowstop filter to the proper heation. The generating function $G_{\rm ho}(Z)$ is then given by

$$||\phi_{1,1}(x)-1|| \left\{ |\phi_{1,1}(x)| + \frac{\frac{1}{2} - \phi_{1,1}(x)}{\frac{1}{2} + \frac{1}{2} + \frac{1}{2}} \frac{1}{2} \frac{1}{2} \frac{1}{2} \frac{1}{2} \right\} ||.$$

AT CONCLUSIONS

Objective of the foregreen extracting function, further choice tensions $\rho_{\rm c}(r) = \rho_{\rm c}$ of the FR recursive-type digital procedure to be used in the realization of the ripe. The the XLMRAD tests, the application of the Tdirect's $\rho_{\rm c}^{\rm c}(N) = \frac{N^4}{4}$ for the digital reclination that was highly sensitive to the accuracy of the constants by the Laplace factor foregament that the Laplace and damonical" form $\frac{N^4}{4}$ was much expect to the Laplace to the reproduction with a principle factor as it is close to the accuracy of the constants.

View NI VIIA) receive enterty very a builded insing the transfer functions of entries of the first of the second of the Care CO4, type in recalled filters can the coefficient of the coefficient of the description of seconds, but the coefficient of the first of the figured coefficient, Plots of a second of the coefficient of the coeffi

The control of the co

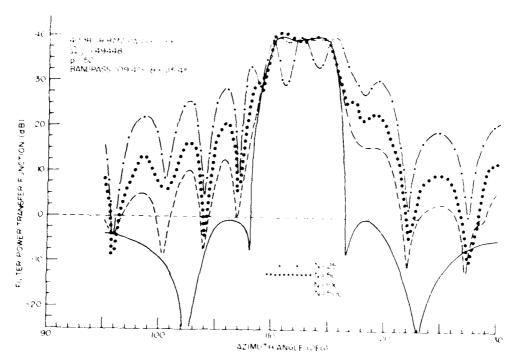


Figure A4. IIR Digital Filter Response Times

Appendix B

Complex Nonrecursive Finite Impulse Response FIR Digital Filters

BL. FREQUENCY SAMPLING DESIGN METHOD

Using the frequency sampling in a convergiven on Rahmer et al. ⁴⁷⁷ Lift holds a case and bonds on rightal filters can be designed that have response three of Li. 33, we can 126 balses. This precedure forces the filter response for the conscious three as secretic values at equally spaced be tals in frequency. The insertic values in the basis band are converged as unit prediscrete values in the report regard one chase mas zero. The design is officient, with respect to suppress, in fifth one attaining respect so that the transfer of the mass in the respect to the regard of the mass in the respect to the value of the mass in the transfer of the mass in the transfer of the mass in the transfer of the condition of the regard transfer or regard to the second of the regard transfer or regard to the condition of the second of the regard transfer or the condition of the regard transfer or regard to the condition of the regard transfer or regard to the condition of the regard transfer or regard to the regard transfer or regard transfer or regard transfer or regard to the regard transfer or regard to the regard transfer or regard to the regard transfer or regard transfer or regard to the regard transfer or regard to the regard transfer or regard transfer or regard to the regard transfer or regard to the regard transfer or regard to the regard transfer or regard transfe

The maximum of a constraint content of the content of the force product of the content of the c

with the section of the Garage states of the section of the secti

The exploit for the term of the exploit of the transition and the exploit of the

It is the nature of digital filters that their respects a functions are be readed in frequency with period equal to the sampling rate, in this case the NFMR/D oulse repetition frequency. Choosing the prf greater than or equal to twice the elaxical expects i chitter Doppler frequency insures that for a single passhand for stephanib digital filter, there is only one passband for stopband) within the chitter Doppler frequency interval. For the NFMRAD truck experiment, the next is 1034 Hz overthis almost exactly twice the maximum clutter Doppler frequency of 0.15.7 Hz,

B2. MODIFICATIONS TO PRODUCE COMPLEX FILTER AND CASCADING

To achieve a complex single passband filter of the type needed for NEMRAD, a real lowpass FIR filter of the desired bandwidth and discrimination is designed and then rotated in the z plane to position the passband at the desired center frequency. For a single stepband filter, a real lowpass FIR filter whose reject region has the desired stepband width is designed and then rotated in the Z plane by the are ununcessary to locate the stepband at the desired center frequency. The Z plane rotation needed for the stepband filter is essentially that which corresponds to the frequency difference between half the pulse repetition frequency (orf. 2) and the Doppler clutter frequency at the center of the antenna transmit beam.

The action of an n-point bandpass FIR filter, together with an n-point bandstep FIR filter, can be achieved by cascading to form a single (2n-1) point FIR filter. For FIR filters with n = 15, 33, or 65, the response time is far less than for the HR filters described earlier. For this reason, cascaded FIR filters were use for all subsequent investigations.

In the work that follows, FIR filters are designated according to their lesign. Figure B1 shows the design of a 33-point FIR bandpass with 5 points in its bandpass and 2 transition points, T1 and T2. The designation code for this filter, 4 P33-3-2, translates as follows:

- BP bandpass filter (BS bandstop filter)
- 33 NP total number of points in the filter
- 3 NBW measure of width of the bassband time bor of points in the passband = 2-NBW-1
- 2 NM number of transition points.

Caracination of the contract o

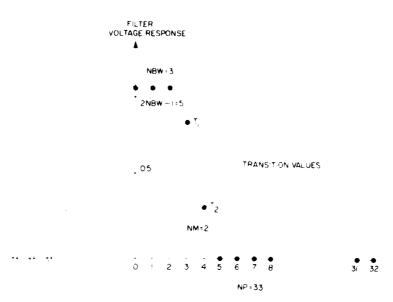


Figure B1. Specification of Filter Response Values for a BP33-3-2 FIR Filter

Table B1 shows some of the filters that were used in the theoretical investigations associated with NFMRAD.

Table B1. FIR Filters Used in NFMRAD Investigation

Bandpass Filters	Bandstop Filters		
BP15-1-1	BS15-7-1		
BP33-1-1	BS33-12-1		
BP33-2-1	BS33-13-1		
BP33-3-2	BS33-14-1		
BP65-3-1	BS65-25-1		
BP65-3-2			

Appendix C

Control Panel Operational Range Equations Range Cell Width = 131.15 ft (40 m) Range Coverage \simeq 2100 ft (640 m)

Figure C1 depicts the three operational range modes of the radar: NEGATIVE, SHORT, and LONG. The position of switches E and F select one of the radar range modes as defined in Table C1.

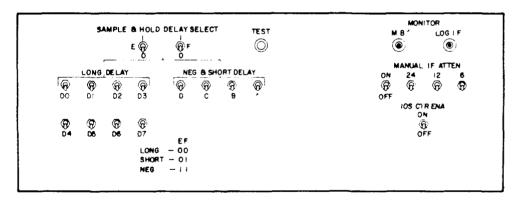


Figure C1. Radar Control Panel

Table C1. Radar Operating Range Mode

	E	F	
LONG	()	0	
SHORT	0	1	
NEGATIVE	1	1	

Equations (C1), (C3), and (C5) express the radar search range as a function of range bin (RB) and control panel configuration (DCBA $_{10}$, D7, etc.). The radar operational range mode is determined by the position of control panel switches L and F.

CL. LONG DELAY RANGE EQUATION

Equation (C1) expresses radar search range (γ) as a function of P0, D1, ... D7 control panel switch position, and the range bin (RB) of interest when in the LONG delay range mode. D_{set} is the control panel switch (D7, D6, D5, ... D0) set during radar operation. To calculate γ when in the LONG delay range mode: Let D7 - 7, D6 - 6, D5 - 5 ... D0 - 0, and RB is an integer representing the range bin of interest such that $1 \le RB \le 16$.

LONG Delay Range Equation

$$\gamma = 65,5763(15(D7-D_{set}) + 10 + 2 \text{ RB}) \text{ ft} - 517,25 \text{ ft}$$
 (C1)

The time delay (Δt) between the transmitter MAIN BAND and the radar 16-bit SAMPLE command is given by Eq. (C2).

LONG Delay Time Equation

$$\Delta^{\dagger} = \frac{2}{15 \text{ MHz}} \left(15 (D7 - D_{\text{set}}) + 10 + 2 \text{ RB} \right)$$
 (C2)

C2. SHORT DELAY RANGE EQUATION

Equation (C3) expresses radar search range (γ) as a function of A, B, C, D control panel switch positions and the range bin (RB) of interest when in the SHORT delay range mode. Control switches A, B, C, D are binary weighted when calculating γ as shown in Table C2.

Table C2. DCBA 10 Equivalent for Range Calculations

Control Panel Switch Position D C B A				Base 10 Equivalent
0	0	0	0	0
0	0	0	1	1
0	0	1	0	2
0	0	1	1	3
		•		
•				·
1	1	1	1	15

SHORT Delay Range Equation

$$\gamma = 131.1525(16.375 + RB - DCBA_{10})$$
 ft - 517.25 ft (C3)

 Δt may be calculated as expressed in Eq. (C4).

SHORT Delay Time Equation

$$\Delta t = \frac{4}{15 \text{ MHz}} (16.375 + RB - DCBA_{10})$$
 (C4)

C3. NEGATIVE DELAY RANGE EQUATION

Equation (C5) expresses the radar search range (γ) as a function of A, B, C, D and RB when in the NEGATIVE delay range mode. A negative result from Eqs. (C5) and (C6) indicates the 16-bit SAMPLE command of interest occurs before the transmitter MAIN BANG. A positive result indicates the SAMPLE command occurs after the MAIN BANG.

NEGATIVE Delay Range Equation

$$\gamma = 131,1525 \text{ (1/2} + \text{RB - DCBA}_{10}) \text{ ft - 517,25 ft}$$
 (C5)

NEGATIVE Delay Time Equation

$$\Delta t = \frac{4}{15 \text{ MHz}} (1/2 + RB - DCBA_{10})$$
 (C6)

Appendix D

ADC Alignment Procedures

The purpose of this procedure is to ensure that the ADC assembly is calibrated and will not introduce additional errors into the receiver/processor system. All comments and adjustments will be made with reference to the I side of the assembly; however, they apply equally to the Q side.

Recommended Equipment

Dual trace oscilloscope

Signal generator

0-5 V dc variable power supply

LED display box (or eight-channel logic analyzer)

BNC to SMA adapters as required

Digital multimeter (DMM)

Two 18-wire ribbon connectors (ML PAC 3552040-01 or equivalent).

D1. 8-BIT ADC ALIGNMENT

D1.1 Initial Setup

Connect an 18-wire cable from the 4-bit ADC power distribution block to the 8-bit ADC assembly under test. The cable must be connected to the 8-bit ADC board row C, pins 19-36. Ensure the black white pair of wires at the ADC board (pins 19-20) is connected to the 4-bit power distribution block (bits 1-2 or 19-21).

Reversing the supply sequence can cause serious damage to the ADC (refer to Figure D1).

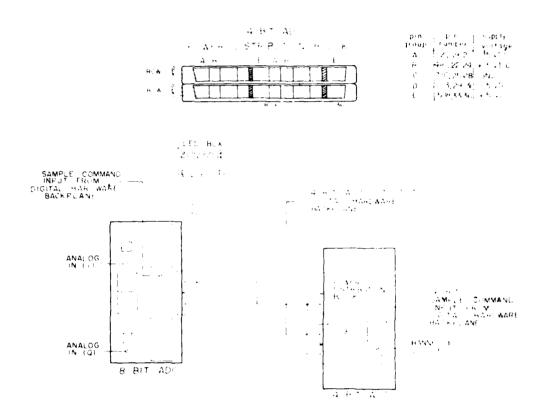


Figure D1. 8-Bit DC Alignment Configuration

Connect a coax cable to the 8-bit SAMPLE command input port from the receiver digital hardware backplane (refer to Figure D2).

Connect the dual trace scope as follows:

- 1. Trace "A" to the analog input
- 2. Trace "B" to the input of the ADC (pins 17 and 18)

(Refer to Figure D3(a) for pin locations,)

Connect the signal generator to the analog input port of the ADC under test. Turn rack power on.

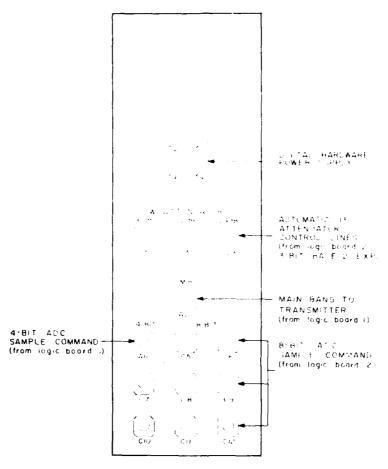
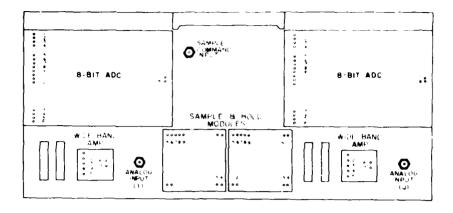


Figure D2. Receiver Digital Hardware (Backplane Connector Panel)

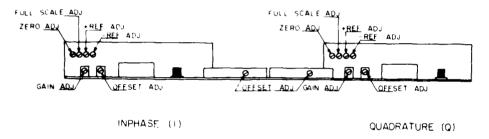
D1.2 ADC Assembly Gain Adjustment (Refer to Figure D3(b))

Ensure the analog input (signal generator) is set for 100 mV peak to peak at 250 KHz as measured with the scope (trace A).

Monitor the input to the ADC (trace B) and adjust the GAIN pot of the wideband amplifier for a gain of $6.3\ (630\ mV)$ output.



(a) Pin Locations (Top View)



(b) Calibration Adjustments (Side View)
Figure D3. 8-Bit ADC Assembly

D1.3 ADC Assembly Offset Adjustment (Refer to Figure D3(b))

The purpose of this adjustment is to ensure the analog input has a 0 V dc offset (with respect to ground) as measured with an oscilloscope. Any dc offset to the analog signal will cause the ADC output to shift a proportional amount and invalidate any gathered data.

Monitor scope trace A and adjust the analog input (signal generator) for 0 V dc offset.

Remove the trace B probe from the ADC (pins 17 and 18) and connect it to the sample and hold unit input (pins 10 and 11). (Refer to Figure D3(a) for pin locations.)

Monitor the scope (trace B), and adjust the OFTSET pot of the wide-band amplifier for 0 V dc offset.

Both and the second property for the position of the second property.

. As the constant of the first property of the second state of th

Burney Commercial

D1.4 8 Bit ADC Output Calibration Setup (Refer to Figures D4 and D5)

In the following areas made, to record with relate the linear energy with a second with all expressions of the first with LADC in that, the expression was a second mode of the LaD fixed with respect to the first with a second with the first with the constant measurement of the first with the constant measurement of the second with the constant with the second with

Commest on the case which from the UTD display begins $P_1 = 0.11$ for some ADC associably to be called defined P_1 on sub-TaO. This are the transfer of the cable is commented to miss P_2 of P_3 . Of his other case is subput from both Land Q sides; however, alled ustractive of the case of some P_3 . To the Uside only,

Connect to V do to the LLD display by a single 446-in, when collective ground connector on the end addigator stips on the other. It up the end to the end of the reach Connect the center of the reach. Connect the center of the reach of the reach the center of the end of the reach the center of the end of the reached hardware and the small clip to ground. Connect BNC connector to the LLD display box.

Remove both scope probes and the signal generator from the ADC assembly. Remove the sample and hold unit from the side to be calibrated.

Connect the 0-5 V dc variable power supply to the input of the ADC (pins 17 and 18).

Connect the DMM to the input of the ADC (pins 17 and 18).

Turn rack power on. Allow 10-min warmup time for the ADC to stabilize.

D1.5 8-Bit A/D Adjustments (Refer to Figure D3(b) for Location of Pots)

Monitoring the DAMM, adjust the variable power supply to -1.115 V de. Adjust the -REF ADJ pot until the LED display indicates the following: (red LED's represent L side, Green LED's represent Q side)

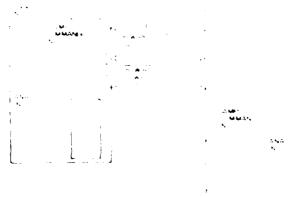
N7, N6, N5 should be on

X4 should be blinking.

As the voltage is decreased to $\text{-1.110}\ \text{V}$ dc, N4 should be on, and as the voltage is increased to $\text{-1.120}\ \text{V}$ dc, N4 should be off.

Monitoring the DMM, adjust the variable power supply to $\pm 1.125~{\rm V}$ dc. Adjust the $\pm {\rm RFF}$ ADJ but until the 44.D display indicates the following:





 $(a_{i+1},\ldots,a_{i+1}) = (a_{i+1},\ldots,a_{i+1},\ldots,a_{i+1})$

The state of the s

Open Colonia April Agris SMEST

(x,y) = (x,y) + (x,y) + (y,y) + (y,y) = 0

The state of the s

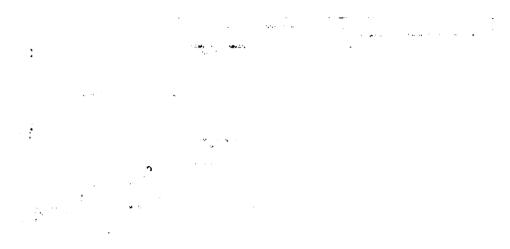


Figure Dr., 4-Fot ADC Assembly

Thirtimen power in sure db title in the committee.

What is some trace A and a fast the object of the 0.3 decouple respect to ground).

Mount in the second true ϵ B and a bust the sample and hold offset our for 0 V fiset (with respect to ground).

D2.3 4 Bit ADC Gain Adjustment

Remove shorting can from the 4-bit ADC analog input pert.

Connect a signal generator to the analog amout. Ensure that the generator is set for 200 KHz at 100 mV peak to beak.

Menth rescope trace A and educe the signal generator for 0 V decoffset.

Montton scope trace B and adult the gain but for a gain of 0, 37 (87 mV beak to be set.

D2.4 4 Bit ADC Output Calibration (Refer to Figures D4 and D6)

In the following proceedings, the LLD display box is used to allow visual monitoring of the solutal ADC output. An eight-schamp religion in diview may be used if desired trefer to Table D1 for the 4-bit ADC output transcription).

Turner o kapes er oge.

. Discontined the loss illescope probes, and signal generator from the 4-bit ADC $\sim 60 c_{\odot}$

Connect in BR-wise cable from the MDC subput connector (row B pins 1-18) to 1.1.0) hasher box too. Figure 1-18),

Table D1. 4-Bit ADC Output

Analog Input (v dts)	Digital Output
-2.400	1111
-1.020	1100
-1,280	1000
-0, 1:0	0001
0.000	0000

(Note: The most negative analog input come sports to fall scales (about)

Comment to V destriction LLD display beginsing a 48-m, proceed of the xights BNC connector (coars) in the end addition reduces the other. Runs trained and allighter choose the uglithe ADC is a to the remark forceway. Connector the end content conductor chaots ground. Connect the ENC challe) connector to the LL position of U.S.

He may the amorte and hold to challe their the 4-bit ADC assertly.

Counset the 0-5 V de variable moves supply to the input of the ADC terms 17 and 15).

Connect the DMM to the most of the ADC (pins 17 and 18).

Turn tack power on anglation 10-min harraup tree.

Women the DWW, adopt the variable power supply to -2,400 V is.

Adjust the FREE and per until the LED display indicates the following:

N7, No. No. X4 should be by

ul. 4-bit ADC uses only these four LLD's).

Atomitoring the DMM, adjust the variable power sumply to a, aa (V ac). The Fi.D display should indicate the following:

St. No. No. 34 should be off.

Since the 4-bit ADC is not a bipolar unit, only the -REE adjus available.

ium no a power off and remove all test equipment.

D3. 4 BFF ADC DC BIAS ADJUSTMENT (Refer to Figure D7)

The numbers of this procedure is to ensure the output of the 4-bit ADC is such that the automatic attenuators begin switching in at the correct power level. If the attenuators switch in too late, the input to the 8-bit ADC's may saturate, convenience did by:

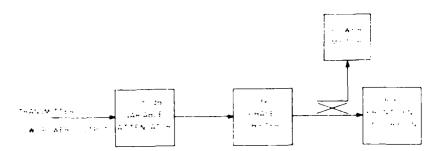


Figure D7. 4-Bit ADC Bit's Admistment

Additional Equipment:

Waveguide attenuator (FXR MDI No. N194A or comivatent)

Waveguide phase shifter (H.P.MD) No. Nac As requivalent)

Waveguide sections as required

Power meter and there isters, unt.

- 1. Configure the ADC deck for normal points in as follows:
 - a. Remove all test equipment
 - b. Reinstall all sample and noid to dules recover in previous procedures.
 - c. Theore that all SAMPLE of read most cable are correctly installed.
 - d. Ensure that all ADC partour parties are properly a nationed to fer the Table D2 & relisting).
 - e. Ensure that all analog amout colles are retrieved needs in (if the Land Q cables for any ADC are stamped, the rate, afterest collide invalid.)
- 2. Configure the transmitter for test persit is as tell of a
 - hasine both wavegut le sant-hes tree set for a resolution to the GROBE test positions).
 - b. At the rear of the transcritter medicine traction to the rearrant install adultional waveguide sections of the intersection of the rearrant tipure D7.
 - c. Disconnect the diode switch driver input odde transfer to it is switches inside the transmitter this will block to the transmitter this will block to the transmitter.
 - d. Set the 0-50 dB variable attenuator for 0 db. Set the total consistent attenuator for 50 dB.
- 3. Furn power on for both transmitter and receiver research Δ . Is a sequence,
 - a. Adjust the transmitter front panel attenuation and in the control of (1 mW) is obtained on the power meter. A terre there is a strong (If 0 dBm cannot be obtained, note the power value of the power attenuation. This will be used at a later through the result of power level.)

Table D2. ADC to Digital Hardware Backplane Cable List (Refer to Ligure 32 for eard locations)

Linetti	100
4-bit ADC	Receiver Hardware
% & B pins 1~18	Card 2 row B pins 19-39
8-bit ADC	
Bill cow B 1-18	Card 4 row A pins 1-18
Bd 2 - row B 1-18	Card 5 rox A pins 1-18
Bd 3 - row B 1-18	Card 6 row A pins 1-18
Bd 4 - row B 1-18	Card 7 rox A pins 1-15
Bd 5 - rox B 1-18	Card 9 row A pins 1-18
Bd 6 - row B 1-18	Card 10 rox A bins 1-18
Bd 7 - rox B 1-18	Card 11 row A ptns 1-18
Bd 8 - row B 1-18	Card 12 row A pins 1-18

- b. Adjust the 0-50 dB attenuator for 50 dB, and the front panel attenuator for maximum attenuation.
- c. Connect the oscilloscope to the IF front end as follows (refer to Figure E1(a) for location IF front end);
 - 1. Trace A to the 6-dB test point.
 - 2. Trace B to the 12-dB test point.
- d. Determine the front panel attenuator setting to be used (refer to the power reading/attenuator setting taken in step 3).
 - 1. If a 1 mW power level was obtained, add the attenuator setting to $-75~\rm{dB}$ to obtain the proper value, that is, attenuation setting

will be the total system attenuation to be inserted via the 0-50 dB attenuator and the front panel attenuator (0-50 dB set to 50 dB and the front panel attenuator set to 27.7 dB).

2. If a 1 mW power level was not obtained, take the power level reading of front panel attenuation and subtract from the total attenuation. Sired, that is, power level reading at -3,2 dBm.

$$\frac{75...3}{-3.2~{\rm dBm}} = \frac{75...3}{71.8~{\rm dB}}$$

total system attenuation.

After the proper attenuation level has been set, monitor the scope and adjust the 4-bit ADC de bias pot (refer to Figure D6) until the 6-dB IF attenuator line just begins to switch in. Ensure the manual attenuation control on the radar control panel is in the OFF position (refer to Figures C1 and E1(a) for location.

 $\underline{\text{Note:}}$ By monitoring the 6- and 12-dB IF attenuator lines, you ensure that 6 dB is being calibrated.

D4. DYNAMIC SYSTEM CHECK (Refer to Figure D8)

The dynamic test for each of the I and Q sides is the same for all eight channels. Channel 1Q will be described because of its accessibility.

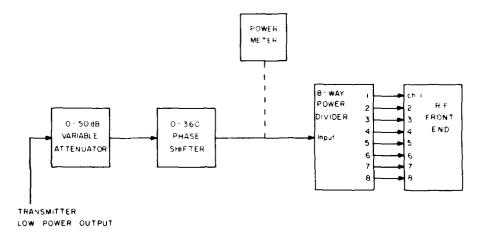


Figure D8. ADC Dynamic Test Configuration

Configure the transmitter for TEST, as outlined in Section D3.2.

Remove the RF input cable from the channel 1 RF input port, and connect this cable end to an eight-way power divider (MERRIMAC PDM-82).

Using eight coax cables (36-in, long), connect each of the output ports of the power divider to the input ports on the RF front end.

In order to determine the saturation point for each of the ADC unit, it may be necessary to measure the total insertion loss of the eight-way power divider from the input cable to each of the eight output cables. This may be accomplished using a network analyzer. (Note: Although use of the eight-way power divider is not mandatory, it does shorten the time required to perform checks on all 16 ADC's.

If not used, the RF input cable must be moved from channel to channel as the test progresses,)

- 1. On the radar control panel, set the IF attenuator switches to 0 dB of manual IF attenuation.
- 2. Connect an oscilloscope to the sample and hold input pins (10 and 11) of the ADC under test. (Refer to Figure D3(a) for pin locations.)
- 3. Set the 0-50 dB attenuator to 50 dB of attenuation. Set the transmitter front panel attenuator to 20 dB of attenuation.
- 4. Turn rack power on (both transmitter and receiver racks). Allow 10 min for warmup. Turn the transmitter "offset oscillator" on.
- 5. Monitoring the scope, adjust the $0-360^{\circ}$ phase shifter for the largest possible signal level (with respect to ground).
- 6. Set the transmitter front panel attenuator to 50 dB. On the radar control panel, set the auto/manual IF attenuator switch to AUTO.
- 7. Monitoring the oscilloscope, begin decreasing the amount of attenuation via the front panel attenuator. At the point where the 6 dB IF attenuator begins to switch in, measure the signal level (reading should be less than 1.25 V peak).
- 8. Continue decreasing the attenuation on the front panel attenuator. As each succeeding IF attenuator begins switching in, note the signal level.

(Note: The full range of 42 dB of IF attenuation may be achieved in the following manner:

After the front panel attenuator has been adjusted through its full range (to 0 dB), set the front panel attenuator to 50 dB and the 0-50 dB attenuator to 0 dB α . attenuation. This will give the system another 50 dB of signal range.)

9. Repeat steps 1. through 7. for the remaining 15 A/D sides.

At no point should the signal level measured in the automatic mode of IF att nuation exceed 1.25 V peak. If the signal level does exceed this amount, the ADC's may saturate.

10. If the signal level for any one of the 16 ADC's exceeds 1.25 V peak, repeat the 4-bit ADC bias adjustment procedure outlined in Section D3.

Appendix E

System Component Identification

The purpose of Appendix E is to identify the equipment located in each of the four equipment racks that make up the NFMRAD (AMTI) systems. As each level is identified within an equipment rack, reference will be made to the chapter within this report and/or other documentation for functional descriptions.

E1. RECEIVER (Refer to Figure E1(a))

level 1

Receiver IF Ref. Section 3.2.4

 $1evel\ 2$

Radar Control Panel Ref. Appendix C

level 3

Receiver Digital Hardware Ref. 4.1, 4.4 through 4.7

level 4

Analog to Digital Converter Ref. 4.2, 4.3, Appendix D (ADC) Deck

level 5 and 6

Power Supplies none

level 7

Rack Blower

E2. TRANSMITTER (Refer to Figure E1(b))

level 1

Ref. 3, 2, 3 Delay Lines

none

level 2

Receiver Front End Ref, 3,2,2

'Transmit'Receive Array Ref. 2.2

level 3

Bef. 3.1 Transmitter

Ref. 4.1.1 a. RI Sources

Ref. 3.1.3 b. Pulse Generation

c. Pulse Generation Ref. 3.1.3

level 4

Power Supplies nome

level i

Traveling Wave Tube Amplifier

(TWTA)

Ref. 3.1.4, also Instruction and Maintenance Manual for Instrumentation Traveling Wave Tube Amplifier Model No. 1277H03 FW L. Hughes Aircraft Co., Electron Dynamics Division, 3100 W. Lamita Blvd., Formance, CA = 90509.

level 6

Rusk Blower none:

E3. CSP-30 MINICOMPUTER (Refer to Figure F2(a))

level 1

Ref. Cartrifile 20 Instruction Manual. Tri-Data Catrifile Unit Tri-Data, 800 Mange Ave., Mountain View, CA 94040

level 2

Ref. CSPI Operation and Maintenance Control panel

Manual, Doc. No. JP3000-000-04. CSPI, 40 Linnel Cr., Billerica, MA

01821

level 3

Upper Mainfraiae Cooling Fans

Ref. none

level 4

Mainframe/Card Nest

Ref. see level 2 above

level 5

Lower Mainframe Cooling Fans

Ref. none

level 6

Power Supplies

Ref. see level 2 above

E4. MAP ARRAY PROCESSOR (Refer to Figure E2(b))

level 1

Display Scope

Tektronix Type 611

Ref. Tektronix Operation and Maintenance Manual, Type 611 Mod. 162C. Tektronix, Inc., P.O. Box 500, Beaverton, OR 97005

level 2

Hard Copy Unit

Tektronix Mod. 4601

Ref. Tektronix Operation and Main-

tenance Manual Mod. 4601.

level 3

MAP Monitor Panel

Ref. Installation and Operation Booklet

No. AS7130-000-01.

level 4

Expansion Power Supply

Ref. Operation Maintenance Manual

AT 6000-004-PRE4.

level 5

MAP-300 Arithmetic Processor

MAP Programmer's Reference Manual

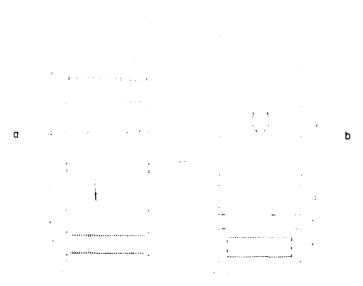


Figure E1. Receiver Transmitter Equipment Racks (i) Receiver, (b) Transmitter



CONTRACTOR CONTRACTOR

MISSION

of

Rome Air Development Center

RADC plans and executes research, development, test and selected acquisition programs in support of Command, Control Communications and Intelligence (C³I) activities. Technical and engineering support within areas of technical competence is provided to ESP Program Offices (POs) and other ESD elements. The principal technical mission areas are communications, electromagnetic guidance and control, surveillance of ground and aerospace objects, intelligence data collection and handling, information system technology, ionospheric propagation, solid state sciences, microwave physics and electronic reliability, maintainability and compatibility.

DATE FILMED

DTIC